

FEEDBACKS AMONG CLIMATE, SOILS, VEGETATION, AND EROSION  
DRIVE VALLEY ASYMMETRY DEVELOPMENT  
IN THE MOUNTAINS OF CENTRAL IDAHO

by

Michael John Poulos

A dissertation  
submitted in partial fulfillment  
of the requirements for the degree of  
Doctor of Philosophy in Geosciences  
Boise State University

August 2016

© 2016

Michael John Poulos

ALL RIGHTS RESERVED

BOISE STATE UNIVERSITY GRADUATE COLLEGE

**DEFENSE COMMITTEE AND FINAL READING APPROVALS**

of the dissertation submitted by

Michael John Poulos

Dissertation Title: Feedbacks Among Climate, Soils, Vegetation, and Erosion Drive Valley Asymmetry Development in the Mountains of Central Idaho

Date of Final Oral Examination: 05 May 2016

The following individuals read and discussed the dissertation submitted by student Michael John Poulos, and they evaluated his presentation and response to questions during the final oral examination. They found that the student passed the final oral examination.

Jennifer Pierce, Ph.D.	Chair, Supervisory Committee
Shawn Benner, Ph.D.	Member, Supervisory Committee
James P. McNamara, Ph.D.	Member, Supervisory Committee
Alejandro N. Flores, Ph.D.	Member, Supervisory Committee
Erkan Istanbuluoglu, Ph.D.	External Examiner

The final reading approval of the dissertation was granted by Jennifer Pierce, Ph.D., Chair of the Supervisory Committee. The dissertation was approved for the Graduate College by Jodi Chilson, M.F.A., Coordinator of Theses and Dissertations.

## ACKNOWLEDGEMENTS

This work would not have been possible without the extensive support and encouragement of my family, my committee, the Department of Geosciences, my colleagues, and my students. Thank you all.

Specifically, Dr. Jen Pierce has provided many opportunities for me to further my intellectual and academic development, and I am deeply grateful for the opportunity to work with her. Valerie and Mesa Greear have provided motivation and encouragement, and I thank them for their companionship. I thank my parents and siblings for encouraging and facilitating my pursuit of a higher education. Thank you to the many colleagues that have helped me over the years, including, but not limited to, Pam Aishlin, Chris Stanbery, Jim Edgemon, Phil Hummer, Brian Stark, Josh Ekhoﬀ, Lucy Gelb, and Austin Hopkins. Thank you to Kerrie Weppner, whose feedback greatly improved my technical writing.

I am grateful for the financial support, teaching opportunities, computing resources, and logistics provided by the Department of Geosciences at Boise State University, USA. This research would not have been possible without the extensive body of work focused on the Dry Creek Experimental Watershed. Additional financial support was provided by the NSF Idaho EPSCoR (EPS – 0814387). Analytical assistance was provided by Lawrence Livermore National Laboratory.

## ABSTRACT

Aspect has long been recognized as a significant source of landscape variability, which is induced by the orientation of land surfaces relative to solar incidence. Insolation differences on opposing aspects (e.g., north and south-facing slopes) act as localized climatic perturbations, altering surface energy balances and temperatures. Over shorter timescales, aspect-induced changes to the energy balance alter snow pack dynamics, soil water input rates and seasonality, and plant available water and water stress. Over longer timescales, aspect-induced insolation variability affects bedrock weathering rates and depths, soil and regolith development, vegetation type and density, erosion rates and processes, and ultimately hillslope and drainage forms. In turn, differences in landscape evolution on the opposite sides of valleys lead to valley asymmetry development.

The primary goals of this work are to 1) summarize available aspect-related hydrologic, ecologic and pedologic data for the Dry Creek Experimental Watershed (DCEW), fill knowledge gaps by investigating aspect-related differences in geomorphic characteristics and processes, and develop an integrative conceptual framework for how landscapes respond to aspect-induced insolation variability and how valley asymmetry develops. In particular, we assess 1) how aspect drives differences in fire and erosion rates, 2) how critical zone characteristics vary with aspect and how aspect-sensitivity changes with elevation, and 3) how aspect-related differences in critical zone response alter runoff production, drainage incision, and catchment competition, which drive valley asymmetry development.

Surprisingly, erosion rates for north and south-facing catchments do not appear to have varied significantly during the Holocene, despite dramatic differences in landscape characteristics (e.g., vegetation cover, soils, hydrologic processes, and landforms). This suggests that the valley asymmetry has not been actively developing, and is a relict feature of either initial landscape response to aspect, or specific climate intervals (e.g., glacial periods). Erosion rates for the margin of the Idaho batholith are lower than those in the interior batholith, reflecting lower rates of incision.

Elevation appears to modify the sensitivity of landscapes to aspect-induced climate perturbation. Critical zone properties appear to be most sensitive to aspect-induced climate perturbation at lower elevations (~1,100 m), and aspect-sensitivity diminishes towards higher elevations (~2,100 m). Changes in precipitation and temperature with increasing elevation appear to alleviate moisture stress, causing aspect-induced insolation and temperature variability to have less of an effect. Reduced landscape sensitivity to aspect at higher elevations explains why previously mapped slope asymmetry diminishes towards these elevations throughout the region.

Drainage incision and expansion are more pronounced on south-facing valley sides. South-facing catchments have shallower, coarser soils that yield more runoff per unit drainage area. Changes to the water balance at pedon-scales appear to influence how fluvial process scale with drainage area, which impacts catchment-scale erosive efficiency. Enhanced drainage incision in south-facing catchments, in conjunction with more effective diffusive erosion, appears to have promoted divide migration and land surface elongation.

Importantly, land surface degradation and elongation reduce geomorphic gradients, which serve as negative feedbacks by reducing denudation differences between north and south-facing valley sides, and effectively drive valley asymmetry development towards dynamic equilibrium. This suggests that although valley asymmetry clearly reflects differences in past erosion, it may actually develop as a landscape response to counteract aspect-induced differences in erosion. Where valley asymmetry is most pronounced, we suspect there may be little difference in rates of erosion. Valley asymmetry may be a remotely measurable characteristic of landscapes that reflect their proximity to stable states.

## TABLE OF CONTENTS

ACKNOWLEDGEMENTS .....	iv
ABSTRACT.....	v
LIST OF TABLES .....	xi
LIST OF FIGURES .....	xii
LIST OF ABBREVIATIONS.....	xviii
CHAPTER ONE: COUPLING ALLUVIAL FANS RECORDS WITH LIDAR TO COMPARE HOLOCENE EROSION RATES OF NORTH AND SOUTH-FACING CATCHMENTS IN THE IDAHO BATHOLITH.....	1
Abstract.....	1
1.1 Introduction.....	2
1.2 Background.....	4
1.3 Study Area and Prior Work.....	6
1.3.1 Overview .....	6
1.3.2 Geologic Setting.....	7
1.3.3 Modern Climate and Vegetation.....	8
1.3.4 Aspect-Related Research in the Dry Creek Experimental Watershed.....	8
1.4 Methods.....	9
1.4.1 Methods Overview.....	9
1.4.2 Fan Identification, Radiocarbon Dating, and Depth Correction .....	10
1.4.3 Fan Reconstruction, Volumetric Deposition, and Catchment- Averaged Denudation .....	11

1.5 Results.....	12
1.6 Discussion.....	15
1.6.1 Regional Synthesis of Erosion Rates and Sediment Yields.....	15
1.6.2 How Do Erosive Processes Vary with Aspect?.....	18
1.6.3 Relationships Among Fire, Slope Aspect, and Erosion.....	20
1.6.4 Aspect-Related Implications.....	24
1.7 Conclusions.....	27
1.8 References.....	29
CHAPTER TWO: ELEVATION MODIFIES THE SENSITIVITY OF REGOLITH PROPERTIES TO TERRAIN ASPECT .....	46
Abstract.....	46
2.1 Introduction.....	47
2.2 Background.....	49
2.3 Study Area .....	53
2.4 Methods.....	54
2.5 Results.....	57
2.6 Discussion.....	61
2.6.1 Elevation and Aspect Variability .....	62
2.6.2 Hillslope-Scale Variability.....	69
2.7 Conclusions.....	73
2.8 References.....	76
CHAPTER THREE: ASPECT-INDUCED ASYMMETRIC DEGRADATION, DIVIDE MIGRATION, AND LAND SURFACE ELONGATION DRIVE VALLEY ASYMMETRY DEVELOPMENT TOWARDS A DYNAMIC EQUILIBRIUM .....	93
Abstract.....	93

3.1 Introduction.....	94
3.2 Study Area .....	97
3.3 Methods.....	99
3.4 Results.....	101
3.5 Discussion.....	106
3.5.1 North-Facing Catchment Response to Decreased Insolation.....	106
3.5.2 South-Facing Catchment Response to Increased Insolation .....	108
3.5.3 Fluvial-Diffusive Process Coupling and Incision Signal Propagation	109
3.5.4 Catchment Competition, Divide Migration, and Valley Asymmetry Development .....	111
3.6 Conclusions.....	113
3.7 References.....	115
APPENDIX A.....	130
Expanded Methods for Chapter 1: Coupling Alluvial Fans Records with Lidar to Compare Holocene Erosion Rates of North and South-Facing Catchments in the Idaho Batholith.....	130
APPENDIX B .....	141
Supplemental Figures for Chapter 3: Aspect-Induced Asymmetric Degradation, Divide Migration, and Land Surface Elongation Drive Valley Asymmetry Development towards a Dynamic Equilibrium.....	141

## LIST OF TABLES

Table 1.1	Alluvial fan deposit charcoal ages and sampling depths. ....	44
Table 1.2	Alluvial fan aggradation rates, reconstructed surface areas, and volumetric rates of deposition. ....	44
Table 1.3	Source catchment areas, catchment averaged denudation rates, and sediment yields. ....	45
Table 1.4	Individual deposit thicknesses, volumes, and sediment yields for years of events. ....	45
Table 2.1	Penetration-based regolith depth (thickness) measurements along a valley transect. Note that actual mean depths are likely higher where depths exceeded measurement capabilities (bold values), and the means for each aspect represent minimum values. Average surface-normal depths are plotted in cross-section in Figure 2.3. ....	91
Table 2.2	Soil thickness and compiled land surface characteristics for each soil augering site, sorted from north to south. ....	92
Table 3.1	Summary of aspect-related variability in soils, water, and vegetation in the DCEW. ....	121
Table 3.2	Summary of characteristics of catchments shown in Figure 3.3. ....	127

## LIST OF FIGURES

Figure 1.1	Aspect-related variability in vegetation cover and landforms in the Dry Creek Experimental Watershed (DCEW). Note asymmetries in hillslope steepness, ridgeline linearity, land surface length, and vegetation cover. ....	38
Figure 1.2	Location and overview of the Dry Creek Experimental Watershed (DCEW). Note steeper northern aspects, with shorter and less developed drainages. Right panel shows alluvial fan charcoal excavation sites and source catchments. Note differences in coniferous forest cover.....	38
Figure 1.3	Example of alluvial fan reconstruction: a.) Alluvial fan location within large valley, b.) 50 cm resolution bare-earth DEM of modern fan surface, and c.) Reconstructed fan surface bound by confining geometry.....	39
Figure 1.4	a.) Relationship between charcoal age and burial depth, tangential to the fan surface, for north and south-facing catchments. Slopes of lines for fan profiles with multiple samples represent aggradation rates. b.) Relationship between charcoal age and catchment-averaged denudation. Slopes of lines for fans profiles with multiple samples represent rates of denudation. ....	40
Figure 1.5	Stratigraphic profiles of fan deposits for two fans. Most fan deposits for south-facing catchments did not exhibit distinct boundaries or stratigraphy related to processes (e.g. sheetflood couplets, large matrix-supported clasts, sediment sorting, and charcoal-rich layers etc.). Note that bottom of pit is seen obliquely in these HDR vertically-stitched photos, falsely giving the appearance of plate-like structure in the south-facing pit. ....	41
Figure 1.6	Fire record showing the summed calibrated age probabilities (top) for charcoal from north (n=13) and south-facing (n=7) catchments. (bottom) samples making up each probability distribution plotted as weighted mean sample ages with 2-sigma age ranges (error bars). Vertical position on lower graph is sorted by aspect and age for display. Overlapping age distributions indicate samples are likely from the same episode of fire-related erosion, and in some cases the same deposit. The absence of samples younger than 500 cal yr BP may reflect the preference for dating of samples from deeper in the deposits in order to obtain time-averaged erosion rates. ....	42

Figure 1.7	a.) Aggradation, b.) volumetric deposition, and c.) catchment-averaged denudation rates calculated using the deepest samples for each north (n=5) and south-facing (n=3) catchment fan. Differences between aspects become greater for volumetric deposition because south-facing fans were larger on average, but decrease for catchment-averaged denudation rates (i.e. source-area normalized) because south-facing catchments are also larger.....	42
Figure 1.8	a.) Time-averaged sediment yields with propagated uncertainty ranges and timescales of measurement. b.) The time-averaged sediment yields and yields from individual deposits are compared to sediment yields from elsewhere in the region.....	43
Figure 1.9	Conceptual model of valley asymmetry development as a landscape adjusts towards dynamic equilibrium. Initially, south-facing valley sides degrade faster, but attenuate towards long-term denudation rates similar to north-facing valley sides, and valley asymmetry evolves towards a stable asymmetric form. Short-term denudation rates may be highly variable, due to differences in the frequency and magnitude of erosional processes, but result in similar long-term rates.....	43
Figure 2.1	Location map of the Dry Creek Experimental Watershed (DCEW), with locations of depth and texture measurements of regolith and soil y this study and previous studies. Penetration inputs were used in a soil depth model by Tesfa et al. (2009). Pit textures, depths and moisture measurements were assessed by Smith et al. (2012). Surficial soil and hydraulic properties were assessed by Geroy et al. (2012).....	82
Figure 2.2	Example of penetration rod and auger piercing the upper darker, finer-grained mobile regolith, and set into the underlying coarser immobile regolith (granodiorite). The methods yielded similar results when tested side-by-side.....	83
Figure 2.3	Cross-sectional view of regolith 'blind' penetration transect showing thicker, and possibly less variable, unconsolidated regolith. Each circle shows the average of 2-3 measurements, with sites where at least one measurement exceeded the maximum measurable depth indicated with crosses. ....	83
Figure 2.4	Comparison of lab textures (circles) with field classification. Blue circles indicate that field classification correctly identified the correct soil class, while red circles indicate incorrect classification and include a red arrow pointing to the texture class or intermediate boundary (e.g. SaLo/Lo boundary) identified in the field. ....	84

Figure 2.5	Example auger samples from a site with relatively thick mobile regolith (152 cm), located on a gentle upland of a south-facing ridgeline supporting dense sagebrush cover. Note the change to immobile regolith (saprolitic granodiorite bedrock) is characterized by an increase in gravel content, a transition to a loamy sand or sand texture, and a lighter and redder color. ....	84
Figure 2.6	Augering transect figure showing, from top to bottom, grain-size data, land surface and mobile/immobile regolith transition profiles, local slope, and local northness, which is calculated from aspect. ....	85
Figure 2.7	Zoomed in figure showing soil textures and mobile regolith (i.e. soil) depths for the north and south-facing hillslopes in the middle of the transect (facets). ....	85
Figure 2.8	a.) Summary of aspect-related differences in soil depth and variability with elevation (replotted from Smith, 2010), and b.) Aspect-related differences in surficial soil texture and density (graphs from Geroy et al., 2011). ....	86
Figure 2.9	Differences in regolith textures (sub-2mm fraction) vary the most with between north and south-facing slopes at low elevations, but differences with aspect decrease with increasing elevation. Replotted using laser-diffraction texture data from Smith (2010). Grain-size data displayed similar trends with aspect and elevation for 0-2 cm, 2-15 cm, and bedrock depths. ....	86
Figure 2.10	a.) Valley cross-section with no vertical exaggeration of topography, showing augered mobile regolith thicknesses with GAM modeled penetrable regolith thickness, which are exaggerated 20 times to make changes in regolith thickness more visible on graphs. ....	87
Figure 2.11	Augered mobile regolith depths plotted over modeled penetrable regolith depths (Tesfa et al, 2009), with added slope-shaded to show topography. ....	88
Figure 2.12	Auger-based mobile regolith thickness transect plotted over color-infrared aerial photograph showing increased vegetation reflectance of infrared (red colors above). Note that, at least on the south-facing slope, thicker soils occur where near-infrared is brighter, which is generally characteristic of productive vegetation. ....	89
Figure 2.13	Annual time-series of insolation and temperature, with overlays of growing season durations and timing of peak NDVI (vegetation productivity), with vertical positions denoting general elevations (not to scale). ....	90

Figure 2.14	Down-valley view of the location of the augering transect. Note the gentler ridgeline segments on the south-facing valley side (i.e. stair-steps in ridgelines), which contrast with the linear north-facing ridgelines.....	90
Figure 3.1	Aerial photo of the Dry Creek Experimental Watershed (DCEW) showing forest cover (i.e. the moisture-limited lower treeline) extending to lower elevations on north-facing valley sides, and locations of instruments stratified across aspects and elevations. Note that drainage networks on south-facing land surfaces are generally more extensive and complex.....	120
Figure 3.2	Up-valley photos at a.) ~1400-1800 m elevation and b.) 1000-1400 m elevation. Note landform asymmetry, and position of the tree-line at lower elevations on northern aspects. ....	120
Figure 3.3	Binned slope angle map showing difference in slope steepness between north and south-facing valley side-slopes. Note that north-facing slopes are consistently over 30° for the north-facing slopes along the major east-west trending drainages. The characteristics of the outlined north and south-facing catchments are summarized in Table 3.2. ....	122
Figure 3.4	Non-parametric probability density function of aspect-binned (90° each) slope angles for north and south-facing slopes. ....	123
Figure 3.5	Topography-modeled insolation distributions for the cardinal directions. Insolation values represent annual cloud-free totals. ....	123
Figure 3.6	Scatter plot showing the inverse correlation between aspect-binned slope and insolation.....	124
Figure 3.7	Summary of aspect-related differences in stream and ridgeline forms. South-facing land surface extends beyond the photo extent. Data for all three valley segments can be viewed in Figures B4-B7 in Appendix B. ....	125
Figure 3.8	a.) Changes in median slope with drainage area, with interquartile range envelopes, labeled slope turnover points, and transitional and channelized trends and power-law functions denoting scaling relationships. b.) Changes in curvature with drainage area, with interquartile range envelopes and the transitional drainage area from convex to concave topography labeled. c.) Drainage area pixel counts, normalized by bin size, depicting differences in total land surface area at different drainage areas. d.) Probabilities of exceeding given drainage areas, with trends and power-law functions for the linear sections of the distributions denoting scaling relationships.....	126

Figure 3.9	Conceptual water balance model of interactions among modern aspect-related variability of vegetation, subsurface characteristics, water storage, hydrologic partitioning, runoff potential, and hillslope and drainage form.....	128
Figure 3.10	Conceptual model of valley asymmetry development and dynamic equilibrium. a.) Valley geometry changes from a heterogeneously-lowering symmetric form to a homogeneously-lowering asymmetric form. b.) South-facing valley sides degrade faster initially, but negative feedbacks cause long-term denudation rates to attenuate to values similar to north-facing valley sides. Valley asymmetry also attenuates towards a stable asymmetric form. Although short-term denudation rates may be highly variable, due to differences in the frequency, magnitude, and type of erosional processes, long-term rates may still be similar. c.) Cross-section of valleys showing the combined effect of asymmetry development and trunk stream incision. Denudation rates between time-steps T0 and T1 vary with aspect, but are uniform between T1 and T2 when dynamic equilibrium has been achieved. ....	129
Figure B1	Before (left) and after (right) hillshades showing how ridgeline elevations were interpolated to fill catchments and estimate the minimum volume of material removed. Ridgelines have likely eroded over time as well, so these volumes should not be viewed as total amounts of erosion, but are treated as a metric of the depth of drainage incision below ridgelines. ....	142
Figure B2	Changes in slope with aspect. Colored data show the frequency of specific combinations of aspect and slope bins. The black line is the median slope value within each 1° aspect bin. The gap in the distribution at ~10 to 80° reflects the low abundance of north-east facing slopes. ....	143
Figure B3	Changes in insolation with aspect. Colored data show the frequency of specific combinations of aspect and insolation bins. The black line is the median insolation value within each 1° aspect bin. ....	144
Figure B4	Locations of stream profiles shown in Figure B5 for catchments incised into north and south-facing valley side-slopes. From top to bottom, these valleys are Upper Dry Creek, Shingle Creek, and Lower Dry Creek. Note the shorter length and more linear form of streams draining from north-facing slopes.....	145
Figure B5	Stream longitudinal profiles plotted draining to trunk streams for catchments incised into north and south-facing valley side-slopes along upper Dry Creek (a.), Shingle Creek (b.) and lower Dry Creek (c.). See Figure B4 for locations. Note that stream profiles for south-facing slopes less linear and longer horizontally, but similar in vertical relief,	

	except along lower Dry Creek where south-facing landsurfaces have more relief. ....	146
Figure B6	Locations of profiles along ridgelines between catchments incised into north and south-facing valley side-slopes. From top to bottom, these valleys are Upper Dry Creek, Shingle Creek, and Lower Dry Creek. Note the shorter length of ridgelines, in general, for north-facing slopes. See Figure B7 for rideline profiles.....	147
Figure B7	Ridgeline (see Figure B6 for locations) profiles for ridgelines formed between catchments incised into north and south-facing valley side slopes along upper Dry Creek (a.), Shingle Creek (b.) and lower Dry Creek (c.). Distances are plotted relative to where each ridgeline intersects the divide between north and south-facing valley land surfaces. Ridgelines on south-facing slopes are longer horizontally, but similar in vertical relief, except in lower Dry Creek where south-trending ridgelines have more relief. ....	148

## LIST OF ABBREVIATIONS

$^{14}\text{C}$ yr	Radiocarbon age (uncalibrated)
cal yr BP	Calibrated radiocarbon age in years before present
CRN	Cosmogenic Radionuclide
CZO	Critical Zone Observatory
DCEW	Dry Creek Experimental Watershed, Idaho, USA
DEM	Digital Elevation Model
LiDAR	Light Detection and Ranging: A laser-based measurement of landsurface elevations.
NDVI	Normalized Difference Vegetation Index
OSL	Optically Stimulated Luminescence
TIN	Triangulated Irregular Network

CHAPTER ONE: COUPLING ALLUVIAL FANS RECORDS WITH LIDAR TO  
COMPARE HOLOCENE EROSION RATES OF NORTH AND SOUTH-FACING  
CATCHMENTS IN THE IDAHO BATHOLITH

**Abstract**

Alluvial fans provide natural, albeit leaky, sediment traps useful for estimating erosion rates if the timing and volume of deposition can be established. We combine high-resolution alluvial fan volume reconstructions with radiocarbon dating of deposits to estimate Holocene erosion rates for small steep ephemeral headwater catchments of south-central Idaho. Comparison of sediment yields from individual debris flows and sheetfloods, time-averaged Holocene sediment yields, and longer-term estimates of uplift and erosion reveals 1) episodic events, often triggered by wildfire, contribute the majority of sediment to alluvial fans and 2) minimum constrainable sediment yields for individual events are expectedly lower than those for larger, more rapidly incising catchments in the region. Interestingly, despite dramatic valley asymmetry and associated aspect-related differences in vegetation and landforms, Holocene erosion rates estimated for north and south-facing catchments are not significantly different. North-facing catchments produce larger and less frequent fire-driven debris flows, while south-facing catchments yield more frequent but lower volume sheetfloods. Tradeoffs between erosional frequency and magnitude appear to produce similar time-averaged Holocene erosion rates on opposite valley sides, suggesting that valleys develop asymmetry to counteract aspect-induced

erosion differences and evolve towards dynamic equilibrium (i.e. homogenous steady state denudation rates).

## 1.1 Introduction

Quantifying erosion rates is fundamental to understanding how climate variability affects landscape evolution. Alluvial fans provide useful records of erosion, which have been underutilized in part due to difficulty of reconstructing and measuring deposit volumes. We provide a novel method that couples alluvial fan deposit dating with volume reconstruction to yield time-averaged erosion rates. Fan aggradation rates are constrained by radiocarbon dating charcoal within alluvial fan deposits. Dissected alluvial fan surfaces often prohibit direct measurement of fan volumes; therefore, alluvial fan geometries were reconstructed from fan surface remnants evident in high-resolution elevation data (0.5 m) derived from airborne LiDAR (Light Detection and Ranging). Extrapolation of alluvial fan aggradation rates across reconstructed fan surfaces provides rates of volumetric deposition, which, when normalized by source-catchment area, yields catchment-averaged denudation rates.

We apply the approach to small (<0.5 km<sup>2</sup>), steep (30-35°), semi-arid, fire-prone, ephemeral headwater catchments in the Idaho batholith. Small catchments generally lack the drainage area for regularly recurring fluvial erosion, but erode rapidly following episodic extreme events (e.g. fire, rain-on-snow, and/or cloudbursts) that produce sediment-rich flows and form alluvial fans at catchment outlets. Prior work in similar environments found that episodic, large alluvial fan-building events account for the bulk of the time-averaged erosion rates (Meyer et al., 2001; Meyer and Pierce, 2003; Riley et al., 2015; Orem and Pelletier, 2016). The episodicity and magnitude of fan deposition are

examined within the context of erosion rate studies in the Idaho Batholith (e.g. Sweetkind and Blackwell, 1989; Kirchner et al., 2001; Meyer et al., 2001; Meyer and Pierce, 2003; Pierce et al., 2011; Riley et al., 2015). We expected that, despite similar catchment characteristics, erosion rates in our study area will be lower than those in the more actively incising region of central Idaho.

Small catchments are particularly sensitive to the topographic variability in climate caused by aspect-induced insolation and temperature variability, which drives feedbacks that alter vegetation, soils, hydrologic processes, and landforms (Istanbulluoglu et al., 2008; Yetemen et al., 2015). Aspect-induced differences in climate have long been recognized as a source of valley asymmetry (e.g. Powell, 1874; Gilbert, 1904; Hack and Goodlet, 1960). Systematic mapping of aspect-related differences in slope angles across the American Cordillera (60° N to 60°S) revealed that aspect-induced asymmetry is widespread and highly variable, displaying changes in slope asymmetry with latitude, elevation, and across mountain ranges (Poulos et al., 2012).

On opposite sides of ~1.2 km wide asymmetric valleys in a semi-arid montane region of the southwestern Idaho batholith, we compare the erosion rates of small catchments (<0.5 km<sup>2</sup>) incised into larger-scale north and south-facing land surfaces. Persistent aspect-induced differences in climate in these basins have produced somewhat counterintuitive effects on catchment erosion and landscape evolution. On drier south-facing slopes, drainages are generally larger and more complex than north-facing slopes. Valley side slopes have clearly experienced different amounts of land surface lowering (i.e. degradation), but it is unclear whether valley asymmetry is actively developing or a relict feature. Erosion rates over 10<sup>3</sup>-10<sup>5</sup> yr timescales appear to vary with aspect in some

environments (e.g. Foster et al., 2015), but not in others, despite dramatic aspect-related landscape variability (West et al., 2014).

We hypothesize that if valley asymmetry is actively developing, then the gentler, longer, less vegetated, and more dissected south-facing slopes should have higher erosion rates. Alternatively, we hypothesize that erosion rates cannot vary with aspect if the system is near steady state conditions, which mandate equal denudation rates throughout a landscape. We suggest that differences in erosion rates with aspect, and resulting valley asymmetries, indicate the proximity of valley asymmetry to steady state conditions; the greater the difference in erosion rates with aspect, the farther the system is from dynamic equilibrium.

## **1.2 Background**

The recent renaissance of research into ‘critical zone’ structure and function (i.e. the life supporting zone that extends from the tops of trees to the depth of weathered bedrock) as well as advances in cosmogenic dating of soil profiles (e.g. Heimsath et al., 1999; West et al., 2014; Foster et al., 2015) has increased research efforts on how hillslope erosion rates and processes relate to eco-pedo-hydro-geomorphic feedbacks and landscape evolution. Studying aspect-related land surface variability is particularly valuable because it reflects how the critical zone responds to persistent climate differences caused by aspect-induced insolation and temperature variability (Istanbulluoglu et al., 2008; Yetemen et al., 2015). Valleys form natural laboratories for studying aspect because many complicating factors can be assumed constant for adjacent slopes (e.g. lithology, regional climate, and changes in base level). The landscape response to the relatively warmer conditions on south-facing slopes can be used in a

space-for-time substitution to represent how north-facing slopes might respond to persistent global warming over long timescales (e.g.  $10^3$ - $10^6$  yrs).

While non-climatic influences can cause valley asymmetry (e.g. Powell, 1874; Hack and Goodlet, 1960; Garrote et al. 2006), most studies of valley asymmetry focus on how aspect-induced changes in microclimate drive eco-hydro-pedo-geomorphic feedbacks that alter land surface characteristics, erosion rates, and valley asymmetry evolution (e.g. Powell, 1874; Gilbert, 1904; Tuck, 1935; Hack and Goodlet, 1960; Melton, 1960; Dohrenwend, 1978; Wende, 1995; Gutiérrez-Jurado et al., 2007; Burnett et al., 2008). However, fewer studies have investigated the timing and rate of valley asymmetry development (e.g. Istanbuloglu et al., 2008; McGuire et al., 2014; West et al., 2014; Foster et al., 2015).

Fire is an important component of erosion in steep, mountainous, fire-prone terrain. Holocene fire-related sheetfloods and debris flows compose a large proportion of alluvial fan sediment, and climate-driven shifts in fire activity alter the timing and magnitude of sediment inputs to alluvial fans over Holocene timescales (Meyer and Pierce, 2003; Pierce et al., 2004; Nelson and Pierce, 2010; Riley et al., 2015). In the Jemez Mountains of New Mexico, fire-related deposits comprised only 39% of the alluvial fan thicknesses for south-facing slopes, compared to 77% for north-facing slopes, suggesting that aspect alters landscape response to fire (Fitch and Meyer, 2016). Radiocarbon dating of charcoal within alluvial fan deposits provides relatively cost-effective records of both erosion and fire, and facilitates assessment of how aspect influences fire timing and erosional response.

The combination of alluvial fan volumes and radiocarbon dating of organic matter in Holocene alluvial fan sediments provides an underutilized mechanism for estimating minimum erosion rates in small ephemeral catchments. Cosmogenic nuclide accumulations are often used to estimate erosion rates, but catchment-scale bulk cosmogenic ages have high uncertainties in landscapes where mass-wasting (e.g. shallow landsliding and debris flows) excavates deeply buried materials that are not exposed to cosmogenic nuclides (Niemi et al., 2005). Cosmogenic accumulation in soil profiles can be used to measure the erosion rate at a given point (e.g. Heimsath et al., 1999), but require numerous costly samples per profile, and point measurements may not be representative of land surface or catchment as a whole.

We are unaware of other studies that use alluvial fan sediments to compare aspect-related differences in erosion rates. While some studies survey catchment erosion and alluvial fan deposition following single modern events (e.g. Meyer et al., 2001; Benda et al., 2003), fewer studies (e.g. Meyer et al., 2001; Riley, 2012) link deposit volumes and ages to produce time-averaged erosion rates of the source catchments, in part because estimating the volume of material within an entire alluvial fan, and ascertaining the ages of that deposited material is difficult.

### **1.3 Study Area and Prior Work**

#### **1.3.1 Overview**

The Dry Creek Experimental Watershed (DCEW; Figures 1.1 and 1.2) is located within the Boise Foothills in the Northern Rockies. The drainages are incised into hydrothermally altered granodiorite on the southwestern margin of the Cretaceous Idaho batholith (Clayton et al., 1979; Criss et al., 1982). The DCEW spans an elevation range

from 1025 to 2130 m.a.s.l. and exhibits dramatic aspect-related variability in landscape characteristics (Figure 1.1). Within the DCEW, we focused on two east-west trending valley segments with side-slopes spanning elevations between 1350 and 1700 m.a.s.l.

The valleys are large and deeply incised, with widths of ~ 1.5 km, and vertical relief of ~200-250 m. Valley side-slopes have been dissected by ephemerally flowing small (<0.5 km<sup>2</sup>), steep (up to ~40°) catchments, which have produced alluvial fans at their outlets. Drainages are generally more developed (i.e. larger and more complex) on south-facing slopes (Figure 1.2).

### 1.3.2 Geologic Setting

The southern lobe of the Idaho Batholith was emplaced between 100 to 75 Ma (Armstrong et al., 1977) in the subsurface as a series of coalescing plutons. However, the batholith was not unroofed and exposed at the surface until ~10 Ma, after which time it has experienced an average of ~30 cm/ka of uplift (Sweetkind and Blackwell, 1989). As such, the drainages and landforms in the study area may have been developing since ~10 Ma. The DCEW is located on the southwestern margin of the batholith, which is bounded by a normal fault.

For ~8 of the last ~9.5 Ma, the study area drained to a local base level defined by paleo “Lake Idaho” (Wood and Burnham, 1982; Othberg, 1994; Wood and Clemens, 2002). For roughly half this period, the lake was an internally-drained basin disconnected from the ocean (Swirydczuk et al., 1979; Straccia et al., 1990). Although lake level fluctuations might cause variations in erosion, the presence of a lake consistently raised the local base level and reduced geomorphic gradients during 8 of the last 9.5 million years.

### 1.3.3 Modern Climate and Vegetation

Based upon 12 years of precipitation gauge data within the watershed at a representative 1610 m.a.s.l., and linearly increasing precipitation trends with elevation (Aishlin and McNamara, 2011; Anderson et al., 2014), the east-west trending valleys studied received between ~30 to 60 cm of precipitation annually that increases with elevation. Roughly half of the modern precipitation falls as snow, with more snow at higher elevations (McNamara et al., 2005; Anderson et al., 2014).

Vegetation in the DCEW varies dramatically with both aspect and elevation (Figures 1.1 and 1.2). Within the valley segments studied, north-facing slopes predominantly support coniferous forests, composed primarily of Douglas fir (*Pseudotsuga menziesii*) and ponderosa pine (*Pinus ponderosa*). South-facing slopes exhibit more bare ground and ecosystems composed of big sagebrush (*Artemisia tridentata*), rubber rabbitbrush (*Ericameria nauseosa*), antelope bitterbrush (*Purshia tridentata*), cheatgrass (*Bromus tectorum*; invasive), rush skeletonweed (*Chondrilla juncea*; invasive), and other forbes in lesser quantities (Smith, 2010; Loughridge, 2014).

### 1.3.4 Aspect-Related Research in the Dry Creek Experimental Watershed

Prior research in the DCEW has characterized aspect related variability in hydrologic processes, soil and regolith characteristics, and vegetation. On north-facing slopes, snow and moisture persist longer, and soils are deeper, finer-grained, and contain more organic matter, which increases water storage and persistence and results in longer growing seasons that promote denser and more productive vegetation (Tesfa et al., 2009; Smith, 2010; Smith et al., 2011; Geroy et al., 2011; Kunkel et al., 2011; Anderson et al., 2014). Differences in regolith thickness and texture with aspect may reflect changes in

weathering rates, residence times, and dust accumulation (Stark, 2012). Differences in soil storage also affect subsurface drainage and runoff production (Kormos et al., 2015), which likely affects the geomorphic efficacy of fluvial processes.

In the DCEW, relatively homogenous bedrock and an absence of faults within the study area suggest tectonic tilting and valley-parallel faulting are not likely mechanisms for valley asymmetry development. Normal faults associated with basin and range extension bound the surrounding terrain. However, hillslope asymmetry in the area varies little across the faults, and correlates with elevation (Poulos et al., 2012), which implies that changes in climate and eco-hydro-geomorphic feedbacks associated with aspect are likely responsible. Additionally, if bedrock structure caused valley asymmetry, one would expect increased erosion from the steepened slope, whereas the landscape characteristics (e.g. thicker soils and denser vegetation) suggest greater stability.

## **1.4 Methods**

### 1.4.1 Methods Overview

For small steep ephemeral catchments incised into north and south-facing land surfaces (i.e. valley sides), small alluvial fans deposited at their outlets were used as records of fire and erosion. Our approach for estimating catchment-averaged erosion rates from alluvial fan deposits required: 1) radiocarbon dating of charcoal within deposits, 2) determining the corresponding deposit volumes, 3) normalizing deposit volumes by source catchment areas, and 4) assessing uncertainties and limitations. Detailed methods are available in Appendix A.

Denudation rates were compared among small, steep ephemeral catchments incised into larger-scale north and south-facing valley side-slopes to investigate whether

erosion rates vary with aspect. Catchment-averaged denudation rates were also compared to established data for the Idaho Batholith to 1) validate our methodology, 2) investigate changes in denudation over time, and 3) examine changes in denudation with uplift and incision.

#### 1.4.2 Fan Identification, Radiocarbon Dating, and Depth Correction

Catchment-scale erosion rates were measured using eight alluvial fan records for north-facing (n=3) and south-facing (n=5) catchments (Figure 1.2). Where possible, we cleanly collected larger individual charcoal fragments from discrete depths in vertically cut pit faces. Where fragments were small and difficult to find, bulk sediment was collected from depth intervals, washed to remove charcoal, and combined into single samples.

Twenty charcoal samples were radiocarbon ( $^{14}\text{C}$ ) dated at the Lawrence Livermore National Laboratory. We selected younger twigs when available to reduce error from the age variance among small fragments and the inbuilt age of the vegetation prior to the fire (Gavin, 2001). Two larger samples were subsampled into duplicates and dated to assess analytical replicability. The results are comparable, varying within the range of the estimated laboratory uncertainty (Sample B16\_P1\_S02:  $585\pm 30$  and  $555\pm 35$   $^{14}\text{C}$  yr, and Sample B09\_P01\_CH1:  $3675\pm 30$  and  $3665\pm 30$   $^{14}\text{C}$  yr).

Radiocarbon dates were calibrated using the IntCal13 curve in Calib 7.0.2 software (Stuiver and Reimer, 1993; [calib.qub.ac.uk](http://calib.qub.ac.uk)), yielding age probability distributions. Weighted means for each age probability distribution, which are most representative of radiocarbon age distributions (Telford et al., 2004), were calculated in Oxcal 4.2 (Ramsey, 2009; [c14.arch.ox.ac.uk](http://c14.arch.ox.ac.uk)).

### 1.4.3 Fan Reconstruction, Volumetric Deposition, and Catchment-Averaged Denudation

Fan surfaces were reconstructed by fitting a conical surface through fan surface remnants, evident in high-resolution (0.5 m resolution) elevation data derived from airborne LiDAR point clouds. Sample depths and ages were extrapolated across reconstructed fan surfaces to yield deposit volumes and volumetric rates of deposition. Deposition rates were normalized by source-catchment surface areas to yield catchment-averaged denudation rates.

Sample depths are often measured vertically in soil pits; however, fans generally aggrade parallel to the surface, and the surface-normal depth better represents the volume of material deposited above a specific depth. Vertical depths were converted to surface-normal depths using field measurements of fan slope, which were consistent within  $1^\circ$  with average fan surface slopes derived from high-resolution elevation data. We recognize that fan deposits are non-uniform in thickness and continuity, and age/depth trends will vary laterally. It was not possible to assess this variability, due to poor exposure and absence of marker deposits. Rather we collected samples from as deep as possible in order to smooth out the episodicity of events. Our methods assume the sample depths are representative of corresponding fan depositional volumes (i.e. deposits less than a specific age are of uniform thickness, lie parallel to the surface, and cover the entire fan). This assumption certainly is not valid over short time-scales; deposition on alluvial fans is often restricted to channels and lobes and deposits vary in thickness laterally. However, over millennial time-scales, time-averaged aggradation rates are relatively even across a fan, because aggradation and avulsion shift deposition back and

forth across alluvial fans (Denny, 1967; Blair and McPherson, 1994; Parker et al., 1998; Field, 2001).

Alluvial fan 3D surfaces were reconstructed by fitting conical trend surfaces through fan surface remnants evident in airborne LiDAR data (Figure 1.3). 3D surface areas were necessary to avoid a slope bias (e.g. steeper slopes have a lower surface area in 2D plan view). Multiplying reconstructed fan 3D surface areas by surface-normal sample depths yielded fan volume estimates above each sample. Fan deposition rates were calculated by dividing the volumes by the weighted-mean calibrated age. Fan aggradation rates were converted to inferred catchment-averaged denudation rates by dividing by 3D surface areas of fan source-catchments. This complete calculation is summarized as follows:

$$\mathbf{Denudation\ rate} \left( \frac{mm}{yr} \right) = \frac{\mathbf{Deposit\ Thickness} * \mathbf{Fan\ Area}}{\mathbf{Deposit\ Age} * \mathbf{Source\ Catchment\ Area}} \quad \frac{cm * m^2}{yr * m^2} \quad \text{[Equation 1]}$$

Maximum and minimum uncertainty ranges of fan aggradation and catchment averaged denudation rates were determined by propagating individual errors and uncertainties through the calculations (i.e. Equation 1; see Appendix A for full discussion of error propagation).

## 1.5 Results

Time-averaged fan aggradation rates, calculated using the deepest charcoal sample for each of the five north-facing catchments and three south-facing catchments, ranged from 55 to 122 cm/ka, with average rates of 62 and 84 cm/ka for north- and south-

facing catchments, respectively (Table 1.2). For individual fan profiles with multiple dated samples, linear aggradation trend slopes ranged from ~45 to ~79 cm/ka (n=4; Figure 1.4a).

Aggradation time-series show the expected increase in age with profile depth (Figure 1.4a), indicating that none of the deposits lower in the profiles were inverted in age; there is neither evidence of cut and fill cycles producing inset younger deposits, nor evidence of reworked charcoal from older fire events included in younger deposits. No trend was calculated for Catchment 11 because all 3 samples appear to be within the same deposit and are not significantly different in age.

The alluvial fan deposits for south-facing catchments were generally better sorted, with less silt and clay sized-material, and more frequently displayed evidence of sheetfloods (e.g. sheetflood couplets and massive units; Figure 1.5). Charcoal fragments were scarcer and smaller in fan deposits from the mostly unforested south-facing catchments. South-facing fans more often required bulk sampling in order to aggregate enough charcoal mass for dating. North-facing fans contained more debris flow deposits, with angular cobble-sized clasts and abundant charcoal (Figure 1.5). There were more samples for north-facing slopes (n=13) than for south-facing slopes (n=7), because charcoal was scarce in deposits from south-facing slopes, and some samples contained insufficient charcoal.

Calibrated alluvial fan weighted-mean charcoal ages ranged from 8,002 to 595 cal yr BP (Table 1.1), with an average 2-sigma (i.e. 2 standard deviation) range of  $\pm 92$  cal yr BP. Charcoal age probability distributions for north and south-facing slopes generally spanned different time periods, except ~1000-500 cal yr BP when numerous samples for

both north and south-facing slopes were dated (Figure 1.6). Charcoal samples from north-facing catchments also exhibited more overlapping (i.e. possibly concurrent) age distributions from different catchments.

The alluvial fan in south-facing Catchment 12 aggraded earlier than the other fans, and its aggradation trend is quite linear (Figure 1.4a). If it were a relict, abandoned alluvial surface, this could yield erroneously low aggradation rates if averaged over the time period of inactivity. The Catchment 12 aggradation trend was extrapolated to intersect the age axis, yielding a possible time of abandonment between ~5,100 and 5,300 cal yr BP, based on the average error of the samples defining the trend. The aggradation trend from Catchment 12 was used to limit aggradation rate calculations to the time period of fan activity, and the minimum and maximum ranges were propagated as errors. Aggradation trends for the rest of the fans appear to intersect the origin (i.e. modern time), so we did not perform abandonment corrections for these fans.

The reconstructed surface areas of alluvial fans ranged from 301 to 2,124 m<sup>2</sup>, with average values of 1,082 and 1,849 m<sup>2</sup> for north- and south-facing catchments, respectively (Table 1.2). Extrapolating the aggradation rates across the fan surface areas yielded volumetric fan deposition rates ranging from 0.17 to 2.58 m<sup>3</sup>/yr. Average deposition rates for north-facing slopes (0.66 m<sup>3</sup>/yr) are lower than those for south-facing slopes (1.60 m<sup>3</sup>/yr).

The source catchment surface areas for north-facing slopes are also lower than for south-facing catchments: north-facing catchments were ~94,000 m<sup>2</sup>, on average, while south-facing catchments were ~201,000 m<sup>2</sup> (Table 1.3). Since both fan and catchment

surface areas were greater on south-facing valley sides, normalizing by source catchment areas counteracted their larger fans (e.g. larger catchments naturally produce larger fans).

Catchment-averaged land surface denudation rates varied by nearly an order of magnitude (Figure 1.4b; Table 1.3), ranging from 0.25 to 1.54 cm/ka for north-facing catchments (0.77 cm/ka average), and 0.63 to 1.47 for south-facing catchments (1.01 cm/ka average). Individual fan aggradation and catchment denudation rates vary within aspect groupings, and the variability increased with each step of the calculation (Figure 1.7). Much of the differences in average erosion and deposition values with aspect are due to the inclusion of the Catchment 11 values, which records a single large event within a relatively short time frame (i.e. within the last 1,000 years). The increase in variability through the calculations is primarily due to variability in the surface areas of both the fans and catchments.

The minimum sediment yields for individual debris flow and sheetflooding events, constrained by samples of similar age at different depths, ranged from 2,170 to 6,835 Mg/km<sup>2</sup> yr (Table 1.4). The average of the three values for north-facing slopes was 4,890 Mg/km<sup>2</sup>yr, whereas the lone value for south-facing slopes was 3,140 Mg/km<sup>2</sup>.

## **1.6 Discussion**

### **1.6.1 Regional Synthesis of Erosion Rates and Sediment Yields**

Inferred erosion rates in the Dry Creek Experimental Watershed are comparable to, but lower than erosion rates measured in the interior Idaho batholith (Figure 1.8).

Lower rates of erosion may be explained by 1) lower rates of uplift, and 2) lack of drainage integration during the late Miocene. Erosion rates are generally thought to keep pace with uplift over  $>10^5$  year timescales (Reiners and Brandon, 2006). Longer

timescale ( $10^7$  year) land surface lowering rates in the *interior* Idaho batholith, inferred from apatite fission-track uplift rates, are  $\sim 20$  cm/ka (Sweetkind and Blackwell, 1989; Meyer and Pierce, 2003). Offset of dated volcanic strata in the foothills containing the DCEW (Clemens, 1993) suggest that the *margin* of the Idaho batholith has experienced slower uplift rates of  $\sim 2$  cm/ka, on average during the last  $\sim 10$  Ma.

Changes in base level associated with drainage incision alter landscape relief and can also affect land surface lowering rates. The Boise River, which serves as a local base level for the DCEW study area, has only been hydrologically connected to sea level for  $\sim 1.5$  Ma and drained to the internally drained 'Lake Idaho' from  $\sim 12$ - $1.5$  Ma. The DCEW foothills may have eroded more slowly prior to capture of Lake Idaho and integration with the greater Columbia River drainage network. The Boise River, located at the base of the Boise foothills and the DCEW watershed incised episodically beginning around  $\sim 1.5$  Ma (Othberg, 1994) producing a flight of terraces which effectively record base level lowering for tributary drainages of the Boise River, including Dry Creek. Near Dry Creek's confluence with the Boise River, the river has incised  $\sim 50$  m vertically from a  $0.974 \pm 0.098$  Ma old terrace (Othberg and Stanford, 1992). This constrains the time-averaged incision rate of the Boise River to  $\sim 5$  cm/ka over the last  $\sim 1$  Ma, which is more than double the  $\sim 2$  cm/ka uplift rates over the last  $\sim 10$  Ma (Clemens, 1993). This suggests that base level fall has exerted a stronger control on erosion during the last million years in the Boise foothills. Drainage incision may be accelerated while the landscape catches up with uplift that occurred while the area drained to a local base level.

Incision of the South Fork Payette River,  $\sim 50$  km northeast of Dry Creek within the interior of the Idaho batholith, has also outpaced uplift, with time-averaged incision

rates of ~90 cm/ka over 7 ka timescales (Pierce et al. 2011) compared to uplift rates of only ~20 cm/ka (Sweetkind and Blackwell, 1989; Meyer and Pierce, 2003). Likewise, post-glacial incision rates for the Middle Fork Salmon River in the interior Idaho batholith were ~80 cm/ka (Meyer and Leidecker, 1999). Based upon a late Pleistocene terrace, however, the Boise River only incised by 15 cm/ka over ~20 ka timescales. River incision in the interior Idaho batholith greatly outpaced river incision of the Boise River.

Modern sediment yields in the interior of the Idaho Batholith, measured from sediment trapping and gaging in the absence of large events, are ~9 Mg/km<sup>2</sup>yr (Figure 1.8; Megahan and Kidd, 1972; Clayton et al., 1979; Clayton and Megahan, 1986). Sediment yields over 10<sup>3</sup> to 10<sup>4</sup> timescales measured from cosmogenic samples in the interior Idaho Batholith average 112 Mg/km<sup>2</sup>yr (Kirchner et al., 2001). Following a rain-on-snow event in 1997, individual large debris flow events, measured from ~0.5 km<sup>2</sup> basins along the South Fork Payette River, provide by far the largest inputs of sediment (~43,000 Mg/km<sup>2</sup>yr ; Meyer et al., 2001; Meyer and Pierce, 2003). These large events are offset by intervals of quiescence; between 7400-6600 cal yr B.P., small sheetflood events only contributed ~16 Mg/km<sup>2</sup>yr to South Fork Payette alluvial fans (Meyer and Pierce, 2003).

Time averaged sediment yields from the small catchments within the Dry Creek Experimental Watershed (DCEW) range from ~3 to 29 Mg/km<sup>2</sup>yr, over ~0.5 to 8 ka timescales, which are of similar magnitude to with sediment yields of ~16 Mg/km<sup>2</sup>yr, over 1 ka, measured by Meyer et al. (2001) for the South Fork Payette River (Figure 1.8). However, the sediment yields for individual events from the DCEW record (~4,000 Mg/km<sup>2</sup>yr, on average; Table 1.4) are up to an order of magnitude lower than individual

events for similar-sized basins along the South Fork Payette (~43,000 Mg/km<sup>2</sup>yr; Figure 1.8). This is possibly because the sediment yields from this study represent the minimum values that could be constrained based on sample depths within the stratigraphy (i.e. they could not be constrained by deposit boundaries), and deposit thickness probably exceeded those constrained by sample positions and ages. However, it seems unlikely, given the observed trends between depth and age, that we underestimated deposit thicknesses by an order of magnitude; often, the fans were not large enough to contain an order of magnitude more sediment. Given the lower regional rates of uplift and incision in the DCEW compared to the South Fork Payette system, as well as the smaller size and higher position of the catchments in the watershed, it makes sense that the catchments have lower sediment yields and erosion rates.

#### 1.6.2 How Do Erosive Processes Vary with Aspect?

South-facing catchments in the DCEW are markedly bigger, less steep, and have more well-developed drainages than opposing north-facing catchments (Poulos et al., 2013; Chapter 3). Logically, it follows that more material eroded from south-facing basins, and they should therefore have higher erosion rates. However, despite dramatic aspect-related differences in land surface characteristics, Holocene erosion rates did not differ significantly between north and south-facing catchments. Although we observed slightly higher average erosion rates for south-facing slopes (Table 1.3), there is also substantial variability within each aspect grouping (Figure 1.7c). The observed differences in catchment-averaged denudation are largely due to south-facing catchment 11, which exhibited a much higher denudation rate.

Alluvial fan aggradation rates for 2 of the 3 south-facing catchments were similar to north-facing catchments. The similarity of aggradation rates among fans may indicate a common control on fan aggradation (e.g. episodic channel incision following base level fall). The exception was Catchment 11, which had a higher aggradation rate, likely because the fan record spans less than 1,000 cal yr BP and contains a relatively large event. Fan aggradation appears to be relatively constant over timescales greater than a thousand years (linearity of trends, Figure 1.4a). An estimated episodic deposition event recurrence interval of 200-600 years suggests that erosion rates measured over thousands of years may effectively average out the episodic nature of erosional processes in steep, mountainous, soil-mantled terrain, and perhaps explains why many of the longer time-scale fan-aggradation trends are linear.

Despite similar aggradation rates, volumetric deposition rates were higher on average for south-facing catchments, due primarily to larger fans; Catchment 11 had both a higher aggradation rate and fan size (Table 1.2). However, the south-facing valley sides also generally have larger catchments, which normalize and reduce catchment-averaged denudation rates. Catchment 11 specifically had a much larger drainage area, but also produced a bigger fan.

Differences in denudation rates for aspect groupings might be more apparent with more samples and catchments, which could reveal statistically distinct erosion rate populations. Variability within aspect groupings might also be lower if erosional time-series were measured over similar and/or longer time scales. The variability within aspect groupings might also reflect the episodic nature of fire-related erosion; the timescales of

measurement and number of events recorded may differ among the alluvial fans, and their record may not have spanned a sufficient timescale to average out episodicity.

### 1.6.3 Relationships Among Fire, Slope Aspect, and Erosion

Fire is a primary driver of erosion in mountainous central Idaho, and differences in fire timing and severity with aspect may have significant effects on erosion rates and processes (Meyer and Pierce, 2003; Pierce et al., 2004; Riley et al., 2015). The trigger for many observed erosional events in the region is fire, based on the presence of charcoal and other characteristics of fire-related deposits (e.g. Meyer et al., 1995; Riley et al., 2015). It is logical that fire might influence asymmetry development: erosion is induced by fire → fire is sensitive to climate → local climate varies with aspect → aspect may modify fire-related erosion. Since the frequency and severity of fire changes with vegetation, and vegetation varies notably with aspect-induced microclimate, it follows that the frequency and severity of erosional events should also vary with aspect. In DCEW, fire return intervals may vary from ~300-400 years for stand-replacing fires in north-facing conifer ecosystems (Heyerdahl et al., 2008; Riley et al., 2015), to 10-200 years for dry south-facing Ponderosa sites or cheatgrass-infested sites (Miller and Tausch, 2001; Baker, 2006).

Time-averaged erosion rates are strongly influenced by the yields and recurrence intervals of individual episodic events (e.g. Kirchner et al., 2001; Meyer and Pierce, 2003). A recurrence interval of 200-600 years for the four individual events is necessary to produce the observed Holocene-average erosion rates for the DCEW catchments. Large erosional responses to fire (e.g. debris flows) occur less frequently than fire, requiring a cloud burst storm or a rain-on-snow event in order to exceed infiltration rates,

saturate soils, and/or produce overland flow (Meyer and Wells, 1997; Cannon et al., 2001; Cannon et al., 2008; Welcker, 2011). Depletion of stored sediment, which requires time to accumulate, may also require a recovery time before mass wasting can occur again. In 1959 in the Boise Foothills, a severe range fire, followed by a summer convective storm, produced sediment-charged floods and muddy debris flows that inundated city streets and removed large amounts of sediment from the foothills (Thomas, 1963). While the relative sediment contribution from north vs. south aspects due to this event has not been assessed, it demonstrates that basins in DCEW are very erosional responsive to fire.

Charcoal ages suggest fires burned on both northern (n=5) and southern (n=3) aspects ~1,000-500 cal yr BP (Figure 1.6). Fires burned on both aspects ~900-700 cal yr BP during the Medieval Climate Anomaly (Cook et al., 2004), but fires were not synchronous between north and south-facing slopes during other intervals. The variable and dry climatic conditions of the Medieval Climate Anomaly (Meyer et al., 1995; Cook et al., 2004; Pierce et al., 2004) promoted fire throughout a range of ecosystems, including high-elevation, moist coniferous forests and drier open forests and sagebrush steppe ecosystems. During the generally cooler Little Ice Age (Luckman, 2000), fires generally burned more frequently, but less severely, in drier forests and sagebrush-steppe (Pierce et al., 2004; Heyerdahl et al., 2008; Nelson and Pierce, 2010; Weppner et al., 2013; Riley et al., 2015) but did not typically burn in high-elevation forests (Meyer et al., 1995). Many of the charcoal ages lie within the primary periods of fire activity highlighted by Nelson and Pierce (2010) in the Wood Creek watershed, which is ~30 km

southeast and has similar vegetation, elevation, lithology, and topographic position (Figure 1.6).

Differences in charcoal ages for north and south-facing slopes during much of the record generally support the notion that aspect-induced microclimate influences the timing and frequency of fire, and associated erosion, in this environment. However, differences in charcoal abundance may also reflect differences in vegetation and processes. The relative scarcity of charcoal in south-facing slopes may be related to the lower chance of preservation for non-woody charcoal (e.g. grasses and leaves) and smaller-stem-diameter shrubs, compared to forested areas (Riley et al., 2015). Additionally, charcoal is less likely to be preserved in sheetflood deposits than in more-poorly sorted debris flows, because it floats and may not be deposited with sediment (Weppner et al., 2013; Riley et al., 2015).

Within the nearby Salmon River watershed, which is also underlain by the Idaho Batholith, Riley et al. (2015) found that higher and lower elevation regions appeared to burn at different times, which they attribute to how Holocene changes in climate act in concert with differences in fuel type and abundance, and plant water stress, with elevation. Low elevation areas appeared to burn less severely, but yielded frequent sheetfloods. Conversely, high-elevation areas burned less frequently but produced relatively large debris flows. North-facing slopes in the DCEW are similar in vegetation cover and cooler temperatures to higher elevations in the Salmon River watershed, whereas south-facing slopes are more similar to lower elevations. The generally coarser-grained, better-sorted deposits for both south-facing catchments in the DCEW and lower elevations in Salmon watershed suggest that runoff-related processes may be more

effective in more arid environments. Conversely, larger fire-related debris flows from both north-facing catchments in the DCEW and higher elevations in the Salmon watershed contribute infrequent but large (Table 1.4) volumes of sediment to alluvial fans.

Sparser vegetation cover on south-facing slopes both reduces fire severity and reduces resistance to erosion, which could deplete locally stored sediment (i.e. soil and regolith thickness) available for remobilization by fire-induced debris flows and decrease event magnitude. In contrast, the denser and deeper-rooted vegetation on north-facing slopes stabilizes the land surface at steeper angles, and reduces non-fire-related erosion rates and sediment storage during inter-fire periods. However, increased soil and root cohesion of north-facing slopes promotes soil retention and thickening on steeper slopes, which makes them more susceptible to debris flows initiated by shallow landslides, which are triggered by the relatively rare combination of severe fire followed by rapid saturation (e.g. rain-on-snow and convective summer thunderstorms).

In the DCEW, the erosional magnitude and processes of individual events likely vary between north and south-facing slopes over short timescales (e.g. following disturbance or extreme climatic events), but varying frequencies and magnitudes of erosional response may produce similar time-averaged rates. For example, although vegetation stabilization and reduced runoff efficacy may inhibit erosion on north-facing slopes between events, increased soil storage and steeper slopes likely leads to a larger erosional response following fire and storms.

#### 1.6.4 Aspect-Related Implications

It is surprising that erosion rates did not differ substantially between north and south-facing catchments, given the dramatic differences in gradients, vegetation cover, and landforms (Figures 1.1 and 1.2). Could the DCEW valleys be approaching, or near, steady state (i.e. dynamic equilibrium) conditions, where land surfaces erode at similar rates throughout a watershed, and landforms are relatively static through time?

It is possible that erosion rates did vary with aspect during the Holocene but that these differences are not reflected within the alluvial fans. Erosion recorded in alluvial fans may be biased by aspect-related differences in erosional and depositional processes. For example, if as our observations suggest, channelized flow is more common on south-facing slopes, fans for south-facing slopes might be 'leakier'; fine sediment and charcoal suspended by fluvial processes, rather than mass wasting, is more likely to be transported downstream, rather than being deposited within alluvial fans. Additionally, channels may incise into fans and be filled by subsequent deposition (i.e. cut-and-fill cycles), yielding an apparently intact fan, in which case our method would underestimate sediment yields. Thus, more active fluvial processes on south-facing slopes may produce biased erosion rates. Regardless, the lack of substantial differences in apparent erosion with aspect is surprising given the dramatic variability in landforms and land cover.

If Holocene erosion rates are indeed similar, aspect-related differences in catchment morphology and valley asymmetry may be relict features reflecting pre-Holocene influences, such as glacial climates (e.g. Istanbuluoglu et al., 2008; McGuire et al., 2014). This is reinforced logically by the observations that the Holocene alluvial fans are two orders of magnitude smaller in surface area than their catchments (Tables 1.2 and

1.3). The amount of geomorphic work performed during the Holocene could not possibly have produced the tens to hundreds of meters of differences in land surface length observed. The Holocene alluvial fans simply do not represent a large enough eroded volume to produce the observed differences in catchment morphology, which have been evolving over  $10^6$  year timescales.

In a related study, West et al. (2014) used meteoric  $^{10}\text{Be}$  to compare erosion rates between north-facing and south-facing slopes in the Susquehanna Shale Hills CZO, but found that regolith flux was similar among north and south-facing hillslopes, despite varying gradients, landforms, vegetation and soils. West et al. (2014) conclude that south-facing slopes have higher transport efficiency, because they transport the same amount of material despite a lower gradient. The lack of differences in erosion rates with aspect, despite differences in transport efficiency, landforms, and vegetation cover, suggests that this landscape also may have had time to adjust to, and counteract, erosion rate differences (i.e. approach steady-state equilibrium).

Aspect-induced valley asymmetry likely develops when a geomorphic system is far from dynamic equilibrium (e.g. steady state), such as during initial valley incision or following episodic changes in climate and vegetation, when valleys must adjust to equalize erosion on opposite valley sides (Figure 1.10). Initially, aspect-induced ecohydrologic feedbacks may cause differences in erosion, but more quickly eroding areas naturally degrade faster, which reduces gradients and serves as a negative feedback that slows the erosion rates. Valley asymmetry is clearly the result of asymmetric degradation, but asymmetric degradation likely counteracts asymmetric erosion and drives valley evolution towards dynamic equilibrium (Figure 1.10).

In more mature landscapes, valley asymmetry may be a relict feature that developed and reached equilibrium long ago, and asymmetry may not have developed significantly over the  $\sim 10^3$  to  $10^5$  year timescale limitations of erosion rate measurements. The landscape that the DCEW lies within has been evolving for over  $10^7$  years (Clemens, 1993), and the Appalachian landscape where the Shale Hills CZO (e.g. West et al., 2014) is located has been evolving for over  $10^8$  years (Matmon et al., 2003). If aspect-induced valley asymmetry develops as an initial system response, it makes sense that it may not be actively developing, and erosion rates will be similar among north and south-facing valley sides after valley asymmetry development nears dynamic equilibrium.

Some landscapes exhibit differences in erosion with aspect, and may be valuable for studying active valley asymmetry development. Erosion rates measured over  $\sim 5$ -100 ka timescales using in-situ and meteoric  $^{10}\text{Be}$  in Gordon Gulch (Boulder CZO), in the Colorado front range of western North America, were  $\sim 1.5$  times greater for a south-facing slope than a north-facing slope (Foster et al, 2015), which is surprising because the Colorado Front Range has been evolving for over  $10^7$  years ( $\sim 40$ -70 Ma; Kelly and Chapin, 2004). The differences in erosion rates with aspect in Gordon Gulch (Foster et al., 2015) do not support the hypothesis that more mature landscapes will have steady-state asymmetry, but the other factors involved may complicate this scenario. Foster et al. (2015) note that the north-facing slope on which erosion was measured is depositional at its foot-slope and disconnected from the stream by a narrow terrace, which could reduce erosion rates, but this effect could be transient over the timescales of erosion measurement. Importantly, the relief of the south-facing slope in Gordon Gulch is  $\sim 2.75$

times greater than the north-facing slopes, which could be a non-climatic influence of land surface lowering rates (i.e. higher relief slopes could simply erode more quickly).

Unfortunately, current methods for measuring hillslope erosion rates typically span <100 ka, which may not capture the longer timescale differences in erosion that produce valley asymmetry. Rates of 1 to 4 cm/ka equate to only 30 to 120 cm of land surface lowering over 30 ka, whereas hillslopes in asymmetric valleys often differ in length and relief by tens to hundreds of meters. As such, current methods for measuring erosion rates fundamentally limit our ability to assess how aspect-induced asymmetry develops. Longer-term metrics of erosion suitable for hillslope and valley scale analyses would aid in understanding how asymmetry develops.

### **1.7 Conclusions**

Radiocarbon dating of alluvial fan deposits coupled with high-resolution fan surface reconstruction and catchment delineation, yielded reasonable estimates of fan aggradation rates and catchment-averaged denudation rates in the Dry Creek Experimental Watershed. These methods are applicable to small, steep first order catchments where episodic accelerated erosion following disturbance (e.g. fire) accounts for a majority of the sediment budget, and fluvial processes that tend to erode deposits are relatively inactive. North and south-facing catchments have eroded and evolved differently, which is evident from differences in landforms and gradients, yet Holocene-averaged erosion rates were not significantly different between north and south-facing catchments. If erosion rates truly are not significantly different between north and south-facing valley sides, this implies that 1) valley asymmetry was not actively developing

over Holocene timescales, and/or 2) valley asymmetry may have developed over longer or different timescales than those over which we measured erosion.

We propose that greater overall degradation of south-facing valley sides reduces their gradients and erosional potential, which serves as a negative feedback that drives the system towards a dynamic equilibrium where both valley sides erode at similar rates (i.e. a local steady state). Despite aspect-related differences in erosional processes, event frequency and magnitude appear to be in equilibrium; north-facing catchments produce less frequent, but more catastrophic debris flows, whereas south-facing catchments produce more frequent, but less severe sheetfloods, resulting in similar time-averaged erosion rates. If valley asymmetry development truly counteracts aspect-induced differences in erosion, the degree of valley asymmetry may be a useful metric for remotely assessing the proximity of landscapes to dynamic equilibrium.

## 1.8 References

- Aishlin, P., & McNamara, J. P. (2011). Bedrock infiltration and mountain block recharge accounting using chloride mass balance. *Hydrological Processes*, 25(12), 1934-1948.
- Anderson, B. T., McNamara, J. P., Marshall, H. P., & Flores, A. N. (2014). Insights into the physical processes controlling correlations between snow distribution and terrain properties. *Water Resources Research*, 50(6), 4545-4563.
- Armstrong, R. L., Taubeneck, W. H., & Hales, P. O. (1977). Rb-Sr and K-Ar geochronometry of Mesozoic granitic rocks and their Sr isotopic composition, Oregon, Washington, and Idaho. *Geological Society of America Bulletin*, 88(3), 397-411.
- Baker, W. L. (2006). Fire and restoration of sagebrush ecosystems. *Wildlife Society Bulletin*, 34(1), 177-185.
- Benda, L., Miller, D., Bigelow, P., & Andras, K. (2003). Effects of post-wildfire erosion on channel environments, Boise River, Idaho. *Forest Ecology and Management*, 178(1), 105-119.
- Blair, T. C., & McPherson, J. G. (1994). Alluvial fans and their natural distinction from rivers based on morphology, hydraulic processes, sedimentary processes, and facies assemblages. *Journal of sedimentary research*, 64(3).
- Burnett, B. N., Meyer, G. A., & McFadden, L. D. (2008). Aspect-related microclimatic influences on slope forms and processes, northeastern Arizona. *Journal of Geophysical Research: Earth Surface* (2003–2012), 113(F3).
- Cannon, S. H. (2001). Debris-flow generation from recently burned watersheds. *Environmental & Engineering Geoscience*, 7(4), 321-341.
- Cannon, S. H., Gartner, J. E., Wilson, R. C., Bowers, J. C., & Laber, J. L. (2008). Storm rainfall conditions for floods and debris flows from recently burned areas in southwestern Colorado and southern California. *Geomorphology*, 96(3), 250-269.

- Clayton, J. L., & Megahan, W. F. (1986). Erosional and chemical denudation rates in the southwestern Idaho batholith. *Earth Surface Processes and Landforms*, 11(4), 389-400.
- Clayton, J. L., Megahan, W. F., & Hampton, D. (1979). Soil and bedrock properties: Weathering and alteration products and processes in the Idaho Batholith (Vol. 237). Dept. of Agriculture, Forest Service, Intermountain Forest and Range Experiment Station.
- Clemens, D. M. (1993). Tectonics and Silicic Volcanic Stratigraphy of the Western Snake River Plain, Southwestern Idaho (Master's thesis, Arizona State University)
- Cook, E. R., Woodhouse, C. A., Eakin, C. M., Meko, D. M., & Stahle, D. W. (2004). Long-term aridity changes in the western United States. *Science*, 306(5698), 1015-1018.
- Criss, R. E., Lanphere, M. A., & Taylor, H. P. (1982). Effects of regional uplift, deformation, and meteoric-hydrothermal metamorphism on K-Ar Ages of biotites in the southern half of the Idaho batholith. *Journal of Geophysical Research: Solid Earth*, 87(B8), 7029-7046.
- Denny, C. S. (1967). Fans and pediments. *American Journal of Science*, 265(2), 81-105.
- Dohrenwend, J. C. (1978). Systematic valley asymmetry in the central California Coast Ranges. *Geological Society of America Bulletin*, 89(6), 891-900.
- Field, J. (2001). Channel avulsion on alluvial fans in southern Arizona. *Geomorphology*, 37(1), 93-104.
- Fitch, E. P., & Meyer, G. A. (2016). Temporal and spatial climatic controls on Holocene fire-related erosion and sedimentation, Jemez Mountains, New Mexico. *Quaternary Research*, 85(1), 75-86.
- Foster, M. A., Anderson, R. S., Wyshnytzky, C. E., Ouimet, W. B., & Dethier, D. P. (2015). Hillslope lowering rates and mobile-regolith residence times from in situ and meteoric <sup>10</sup>Be analysis, Boulder Creek Critical Zone Observatory, Colorado. *Geological Society of America Bulletin*, B31115-1.

- Garrote, J., Cox, R. T., Swann, C., & Ellis, M. (2006). Tectonic geomorphology of the southeastern Mississippi Embayment in northern Mississippi, USA. *Geological Society of America Bulletin*, 118(9-10), 1160-1170.
- Gavin, D. G. (2001). Estimation of inbuilt age in radiocarbon ages of soil charcoal for fire history studies. *Radiocarbon*, 43(1), 27-44.
- Geroy, I. J., Gribb, M. M., Marshall, H. P., Chandler, D. G., Benner, S. G., & McNamara, J. P. (2011). Aspect influences on soil water retention and storage. *Hydrological Processes*, 25(25), 3836-3842.
- Gilbert, G. K. (1904). Systematic asymmetry of crest lines in the High Sierra of California. *The Journal of Geology*, 12(7), 579-588.
- Gutiérrez-Jurado, H. A., Vivoni, E. R., Istanbuluoglu, E., & Bras, R. L. (2007). Ecohydrological response to a geomorphically significant flood event in a semiarid catchment with contrasting ecosystems. *Geophysical Research Letters*, 34(24).
- Hack, J. T., & Goodlett, J. C. (1960). *Geomorphology and forest ecology of a mountain region in the central Appalachians* (No. 347). United States Government Printing Office.
- Heimsath, A. M., Dietrich, W. E., Nishiizumi, K., & Finkel, R. C. (1999). Cosmogenic nuclides, topography, and the spatial variation of soil depth. *Geomorphology*, 27(1), 151-172.
- Heyerdahl, E. K., Morgan, P., & Riser, J. P. (2008). Multi-season climate synchronized historical fires in dry forests (1650-1900), northern Rockies, USA. *Ecology*, 89(3), 705-716.
- Istanbuluoglu, E., Yetemen, O., Vivoni, E. R., Gutiérrez-Jurado, H. A., & Bras, R. L. (2008). Eco-geomorphic implications of hillslope aspect: Inferences from analysis of landscape morphology in central New Mexico. *Geophysical Research Letters*, 35(14).

- Kelley, S. A., & Chapin, C. E. (2004). Denudation history and internal structure of the Front Range and Wet Mountains, Colorado, based on apatite-fission-track thermochronology. *Tectonics, Geochronology and Volcanism in the Southern Rocky Mountains and Rio Grande Rift: Socorro, New Mexico, New Mexico Bureau of Geology and Mineral Resources Bulletin*, 160, 41-78.
- Kirchner, J. W., Finkel, R. C., Riebe, C. S., Granger, D. E., Clayton, J. L., King, J. G., & Megahan, W. F. (2001). Mountain erosion over 10 yr, 10 ky, and 10 my time scales. *Geology*, 29(7), 591-594.
- Kormos, P. R., McNamara, J. P., Seyfried, M. S., Marshall, H. P., Marks, D., & Flores, A. N. (2015). Bedrock infiltration estimates from a catchment water storage-based modeling approach in the rain snow transition zone. *Journal of Hydrology*, 525, 231-248.
- Kunkel, M. L., Flores, A. N., Smith, T. J., McNamara, J. P., & Benner, S. G. (2011). A simplified approach for estimating soil carbon and nitrogen stocks in semi-arid complex terrain. *Geoderma*, 165(1), 1-11.
- Loughridge, R. (2014). Identifying Topographic Controls of Terrestrial Vegetation Using Remote Sensing Data in a Semiarid Mountain Watershed, Idaho, USA. (Master's thesis, Boise State University)
- Luckman, B. H. (2000). The little ice age in the Canadian Rockies. *Geomorphology*, 32(3), 357-384.
- Matmon, A., Bierman, P. R., Larsen, J., Southworth, S., Pavich, M., & Caffee, M. (2003). Temporally and spatially uniform rates of erosion in the southern Appalachian Great Smoky Mountains. *Geology*, 31(2), 155-158.
- McGuire, L. A., Pelletier, J. D., & Roering, J. J. (2014). Development of topographic asymmetry: Insights from dated cinder cones in the western United States. *Journal of Geophysical Research: Earth Surface*, 119(8), 1725-1750.
- McNamara, J. P., Chandler, D., Seyfried, M., & Achet, S. (2005). Soil moisture states, lateral flow, and streamflow generation in a semi-arid, snowmelt-driven catchment. *Hydrological Processes*, 19(20), 4023-4038.

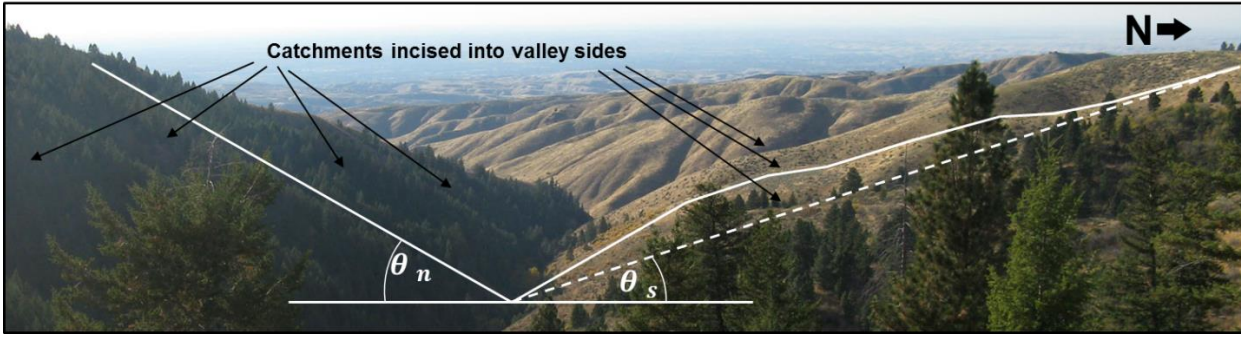
- Megahan, W. F., & Kidd, W. J. (1972). Effects of logging and logging roads on erosion and sediment deposition from steep terrain. *Journal of Forestry*, 70(3), 136-141.
- Melton, M. A. (1960). Intravalley variation in slope angles related to microclimate and erosional environment. *Geological Society of America Bulletin*, 71(2), 133-144.
- Meyer, G. A., Wells, S. G., & Jull, A. T. (1995). Fire and alluvial chronology in Yellowstone National Park: climatic and intrinsic controls on Holocene geomorphic processes. *Geological Society of America Bulletin*, 107(10), 1211-1230.
- Meyer, G. A., & Wells, S. G. (1997). Fire-related sedimentation events on alluvial fans, Yellowstone National Park, USA. *Journal of Sedimentary Research*, 67(5).
- Meyer, G. A., & Leidecker, M. E. (1999). Fluvial terraces along the Middle Fork Salmon River, Idaho, and their relation to glaciation, landslide dams, and incision rates: A preliminary analysis and river-mile guide. *Guidebook to the Geology of Eastern Idaho*. Pocatello (ID): Idaho Museum of Natural History, 219-235.
- Meyer, G. A., Pierce, J. L., Wood, S. H., & Jull, A. J. T. (2001). Fire, storms, and erosional events in the Idaho batholith. *Hydrological Processes*, 15(15), 3025-3038.
- Meyer, G. A., & Pierce, J. L. (2003). Climatic controls on fire-induced sediment pulses in Yellowstone National Park and central Idaho: a long-term perspective. *Forest Ecology and Management*, 178(1), 89-104.
- Miller, R. F., & Tausch, R. J. (2001). The role of fire in juniper and pinyon woodlands: A descriptive analysis. In: Galley KEM and Wilson TP (eds) *Proceedings of the Invasive Species Workshop: The Role of Fire in the Control and Spread of Invasive Species*. Fire Conference 2000: the First National Congress on Fire Ecology, Prevention, and Management. Miscellaneous Publication No. 11, Tallahassee FL: Tall Timbers Research Station, 15-30.
- Niemi, N. A., Oskin, M., Burbank, D. W., Heimsath, A. M., & Gabet, E. J. (2005). Effects of bedrock landslides on cosmogenically determined erosion rates. *Earth and Planetary Science Letters*, 237(3), 480-498.

- Nelson, N. A., & Pierce, J. (2010). Late-Holocene relationships among fire, climate and vegetation in a forest-sagebrush ecotone of southwestern Idaho, USA. *The Holocene*.
- Orem, C. A., & Pelletier, J. D. (2016). The predominance of post-wildfire erosion in the long-term denudation of the Valles Caldera, New Mexico. *Journal of Geophysical Research: Earth Surface*.
- Othberg, K. L., & Stanford, L. R. (1992). Geologic map of the Boise Valley and adjoining area, Western Snake River Plain, Idaho. Idaho Geological Survey, University of Idaho.
- Othberg, K. L. (1994). Geology and geomorphology of the Boise Valley and adjoining areas, western Snake River Plain, Idaho. *Idaho Geological Survey Bulletin*, 29, 54.
- Parker, G., Paola, C., Whipple, K. X., & Mohrig, D. (1998). Alluvial fans formed by channelized fluvial and sheet flow. I: Theory. *Journal of Hydraulic Engineering*, 124(10), 985-995.
- Pierce, J. L., Meyer, G. A., & Jull, A. T. (2004). Fire-induced erosion and millennial-scale climate change in northern ponderosa pine forests. *Nature*, 432(7013), 87-90.
- Pierce, J. L., Meyer, G. A., & Rittenour, T. (2011). The relation of Holocene fluvial terraces to changes in climate and sediment supply, South Fork Payette River, Idaho. *Quaternary Science Reviews*, 30(5), 628-645.
- Poulos, M. J., Pierce, J. L., Flores, A. N., & Benner, S. G. (2012). Hillslope asymmetry maps reveal widespread, multi-scale organization. *Geophysical Research Letters*, 39(6).
- Poulos, M. J., Pierce, J. L., McNamara, J. P., Flores, A. N., & Benner, S. G. (2013). A Multi-Scale Assessment of How Topoclimate-Driven Ecohydrologic Feedbacks Impact Drainage Erosion, Incision and Expansion. In *AGU Fall Meeting Abstracts (Vol. 1, p. 0794)*.

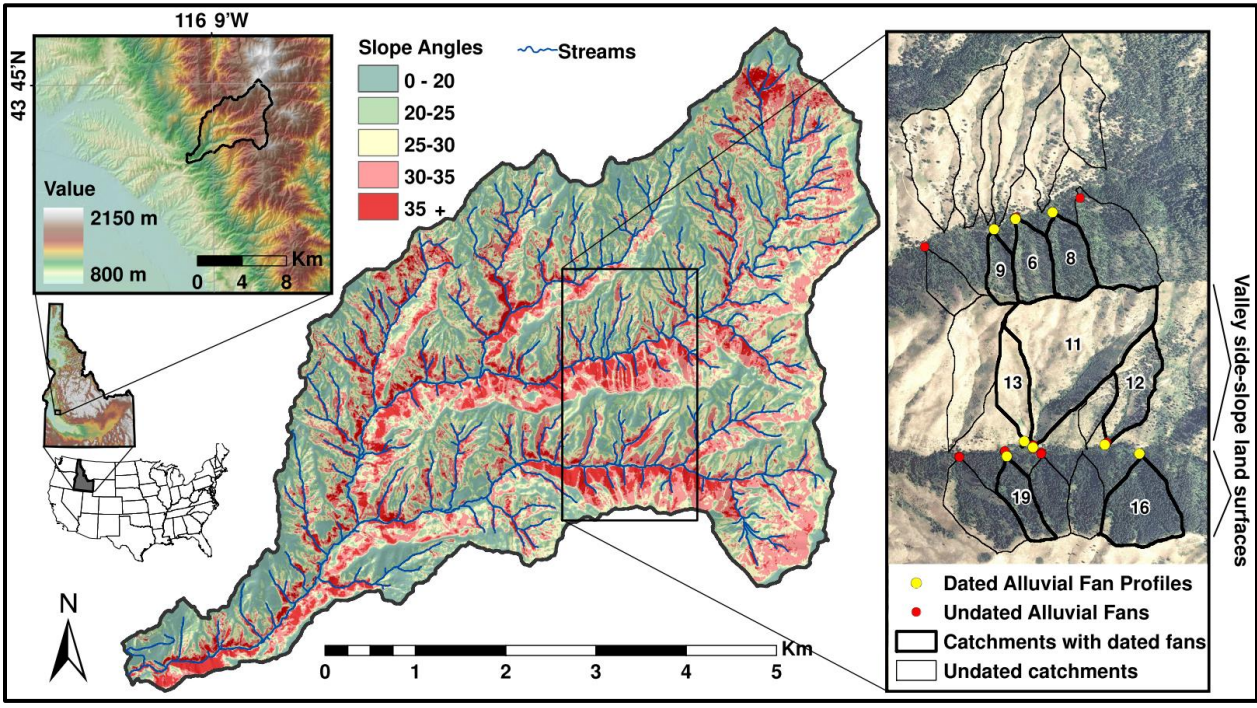
- Powell, J. W. (1874). Remarks on the structural geology of the valley of the Colorado of the West. *Washington Philosophical Society Bulletin*, 1, 48 – 51.
- Ramsey, C. B. (2009). Bayesian analysis of radiocarbon dates. *Radiocarbon*, 51(1), 337-360.
- Reiners, P. W., & Brandon, M. T. (2006). Using thermochronology to understand orogenic erosion. *Annu. Rev. Earth Planet. Sci.*, 34, 419-466.
- Riley, K. E. (2012). A 14,000-year Record of Wildfire and Alluvial Fan Deposition Reveals Relationships Among Fire, Climate, Vegetation, and Sediment Yields in the Middle Fork Salmon River, Idaho.
- Riley, K., Pierce, J., & Meyer, G. A. (2015). Vegetative and climatic controls on Holocene wildfire and erosion recorded in alluvial fans of the Middle Fork Salmon River, Idaho. *The Holocene*, 0959683615571423.
- Smith, T. J. (2010). Using Soil Moisture Trends Across Topographic Gradients to Examine Controls on Semi-arid Ecosystem Dynamics (Master's thesis, Boise State University).
- Smith, T. J., McNamara, J. P., Flores, A. N., Gribb, M. M., Aishlin, P. S., & Benner, S. G. (2011). Small soil storage capacity limits benefit of winter snowpack to upland vegetation. *Hydrological Processes*, 25(25), 3858-3865.
- Stark, B. J. (2012). Assessing Eolian Dust Inputs to Soils in Dry Creek Experimental Watershed, SW Idaho (Master's Thesis, Boise State University).
- Stuiver, M., Reimer, P.J., (1993). Extended 14C database and revised CALIB Radiocarbon Calibration Program. *Radiocarbon* 35, 215–230.
- Straccia, F. G., Wilkinson, B. H., & Smith, G. R. (1990). Miocene lacustrine algal reefs—southwestern Snake River Plain, Idaho. *Sedimentary geology*, 67(1), 7-23.
- Sweetkind, D. S., & Blackwell, D. D. (1989). Fission-track evidence of the Cenozoic thermal history of the Idaho batholith. *Tectonophysics*, 157(4), 241-250.

- Swirydczuk, K., Wilkinson, B. H., & Smith, G. R. (1979). The Pliocene Glens Ferry oolite: Lake-margin carbonate deposition in the southwestern Snake River plain. *Journal of Sedimentary Research*, 49(3).
- Telford, R. J., Heegaard, E., & Birks, H. J. (2004). The intercept is a poor estimate of a calibrated radiocarbon age. *The Holocene*, 14(2), 296-298.
- Tesfa, T. K., Tarboton, D. G., Chandler, D. G., & McNamara, J. P. (2009). Modeling soil depth from topographic and land cover attributes. *Water Resources Research*, 45(10).
- Thomas, C. A. (1963). Cloudburst Floods at Boise, Idaho, August 20, September 22, 26, 1959. United States, Department of the Interior, Geological Survey, 12 p.
- Tuck, R. (1935). Asymmetrical topography in high latitudes resulting from alpine glacial erosion. *The Journal of Geology*, 530-538.
- Welcker, C. (2011). *Bulking Debris Flow Initiation and Impacts*. (Doctoral Dissertation, University of Idaho).
- Wende, R. (1995). Drainage and valley asymmetry in the Tertiary Hills of Lower Bavaria, Germany. *Geomorphology*, 14(3), 255-265.
- Weppner, K. N., Pierce, J. L., & Betancourt, J. L. (2013). Holocene fire occurrence and alluvial responses at the leading edge of pinyon–juniper migration in the Northern Great Basin, USA. *Quaternary Research*, 80(2), 143-157.
- West, N., Kirby, E., Bierman, P., & Clarke, B. A. (2014). Aspect-dependent variations in regolith creep revealed by meteoric  $^{10}\text{Be}$ . *Geology*, 42(6), 507-510.
- Wood, S. H., Burnham, W., & Osterman, D. (1982). *Field Trip Guide to the Boise Foothills, Idaho*. Idaho Association of Professional Geologists.
- Wood, S. H., & Clemens, D. M. (2002). Geologic and tectonic history of the western Snake River Plain, Idaho and Oregon. *Tectonic and Magmatic Evolution of the Snake River Plain Volcanic Province: Idaho Geological Survey Bulletin*.

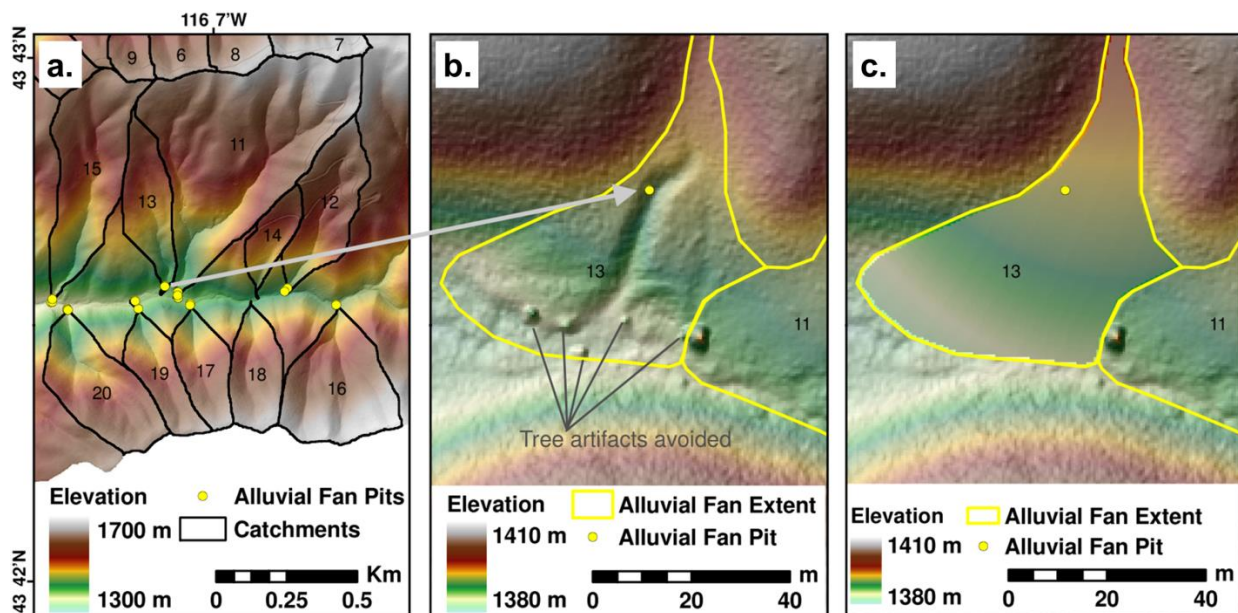
Yetemen, O., Istanbuloglu, E., Flores-Cervantes, J. H., Vivoni, E. R., & Bras, R. L. (2015). Ecohydrologic role of solar radiation on landscape evolution. *Water Resources Research*, 51(2), 1127-1157.



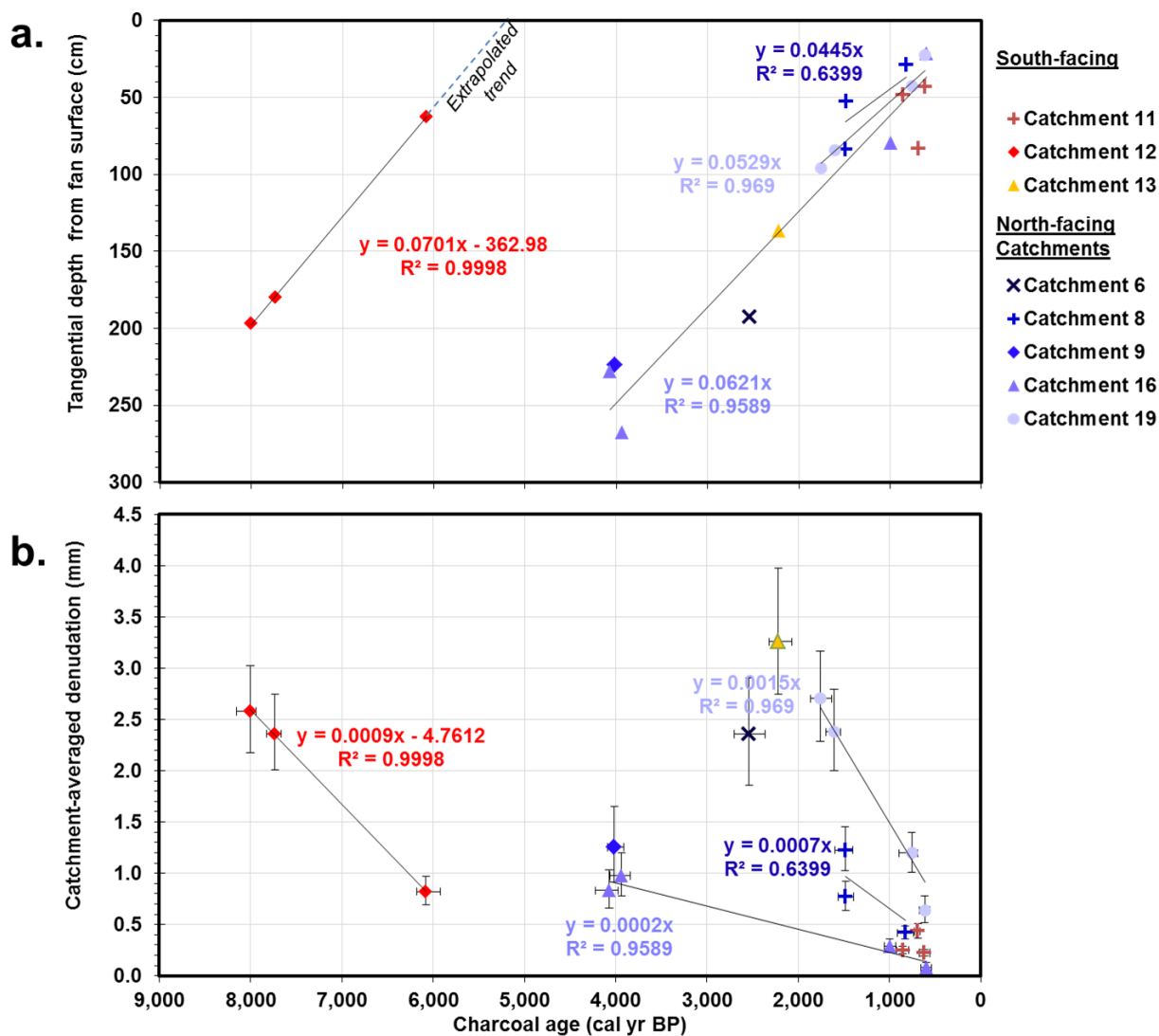
**Figure 1.1** Aspect-related variability in vegetation cover and landforms in the Dry Creek Experimental Watershed (DCEW). Note asymmetries in hillslope steepness, ridgeline linearity, land surface length, and vegetation cover.



**Figure 1.2** Location and overview of the Dry Creek Experimental Watershed (DCEW). Note steeper northern aspects, with shorter and less developed drainages. Right panel shows alluvial fan charcoal excavation sites and source catchments. Note differences in coniferous forest cover.



**Figure 1.3** Example of alluvial fan reconstruction: a.) Alluvial fan location within large valley, b.) 50 cm resolution bare-earth DEM of modern fan surface, and c.) Reconstructed fan surface bound by confining geometry.



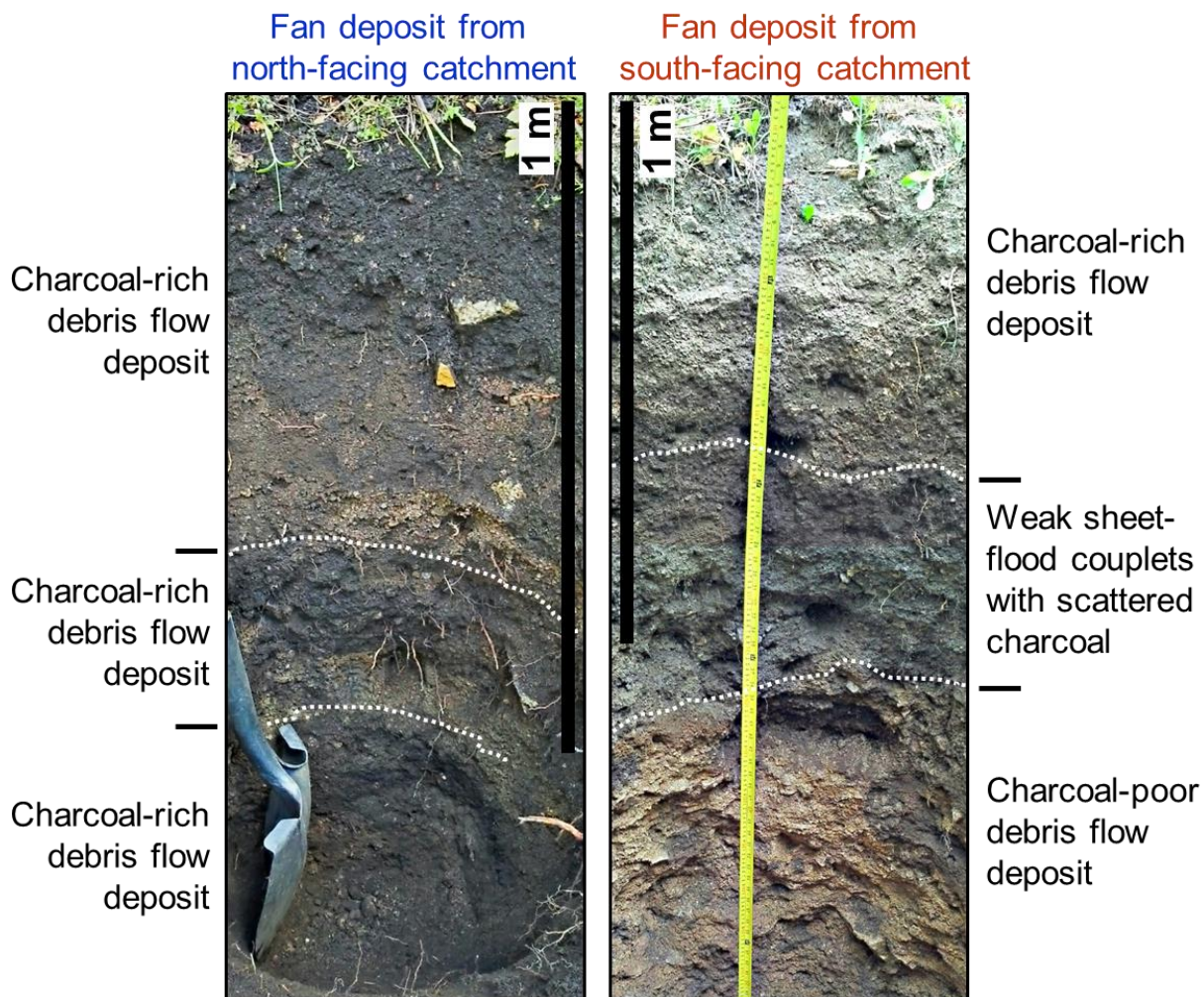


**Figure 1.5** Stratigraphic profiles of fan deposits for two fans. Most fan deposits for south-facing catchments did not exhibit distinct boundaries or stratigraphy related to processes (e.g. sheetflood couplets, large matrix-supported clasts, sediment sorting, and charcoal-rich layers etc.). Note that bottom of pit is seen obliquely in these HDR vertically-stitched photos, falsely giving the appearance of plate-like structure in the south-facing pit.

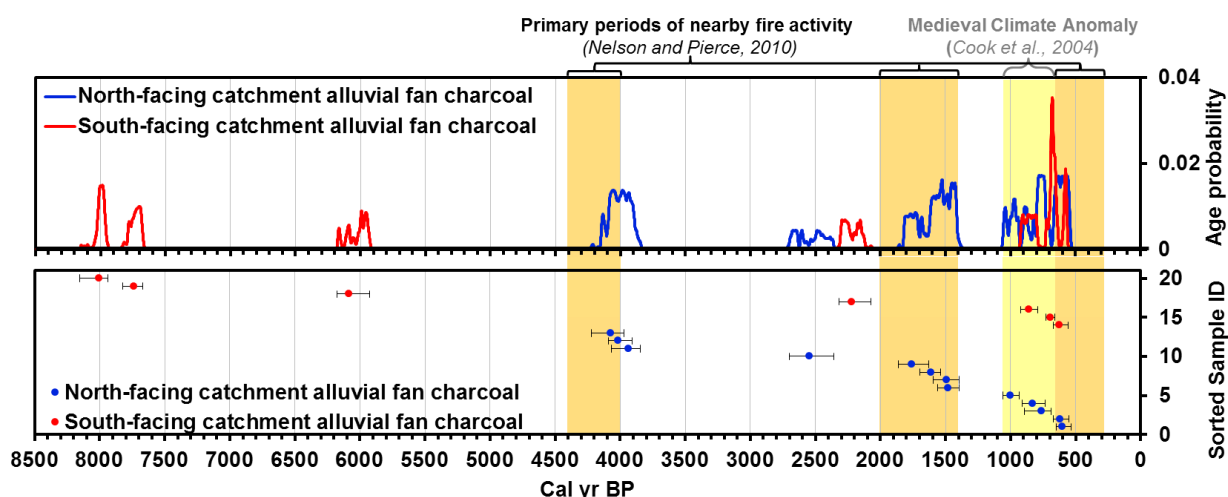


**Figure 1.6** Fire record showing the summed calibrated age probabilities (top) for charcoal from north ( $n=13$ ) and south-facing ( $n=7$ ) catchments. (bottom) samples making up each probability distribution plotted as weighted mean sample ages with 2-sigma age ranges (error bars). Vertical position on lower graph is sorted by aspect and age for display. Overlapping age distributions indicate samples are likely from the same episode of fire-related erosion, and in some cases the same deposit. The absence of samples younger than 500 cal yr BP may reflect the preference for dating of samples from deeper in the deposits in order to obtain time-averaged erosion rates.

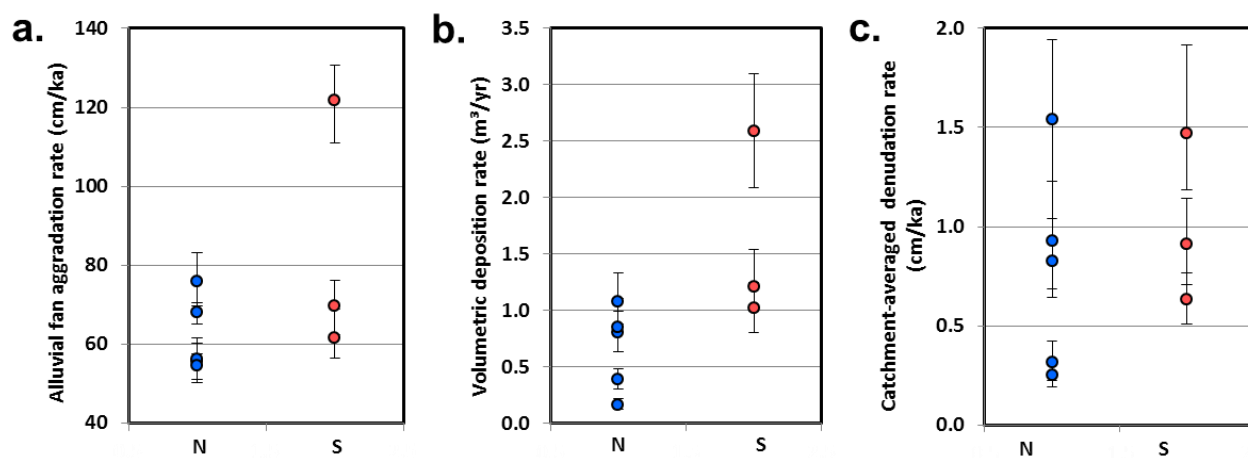


**Figure 1.7** a.) Aggradation, b.) volumetric deposition, and c.) catchment-averaged denudation rates calculated using the deepest samples for each north ( $n=5$ ) and south-facing ( $n=3$ ) catchment fan. Differences between aspects become greater for volumetric deposition because south-facing fans were larger on average, but decrease for catchment-averaged denudation rates (i.e. source-area normalized) because south-facing catchments are also larger.

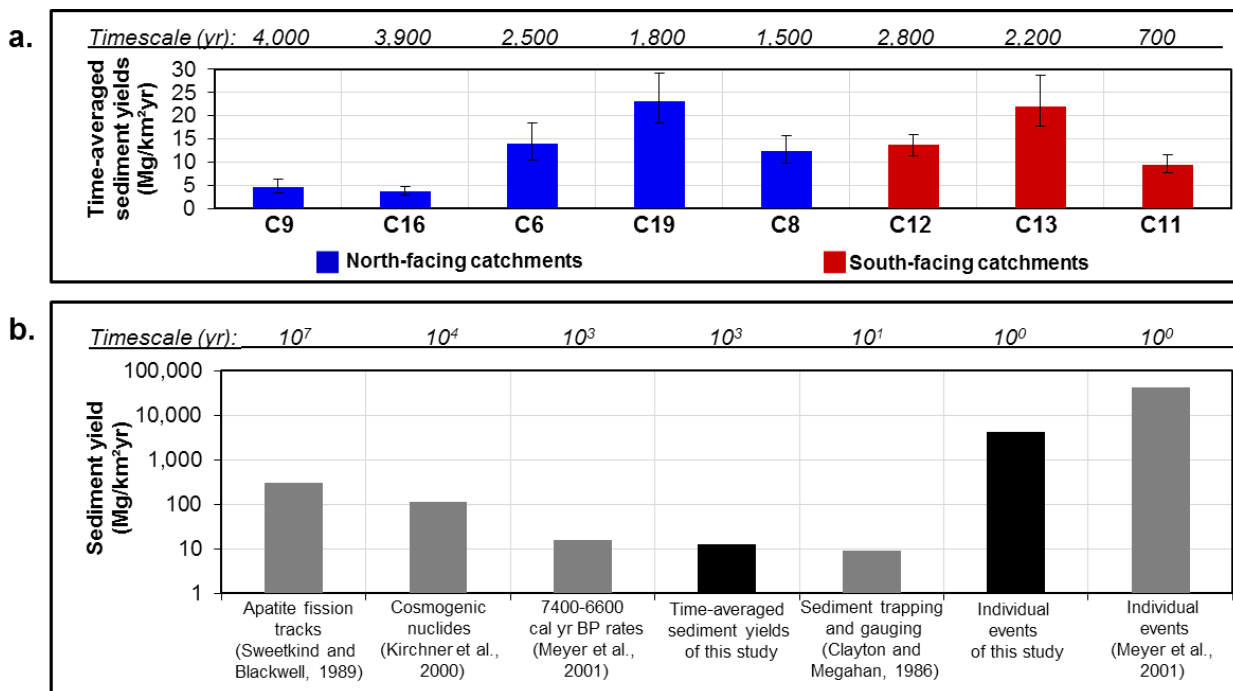


**Figure 1.8** a.) Time-averaged sediment yields with propagated uncertainty ranges and timescales of measurement. b.) The time-averaged sediment yields and yields from individual deposits are compared to sediment yields from elsewhere in the region.

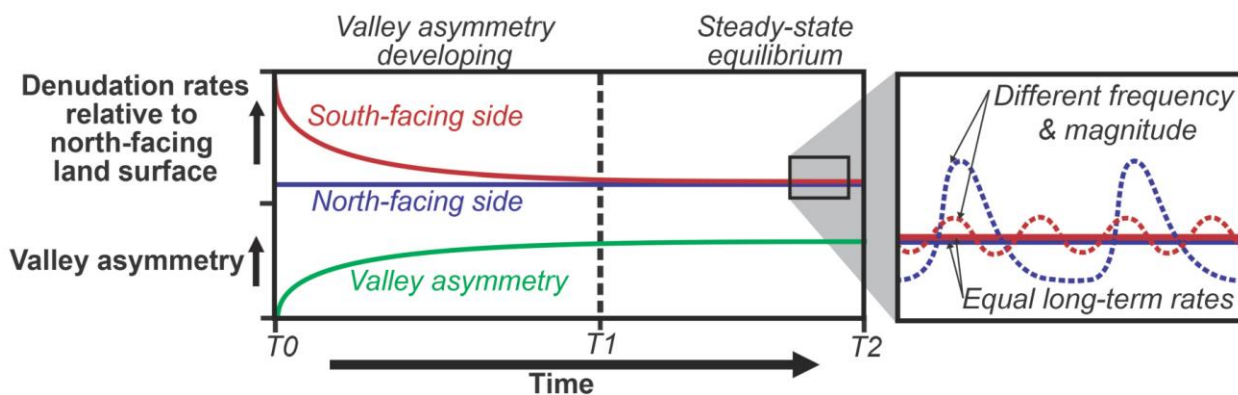


**Figure 1.9** Conceptual model of valley asymmetry development as a landscape adjusts towards dynamic equilibrium. Initially, south-facing valley sides degrade faster, but attenuate towards long-term denudation rates similar to north-facing valley sides, and valley asymmetry evolves towards a stable asymmetric form. Short-term denudation rates may be highly variable, due to differences in the frequency and magnitude of erosional processes, but result in similar long-term rates.

Table 1.1 Alluvial fan deposit charcoal ages and sampling depths.

	Alluvial charcoal sample ID	Radiocarbon age		Calibrated charcoal age			Slope-normal sample depth (cm)		
		<sup>14</sup> C age (yr)	Lab error (±yr)	Weighted mean age (cal yr BP)	2-sigma range min.	2-sigma range max.	Mean sample collection depth	Min. sample collection depth	Max. sample collection depth
North-facing catchments	B09 P01 CH1	3675	30	4,013	3,908	4,089	224	223	225
	B08 P1 S5 30	895	30	825	736	910	29	29	29
	B8 P1 S1	1595	40	1,478	1,394	1,562	53	51	55
	B8 P1 S08 85-90	1605	40	1,485	1,398	1,593	84	81	86
	B06 CH4 P02 twig	2450	30	2,538	2,360	2,703	192	189	196
	B19 P1 S9	655	40	613	553	674	23	21	24
	B19 P1 S6	845	30	755	689	892	42	41	43
	B19 P1 S2 85-90	1695	30	1,606	1,538	1,695	84	82	87
	B19 P1 S01 97-102	1820	30	1,757	1,630	1,860	96	93	98
	B16 P1 S02	585	30	595	535	651	22	14	29
	B16 P1 S05	1080	35	994	932	1,057	79	77	82
	B16 P2 S4	3725	35	4,070	3,973	4,223	228	223	233
B16 P2 S2	3620	30	3,933	3,843	4,066	268	265	270	
South-facing catchments	B13 P2 S01B	2185	35	2,217	2,073	2,318	137	131	143
	B12 P1-1 S05 62-66	5250	35	6,079	5,924	6,177	63	61	65
	B12 P01-3 S03 40-46	6900	35	7,732	7,667	7,823	180	177	183
	B12 P01-3 S04 55-59	7190	35	8,002	7,940	8,151	197	192	201
	B11 P3 CH2 43-44	665	30	618	559	674	43	43	44
	B11 P3 CH3 47-50	935	30	853	789	923	48	47	50
	B11 P3 CH4	745	30	686	662	726	83	80	86

Table 1.2 Alluvial fan aggradation rates, reconstructed surface areas, and volumetric rates of deposition.

	Catchment #	Avg. fan aggradation rate (cm/ka)	Min. fan aggradation rate (cm/ka)	Max. fan aggradation rate (cm/ka)	Fan 3D surface area (m <sup>2</sup> )	Min. fan 3D surface area (m <sup>2</sup> )	Max. fan 3D surface area (m <sup>2</sup> )	Mean total volumetric fan deposition rate (m <sup>3</sup> /yr)	Min. total volumetric fan deposition rate (m <sup>3</sup> /yr)	Max. total volumetric fan deposition rate (m <sup>3</sup> /yr)
North-facing catchments	B09 P01 CH1	56	55	58	301	226	385	0.17	0.12	0.221
	B8 P1 S08 85-90	56	51	62	1,433	1,252	1,622	0.81	0.64	0.999
	B06 CH4 P02 twig	76	70	83	1,120	918	1,330	0.85	0.64	1.106
	B19 P1 S01 97-102	55	50	60	1,975	1,749	2,208	1.08	0.88	1.331
	B16 P2 S2	68	65	70	579	471	695	0.39	0.31	0.489
	<b>Group average</b>	<b>62</b>			<b>1,082</b>			<b>0.66</b>		
South-facing catchment	B13 P2 S01B	62	56	69	1,957	1,763	2,240	1.21	1.00	1.54
	B12 P01-3 S04 55-59	70	62	76	1,465	1,290	1,647	1.02	0.81	1.25
	B11 P3 CH4	122	111	131	2,124	1,884	2,371	2.58	2.09	3.10
		<b>Group average</b>	<b>84</b>			<b>1,849</b>			<b>1.60</b>	

**Table 1.3 Source catchment areas, catchment averaged denudation rates, and sediment yields.**

	Alluvial charcoal sample ID	Mean catchment 3D area (m <sup>2</sup> )	Min. catchment 3D area (m <sup>2</sup> )	Max. catchment 3D area (m <sup>2</sup> )	Catchment-averaged denudation rate (cm/ka)	Min. catchment-averaged denudation rate (cm/ka)	Max. catchment-averaged denudation rate (cm/ka)	Time-averaged fan sediment yield (Mg/km <sup>2</sup> yr)	Min. time-averaged fan sediment yield (Mg/km <sup>2</sup> yr)	Max. time-averaged fan sediment yield (Mg/km <sup>2</sup> yr)
North-facing catchments	B09 P01 CH1	53,679	52,419	54,948	0.31	0.22	0.42	4.7	3.4	6.3
	B8 P1 S08 85-90	97,738	96,122	99,363	0.83	0.64	1.04	12.4	9.6	15.6
	B06 CH4 P02 twig	91,494	89,932	93,062	0.93	0.69	1.23	13.9	10.3	18.4
	B19 P1 S01 97-102	70,054	68,484	71,600	1.54	1.23	1.94	23.1	18.4	29.2
	B16 P2 S2	158,597	156,990	160,089	0.25	0.19	0.31	3.7	2.9	4.7
	<b>Group average</b>	<b>94,313</b>			<b>0.77</b>			<b>11.6</b>		
South-facing catchment	B13 P2 S01B	82,170	80,400	83,948	1.47	1.19	1.92	22.0	17.8	28.8
	B12 P01-3 S04 55-59	111,688	109,750	113,642	0.91	0.71	1.14	13.7	11.4	15.9
	B11 P3 CH4	408,014	404,557	411,478	0.63	0.51	0.77	9.5	7.6	11.5
		<b>Group average</b>	<b>200,624</b>			<b>1.01</b>			<b>15.1</b>	

**Table 1.4 Individual deposit thicknesses, volumes, and sediment yields for years of events.**

Alluvial charcoal sample ID	Individual deposit thickness (cm)	Min. Individual deposit thickness (cm)	Max. Individual deposit thickness (cm)	Individual deposit volume (m <sup>3</sup> )	Min. Individual deposit volume (m <sup>3</sup> )	Max. Individual deposit volume (m <sup>3</sup> )	Sediment yield for year of event (Mg/km <sup>2</sup> yr)	Min. Sediment yield for year of event (Mg/km <sup>2</sup> yr)	Max. Sediment yield for year of event (Mg/km <sup>2</sup> yr)
B8 P1 S08 85-90	31	27	35	445	335	574	6835	5061	8956
B19 P1 S01 97-102	12	7	16	228	118	362	4890	2472	7922
B16 P2 S2	40	32	47	229	150	329	2169	1407	3143
B11 P3 CH4	35	31	40	749	580	942	2754	2115	3494

CHAPTER TWO: ELEVATION MODIFIES THE SENSITIVITY  
OF REGOLITH PROPERTIES TO TERRAIN ASPECT

**Abstract**

Terrain aspect introduces climate variability that can alter eco-pedo-hydro-geomorphic processes and critical zone structure, and culminate in valley asymmetry. In semi-arid lower elevations of the Idaho batholith, pole-facing northern aspects produce thicker, finer-grained, organic-rich, and less dense regolith that retains more water in the near-surface, supports denser vegetation, and stabilizes northern aspects at steeper slope angles. However, slope asymmetry differences between north and south-facing aspects is reduced with increasing elevation throughout the region, and eventually reverses; southern aspects become steeper at higher elevations. It is unclear how aspect-induced differences in regolith properties change with elevation. Across a range of elevations and aspects, we assessed changes in soil thickness, texture, moisture, temperature, vegetation productivity, and growing season length. Regolith varied with aspect most at lower elevations, where northern aspects produced 70% thicker regolith cover and contained more than twice the silt and clay. Importantly, soil textures coarsen with increasing elevation among north-facing slopes, but become finer (i.e. more silt and clay) with elevation among south-facing slopes. These opposing trends converge to similar textures on both aspects at high elevations. Regolith thicknesses, and a suite of associated eco-hydro-pedologic characteristics, also become more similar with increasing elevation. Elevation appears to modify the influence of aspect on critical zone properties; lower

elevations are more sensitive to aspect than higher elevations. Orographic increases in precipitation and decreases in temperature with increasing elevation appear to 1) alleviate moisture stress on south-facing slopes, facilitating regolith thickening and soil development, and 2) increase the dominance of physical weathering processes on north-facing slopes, yielding coarser regolith textures. Elevation-induced changes in the sensitivity of the critical zone to aspect explain slope asymmetry reductions across similar elevations throughout the region, and could contribute to variability in valley asymmetry development throughout the world.

## **2.1 Introduction**

The relatively thin layer of mobile regolith (e.g. soil and weathered rock) mantling the surface of the earth is a zone of mineral and organic mixing that forms a primary reservoir of water and nutrients for life (i.e. the critical zone; NRC, 2001; Brantley et al., 2007). Water controls critical zone evolution by influencing chemical and physical weathering, pedogenesis, ecosystem type and function, and hydrologic and geomorphic processes (Hack and Goodlet, 1960; Clayton et al., 1979; Birkeland, 1984; Istanbuluoglu et al., 2008; Yetemen et al., 2010). Conversely, regolith properties control how water is retained in the subsurface; soil texture, bulk density, and organic content determine water retention per unit volume (i.e. porosity, field capacity, and wilting points; Smith, 2010; Geroy et al., 2011), while the thickness of the mobile regolith layer defines the volume of the subsurface pedo-hydrologic reservoir (Smith, 2010; Smith et al., 2011). The coevolution of eco-pedo-hydro-geomorphic processes at pedon-scales dictates how water is stored and partitioned into evapotranspiration, subsurface recharge, and runoff, which impacts how fluvial processes scale with drainage area, and how

catchments evolve (Chapter 3; Rodríguez-Iturbe and Rinaldo, 2001; Pelletier and Rasmussen, 2009).

The critical zone is sensitive to climate (Birkeland, 1984), and understanding how the critical zone responds to climate variability is vitally important (NRC, 2001; Pelletier et al., 2015). Climate at a given point on a landscape is not dictated simply by regional weather patterns; Elevation and aspect shift the local expression of regional climate. Aspect-induced eco-pedo-hydro-geomorphic feedbacks can alter the evolution of opposite valley sides, culminating in valley asymmetry (e.g. Istanbuluoglu et al., 2008). Maps of slope asymmetry between north and south-facing slopes show that slope asymmetry is globally widespread, but highly variable, with some landscapes responding oppositely to aspect-induced insolation differences (Poulos et al., 2012); The Idaho batholith, in the Northern Rocky Mountains, exhibits steeper northern aspects at lower elevations, but this asymmetry declines towards, and reverses above ~2000 m (i.e. steeper southern aspects). However, we cannot mechanistically explain how elevation modifies the influence aspect on the eco-hydro-pedo-geomorphic feedbacks associated with valley asymmetry. Few studies (e.g. Yetemen et al., 2010; Pelletier et al., 2013; McGuire et al., 2014; Rasmussen et al., 2015) assess how both elevation and aspect affect the critical zone. It is unclear whether the aspect-induced asymmetry of regolith properties within valleys also varies with elevation.

In order to assess how changes in climate with elevation affect the sensitivity of critical zone properties to aspect-induced insolation differences, regolith thickness and texture were assessed across a range of aspects and elevations in the Dry Creek Experiment Watershed (DCEW; Figure 2.1), which lies within the Idaho batholith region

and spans the elevation range across which slope asymmetry diminishes (e.g. Poulos et al., 2012). Regolith data were integrated with ecologic, hydrologic, and geomorphic data to form a conceptual framework of how elevation alters critical zone sensitivity to aspect.

Because elevation appears to control aspect-induced slope asymmetry within the Idaho batholith (Poulos et al., 2012), we suspect that the eco-hydro-pedologic responses to aspect that govern this geomorphic response are also elevation-sensitive. Northern aspects receive less insolation, which alters the surface energy balance, reduces temperatures, allows water to persist for longer, and generally produces thicker and finer-grained regolith that retains more water (Smith, 2010; Smith et al., 2011; Geroy et al., 2011; Stark, 2012). We hypothesize that lower elevations are more sensitive to aspect because they are more sensitive to insolation-induced water stress (i.e. water-limited ecosystems), but that this sensitivity diminishes with increasing elevations as precipitation increases and temperatures decline and evapotranspiration becomes more energy-limited (e.g. Budyko, 1974). Identifying how elevation alters the sensitivity of landscapes to aspect may help explain regional and global patterns in valley asymmetry (e.g. Poulos et al., 2012).

## **2.2 Background**

Feedbacks among regolith production, pedogenesis, and erosion cause them to coevolve and keep pace with each other, which, unless disturbed, results in a characteristic regolith thickness that reflects the dynamic equilibrium between production and erosion (Heimsath et al., 1997). Initially, if erosion outpaces regolith production, regolith thinning exposes less weathered, coarser rock fragments that are more difficult to erode, while greater exposure increases regolith production rates (e.g. more frequent

water infiltration, freeze/thaw and root wedging), both of which act as negative feedbacks that reduce differences between regolith production and erosion. If erosion greatly outpaces weathering, the regolith mantle may be completely removed, exposing bare bedrock and forcing erosion to become weathering-limited (i.e. fundamentally equal rates). Conversely, if erosion rates are too slow, regolith production outpaces removal and the regolith mantle thickens, which buffers the bedrock from interaction with water and roots and effectively slows regolith production (i.e. a negative feedback; Heimsath et al., 1997), while simultaneously increasing erosion rates due to mass wasting via shallow landslides (Roering et al., 1999). In either case, negative feedbacks drive regolith thickness towards a dynamic equilibrium where regolith production and erosion are equal.

The regolith thickness at which regolith production and erosion are in equilibrium is inherently sensitive to climate (Heimsath et al., 1997). For example, many arid lands are dominated by bare bedrock outcrops because moisture is insufficient for bedrock weathering, and erosion outpaces regolith production until it becomes weathering-limited. Conversely, regolith cover in warm, wet tropical climates can be incredibly thick due to stronger and deeper bedrock weathering. Studying the distribution and character of mobile regolith across a range of aspects, elevations, and topographic positions offers a perspective of how the balance between regolith production and erosion relates to climate gradients.

Global weather patterns control the movement of air and the energy (e.g. air temp) and moisture it contains, while elevation controls regional patterns of precipitation extraction and temperature gradients (i.e. adiabatic and orographic effects), aspect (i.e.

terrain orientation) modifies daily and annual insolation and temperature cycles, and topographic position (e.g. hillslope and catchment position) influences water and air fluxes (Yetemen et al., 2010; Barry, 2013). Vegetation type and density also vary with elevation, with the water supply (i.e. soil water storage) limiting evapotranspiration in more arid environments, while the energy supply limits evapotranspiration in wetter, colder environments (Budyko, 1974; Rasmussen et al., 2015). Predicting how climate change will affect the critical zone of a given landscape requires more than just future climate scenarios, we need to understand how elevation and aspect modify regional climate in order to downscale global climate forecasts.

Investigating how climate affects regolith properties is difficult because landscapes respond over long timescales, and may reflect past climates, such as the glacial conditions that have prevailed during the last million years (Howard, 1965; Bull, 1991; McGuire et al., 2014; Rinaldo et al., 1995). Landscapes also respond to climate non-linearly, and can be governed by thresholds and stable states (Pelletier et al., 2015). Regolith forming processes are also inherently complex and involve feedbacks among many variables (Jenny, 1941; Heimsath et al., 1997).

Studying how aspect-induced climate affects regolith properties can be beneficial to constrain many complicating influences. Oppositely facing slopes within valleys have experienced similar past regional climate variability, are often underlain by similar bedrock, are exposed to similar biotic communities, have common uplift and base-level conditions, and are subject to similar regional-scale landscape climate-response thresholds. Aspect serves as a natural persistent forcing that shifts the climate of adjacent

north and south-facing slopes, allowing us to constrain the influence of climate on regolith properties.

Aspect-induced slope asymmetry is a widespread source of landform variability in mountainous landscapes, but elevation modifies how valleys respond and develop asymmetry (Poulos et al., 2012). Aspect-induced climate perturbation shifts adjacent slopes within valleys from regional climate gradients (i.e. SFS are warmer, and NFS are cooler), and may cause slopes of one orientation to cross thresholds or tipping points and produce dramatic critical zone responses (e.g. Pelletier et al., 2015). The response of valleys to aspect-induced topoclimate can be studied to elucidate how insolation affects critical zone evolution (e.g. regolith production, pedogenesis, dust accumulation, and erosion) and how critical zone sensitivity changes along elevation-induced climate gradients. Aspect-sensitivity sensitivity may also reflect threshold and tipping point behavior, and help identify 'landscapes on the edge' (NRC, 2010).

In several environments, despite dramatic valley asymmetry of critical zone characteristics (e.g. slope steepness and vegetation), erosion rates of north-facing and south-facing slopes are surprisingly similar over  $10^3$  to  $10^4$  year timescales (West et al., 2014; Foster et al., 2015; Chapter 1). One possible explanation is that valley asymmetry represents a system response whereby aspect-related differences in erosion diminish as the valley system approaches a dynamic equilibrium; enhanced erosion on one valley side engages negative feedbacks that slow erosion (e.g. gradient reduction and land surface lengthening), which reduces differences in erosion with aspect, and causes north and south-facing slopes to erode at equal rates, while asymmetry is preserved. If valley asymmetry development is truly in dynamic equilibrium, we suspect that regolith

production and erosion are also generally in dynamic equilibrium, which should be reflected in regolith thickness measurements.

### 2.3 Study Area

The Dry Creek Experimental Watershed (DCEW) is a semi-arid research watershed with over 15 years of ecohydrologic data, located at  $\sim 116.1^\circ$  W and  $\sim 43.7^\circ$  N and spanning an elevation range of 1025 to 2130 m in the foothills near Boise, Idaho, USA (Figure 2.1; <http://earth.boisestate.edu/drycreek/>). Average annual precipitation increases from  $\sim 300$  to 1000 mm over the elevation range, with roughly half occurring as snow (McNamara et al., 2005; Aishlin and McNamara, 2011), while air temperatures range from  $-14^\circ\text{C}$  to  $33^\circ\text{C}$  seasonally (Smith et al., 2011). The watershed is incised on the margin of the Idaho batholith of the Northern Rockies into hydrothermally altered Cretaceous granodiorite that is incompetent compared to unaltered granite and forms grus-rich soils (Clayton et al., 1979; Clemens, 1993).

Northern aspects generally exhibit thicker, finer-grained, less dense, organic-enriched regolith that stores more water and supports denser vegetation (Tesfa et al., 2009; Williams et al., 2009; Smith, 2010; Geroy et al., 2011; Kunkel et al., 2011; Nicotina et al., 2011; Smith et al, 2011; Stark, 2012; Loughridge, 2014). Ecosystems vary dramatically with elevation, with higher elevations supporting montane coniferous forest composed of ponderosa pine (*Pinus ponderosa*) and douglas fir (*Pseudotsuga menziesii*), while lower elevations support sagebrush steppe ecosystems composed of big sagebrush (*Artemisia tridentata*), antelope bitterbrush (*Purshia tridentate*), rubber rabbitbrush (*Ericameria nauseosa*), cheatgrass (*Bromus tectorum*), and rush skeletonweed (*Chondrilla juncea*). The boundary between these ecosystems (i.e. ecotone) forms the

lower-elevation moisture-limited treeline. Interestingly, the treeline is effectively shifted down in elevation on north-facing slopes, supporting coniferous forest on only one side of the valleys at mid elevations in the watershed. Lower elevations lack forest cover on both aspects, while both are forested at high elevations.

## 2.4 Methods

In order to assess how mobile regolith thickness and texture vary with elevation and aspect, and study relationships with valley asymmetry, we 1) augered and assessed field textures, colors, and regolith thickness along a mid-elevation valley spanning transect, and 2) measured the depth to competent bedrock using blind penetration tests along a lower-elevation valley-spanning transect (Locations shown in Figure 2.1; example in Figure 2.2). The regolith transect sampling strategy was designed to complement existing data for the study area, in order to fill gaps in spatial characterization of regolith thickness and texture, and develop a conceptual framework of how critical zone properties vary with aspect, elevation, and hillslope position. Our penetration transect corresponds with the lower elevation sites of Smith (2010), while the augering transect correlates with their mid-high elevation sites.

The regolith penetration transect was ~0.3 km in horizontal length. Penetration sites were spaced 10 m apart, along slope, with a total of 40 sites and 114 measurements. Measurement involved pounding a ~2 cm diameter and 200 cm long incremented rod vertically into the ground until it would go no further (i.e. the ‘refusal’ of Tesfa et al., 2009). At each site, 2 or 3 measurements were collected in a triangular pattern with points spaced ~1 m apart to characterize local variability. Vertical depths were converted to surface-normal regolith thicknesses based on local slope. Many of the penetration tests

never reached refusal, indicating that the unconsolidated regolith vertical thickness exceeded the maximum measurement ability of 1.9 m. The inability to measure full thicknesses with penetration tests, and their blind nature, led us to explore augering techniques for more directly characterizing the mobile regolith thickness.

Augering was performed along a mid-elevation 1.4 km valley spanning transect, with 39 auger holes measured 40 m apart, along slope. We augered perpendicular to each hillslope, measured with a clinometer, to avoid the bias of slope angles on depth estimates (i.e. soils appear thicker on steeper slopes if depths are measured vertically). Augered samples were retrieved from discrete depth intervals by measuring the depth of the auger tip, using a scale taped to the auger shaft. For each sample, we augered until the hollow auger bit was filled with soil. The regolith depth interval required to fill the 16.5 cm long by 7.75 cm diameter auger bit varied, but was always less than the full 16.5 cm due to soil disaggregation and inflation. When the top of the auger bit could not be seen, we conservatively augered smaller intervals (e.g. 5 to 10cm) to avoid over-filling and spilling material back into the hole. Immobile saprolitic regolith was often noticeably harder to auger than the overlying mobile regolith; many of the auger holes extend less than 20 cm into this denser material.

Soil texture and color was assessed in the field for every other auger depth interval ( $n = 228$  fields textures from 42 auger holes) by: 1) sieving to measure and remove gravel ( $>2$ mm diameter), 2) determining moistened field textures by manual tests, and 3) determining moist Munsell soil color. Regolith texture classes were determined following the manual methods outlined in the appendix of Birkeland (1984), yielding texture classes that correspond with the Natural Resource Conservation

Service/US Department of Agriculture soil textural classes. Color and texture changes with depth were used to determine mobile regolith thicknesses.

Augered regolith samples were collected from every fourth auger hole, and a range of different soil field textures were analyzed in the lab using hydrometer analysis (n=15). Laboratory measurements of texture are compared with field estimates to evaluate the accuracy of field textures.

Differences in regolith thickness variability with aspect between the augering and penetration transects were interpreted by comparing changes in aspect-related variability with elevation to earlier studies in the watershed. Smith (2010) assessed thirty-two regolith profiles on north and south-facing valley sides (four soil pits on each aspect at four elevations). Regolith profiles were instrumented at four depths with moisture and temperature sensors (128 sensors among 32 pits), and sampled for laboratory soil textural analysis with laser diffraction and hydrometer.

The eco-pedo-hydrologic data of Smith (2010) were compared to the regolith transect data to form a conceptual framework for how elevation modifies the sensitivity of regolith properties to terrain aspect. Soil hydrologic properties and annual time-series of moisture and temperature from soil pit sensors were used to estimate subsurface saturation capacities, field capacities, and wilting points. Precipitation and air temperature were interpolated from elevation trends between three weather stations. Growing season length was constrained with leaf-area index measurements and Landsat-derived peak vegetation productivity. For detailed methods outlining soil pit instrumentation, sampling, laboratory analyses, and calculations, see Smith (2010).

Development of the conceptual framework was guided by additional prior studies in the DCEW. Geroy et al. (2011) performed progressive drainage lab experiments to assess the water retention characteristics of surficial soils (i.e. top 3 cm) collected along a mid-high elevation valley-spanning transect. Kunkel et al. (2011) used an elemental analyzer to compare the organic carbon and nitrogen content of soils in 5 cm increments of depth from 0-30 cm deep at mid-slope for north and south facing slopes at 11 elevations. Tesfa et al. (2009) measured regolith thickness within many smaller catchments within the DCEW, which were used in statistical models, based on relationships with topography and vegetation, to predict regolith thickness throughout the watershed.

## 2.5 Results

Regolith penetration measurements along the transect at lower elevations exhibit at least 73% thicker regolith cover on the north-facing valley side, with average regolith thicknesses of at least 144 cm (n = 48) for the north-facing side and 83 cm (n = 66) for the south-facing side (Figure 2.3; Table 2.1). Thicknesses exceeded our maximum measurement capability on the north-facing side 22 times, compared to only 7 times on south-facing slopes. Differences in average thicknesses may be greater than measured.

On the south-facing valley side, the penetration data exhibit a stair-stepping pattern in the underlying bedrock topography (Figure 2.3). This pattern is not evident in the land surface profile, but is related to variability in the regolith thickness with alternating deeper and shallower pockets of regolith. It is unclear if the north-facing slope is underlain by similar bedrock topography, as most of the thicknesses exceeded our measuring ability.

For the penetration transect, the north-facing valley side is steepest for the lower third of the slope, which appears to be undercut as it is located on the outside of a bend of the basal stream. Interestingly, the steepened lower slope was mantled by regolith thicker than we could measure, despite its steeper gradient, and supports dense choke cherry bushes. In contrast, the middle and upper hillslope supports sagebrush and herbaceous vegetation.

Field textural analyses of augered soils are useful for collecting a large number of texture observations, but prone to misclassification based upon the difficulty of correct identification (e.g. changes in textural characteristics caused by organic matter), and the experience of the individual performing the analysis. Comparing field textures to hydrometer textures measured in the lab ( $n = 15$ ; Figure 2.4) found that the correct soil texture class was identified for about half the samples ( $n=7$ ). Interestingly, clay was overestimated for more clay-rich samples, while silt was overestimated for samples with higher silt and organic matter content and lower amounts of clay. Organic matter produced smoother, less-sticky textures, possibly contributing to overestimation of silt. Samples near soil class boundaries (e.g. LoSa/SaLo boundary) were also prone to misclassification.

Despite uncertainties associated with field textures, when combined with gravel content and color changes, the methods were able to characterize regolith texture and color changes indicative of a change from mobile to immobile regolith. Mobile regolith was generally darker and browner, with more silt and organic matter (see Figures 2.2 and 2.5). Immobile regolith was generally lighter and redder, with more gravel and sand, and was harder and denser to auger through. The transition from mobile to immobile regolith

was characterized by 1) a coarsening in texture from sandy loam to loamy sand, 2) an increase in gravel content above ~40%, and 3) a change in color from a darker brown to a lighter reddish orange (Munsell color above ~4/4 7.5 YR). Clay was sometimes greater within horizons within the mobile regolith, but also sometimes accumulated near the top of the immobile layer.

A trade-off of producing a large number ( $n = 228$ ) of texture measurements using field methods is that sand, silt, and clay contents could not be precisely measured. Given the uncertainty of estimates of percentages of sand, silt, and clay based upon field texture classes, it is not clear from the augering data whether soils are finer grained (e.g. more silt and clay) for northern aspects along the augering transect (Figures 2.6 and 2.7). Field textures were primarily measured, in conjunction with gravel and color measurements, to identify the transition from mobile to immobile regolith; Texture data should be interpreted cautiously given its uncertainty.

Soils generally became coarser grained with depth on both aspects, but changes in texture primarily occurred near the transition from mobile to immobile regolith. The mobile regolith above this interface was often homogenous enough that field-measured soil textures were not distinctively different, although sometimes horizons were evident (e.g. example in Figure 2.5).

Compared to the lower-elevation penetration transect, the mid-elevation augering transect does not exhibit clear differences in regolith thickness, nor any stair-stepping patterns in the underlying topography. Smith (2010) found that the greatest differences in regolith thicknesses occurred at lower elevation sites and differences generally diminished with increasing site elevations (Figure 2.8a). Smith's (2010) mid-high

elevation site is of similar elevation to the augering transect, and did not exhibit significantly different regolith thicknesses. Geroy et al. (2011; Figure 2.8b) and Smith (2010; Figure 2.9), both found that north-facing slopes at mid-high elevations were mantled by finer-grained soils with more silt and clay, as well as lower bulk density, when measured in the lab.

Augering data showed variable regolith thicknesses with hillslope position for both north and south-facing slopes (Figure 2.10). Some of the thickest regolith occurred two-thirds of the way up the slopes, and generally thinned moving down or up from this position. Regolith thickness was variable along ridgelines, with steeper convex ridgelines producing shallower soils and sparser vegetation, and lower-gradient sections of the south-facing ridgelines exhibiting some of the deepest soils and densest sagebrush cover. Neither valley side appeared to be undercut along the augering transect. Average regolith thicknesses were greater for the south-facing valley side (86 vs 75 cm; Table 2.2), but this difference was mainly due to the thick soils on the relatively gentle ridgeline segment. Given the standard deviations of regolith thicknesses for the two valley sides (+/-49 and 54 cm; Table 2.2), differences in regolith thickness were not significant along the augering transect.

The auger-based regolith thickness measurements agreed with statistically modeled regolith thicknesses (Tesfa et al., 2009) for most of the transect, but specific areas appear discordant (Figures 2.10 and 2.11). The model under-predicted regolith thickness on the relatively gentle ridgeline segments, and over predicted for foot slopes and hollows.

Comparing regolith thickness with color infrared imagery (Figure 2.12) revealed that on the south-facing valley side, areas with greater infrared reflectance (i.e. more productive vegetation) exhibited the thickest regolith cover. This pattern was not evident on the north-facing valley side, as infrared reflectance was relatively high across the land surface.

The combined regolith thickness field and model data indicate that regolith cover is generally thicker on northern aspects at lower elevations, but that this difference decreases with increasing elevation. Additionally, soil texture differences appear greatest at lower elevations, and decrease with increasing elevations (e.g. Figure 2.9; Smith, 2010). Importantly, this apparent convergence is associated with opposing trends in texture with elevation for the two aspects; north-facing slopes become coarser-grained with increasing elevation, whereas south-facing slopes become finer-grained with increased elevations.

## **2.6 Discussion**

Elevation appears to affect the sensitivity of valley side slopes to aspect-induced insolation variability. At the lowest elevations, aspect-related differences in regolith thickness and texture are the greatest, with thicker, finer-grained regolith on northern aspects, whereas at the highest elevations they are most similar. Regolith thickness generally increases with increasing elevation among both north and south-facing sites, going from lower to mid-high elevations, but thickening with elevation is more rapid among south-facing sites, allowing them to ‘close the gap’ and reduce differences in thickness between aspects and approach similar thickness values at mid-high and high sites. Regolith textures exhibit opposite trends with elevation for north and south aspects,

with textures fining (i.e. increase in silt and clay) with increasing elevation among southern aspects, while textures coarsen (i.e. increase in sand) with elevation among northern aspects. Bulk density, soil water storage, growing season length, and the timing of peak vegetation productivity (e.g. NDVI) also vary with aspect more at low elevations, and converge to similar values between aspects at high elevations (Figure 2.13). For both aspects, aspect-related variability changes little between mid-high and high elevations, suggesting a limit to elevations influence on regolith thickness.

### 2.6.1 Elevation and Aspect Variability

At mid to lower elevations, relatively higher insolation on southern aspects increases moisture stress and supports sparser vegetation. Initially, this likely reduced stability and increased erosion rates, causing regolith to thin. However, as regolith becomes thinner, water and plants can reach the bedrock more easily, and bedrock weathering accelerates to keep pace with denudation, and the system trends towards a shallow equilibrium regolith thickness (Heimsath et al., 1997).

Conversely, on northern aspects at mid to lower elevations, reduced insolation on northern aspects alleviates moisture stresses, producing denser vegetation and increasing stability, which likely initially reduced erosion rates and caused regolith cover thickening. However, as regolith thickens, the bedrock becomes increasingly distant and buffered from interaction with water and roots, which slows weathering rates and regolith production until they keep pace with erosion rates and a thicker equilibrium thickness is achieved (Heimsath et al., 1997).

At higher elevations, moisture stress on both north and south-facing slopes is reduced by increasing precipitation, and decreasing temperatures. This allows vegetation to grow densely on both aspects, and produces similar equilibrium regolith thicknesses.

Increases in orographic precipitation and reductions in temperature with rising elevation appear to alter the sensitivity of the critical zone to aspect-induced radiation variability and microclimate. This conceptual framework explains regolith thickness and texture variability with aspect and elevation within the Dry Creek Experimental Watershed (DCEW), as well as why, across the larger semi-arid montane region of the Northern Rocky Mountains it lies within, valley asymmetry diminishes across a similar range of elevations and becomes infrequent approaching ~2000 m (Poulos et al., 2012).

In the DCEW, regolith textures (Figure 2.10; Smith, 2010) are generally finer-grained on north-facing slopes but become coarser grained (i.e. sandier) with increasing elevation, whereas regolith on south-facing slopes is coarser-grained and becomes finer-grained (i.e. more silt and clay) with increasing elevation. This results in regolith textures being most different at lower elevations, and gradually becoming more similar with increasing elevation. Regolith thicknesses are also most different between north and south-facing slopes at lower elevations (~1100 m), more similar at mid-low elevations (~1300 m), and not significantly different at mid-high and high elevations (~1450 and ~1825 m). Importantly, regolith changes with elevation are more pronounced for south-facing slopes, suggesting that they are more sensitive to increases in precipitation and reductions in temperature with increasing elevation, likely because both climate changes reduce aspect-induced radiative moisture stress.

The convergence of both regolith textures and thicknesses to similar values for north and south-facing slopes at higher elevations suggests that precipitation increases and temperature reductions with rising elevation (i.e. orographic effects) reduce the sensitivity of landscapes to aspect-induced radiation variability and moisture stress. This interaction makes sense, because both elevation- and aspect-induced climate forcings act to shift the system from regional climate, and determine the topo-climatic setting.

In semi-arid montane environments, increases in precipitation with elevation should ease moisture stress, promoting vegetation stabilization and soil thickening, increasing regolith weathering rates and residence times, and perhaps enhancing dust deposition and/or retention. South-facing slopes fit this model, with soil textures becoming finer-grained and regolith thicknesses generally increasing with elevation. However, regolith on north-facing slopes becomes coarser-grained with increasing elevation, despite increases in precipitation. North-facing slopes may be less sensitive to precipitation because they more effectively retain moisture at all elevations (Geroy et al., 2011; Smith et al., 2011). Rather, temperature reductions with increasing elevation may kinetically limit weathering rates on north-facing slopes, and perhaps promote more physical weathering (e.g. more tree-throw and freeze-thaw).

The coupled convergence of thicknesses and textures, as well as most eco-hydro-pedologic variables, for north and south-facing slopes at higher elevations (1450 - 1825 m) suggest that aspect becomes less important at high elevations. The comprehensive analyses of Smith (2010) indicate that other eco-hydro-pedologic variables are also most different between north and south-facing slopes at lower elevations, and converge to similar values at high elevations. Soil temperatures vary with aspect among the three

mid-to-low elevations, but do not vary with aspect at high elevations. Air temperatures are higher at low elevations, and are most different between high and low elevations during the summer, when water stress is high. Snow cover persists for longer and later into the year on north-facing slopes for the three mid-to-low sites, but persists for similar time lengths and periods on both aspects at high elevation. Soil temperature, soil water capacity, soil bulk density, and soil carbon differences between north and south-facing slopes are all greater at lower elevations, and converge to similar values at high elevations. Growing season lengths are generally longer and decrease with increasing elevation on north-facing slopes, whereas growing season lengths increase with increasing elevation for south-facing slopes, and growing season lengths are similar for both aspects at higher elevations (Figure 2.13). Growing seasons also generally start and end earlier at lower elevations and on south-facing slopes, except at high elevations. More organic carbon was evident at all depths for north-facing slopes, among all elevations except at the high sites, where south-facing slopes had more organic carbon (Smith, 2010). Kunkel et al. (2011) also found that organic carbon and nitrogen increased with both terrain northness and elevation. Solar radiation is reduced by a similar amount on northern aspects at all elevations, indicating the changing response is not due to a reduction of forcings (i.e. aspect-induced climate perturbation). The whole eco-hydro-pedologic system (i.e. the critical zone) appears to become insensitive to aspect-induced insolation differences at higher elevations (~1825 m), not just regolith thickness and texture.

Effectively, the transition from moisture-sensitive to temperature-sensitive regolith development may be shifted to higher elevations on southern aspects due to their

warmer, drier conditions. Regolith thickness did not vary significantly between mid-high and high elevations for either aspect (Figure 2.8a), suggesting a limit to elevation's control on weathering and stability. This makes sense because if these landscapes are less sensitive to aspect-induced microclimate, then it follows that they should also be less sensitive to elevation-induced climate perturbation. Perhaps the consistent regolith thicknesses between mid-high and higher elevations reflect other ubiquitous controls, such as the average rooting depth of trees (e.g. Gabet and Mudd, 2010; Roering et al., 2010). Integration of less-weathered crumbly hydrothermally-altered granodioritic bedrock chunks into the soil due to increasing forest bioturbation (via tree-throw and/or root-wedging) with elevation could explain why regolith textures became sandier (i.e. more *grus*) with increasing elevation on north-facing slopes. Alternatively, the coarser textures at higher elevations among north-facing sites might reflect deeper, more effective freeze-thaw driven physical weathering (e.g. Anderson et al., 2013).

Thicker regolith and finer-grained soils generally occur in areas where controlling factors are relaxed (i.e. moisture or temperature limitations on weathering), where residence times are longer (i.e. erosion is reduced), and/or where dust accumulation is enhanced. Regolith thickness represents a balance between regolith formation from bedrock and dust inputs, and net lateral transport and land surface denudation (e.g. Heimsath et al., 1997; Gabet and Mudd, 2010). On north-facing slopes, and at higher elevations, denser vegetation may help stabilize slopes, promote dust accumulation, reduce erosion, and increase residence times, leading to both thickening and more pronounced weathering (i.e. finer-grained textures). For the semi-arid low to mid-high elevations, moisture and vegetation density increase with both northness and elevation. In

contrast, at higher elevations, forest cover is more homogenous, and both aspects may be equally stable.

Relationships between regolith properties and modern vegetation remain unclear, as the greatest aspect-related differences in thickness and texture occur at lower elevations, whereas differences in the dominant functional type (e.g. trees vs. shrubs) and density of vegetation are greatest at mid-high elevations. Tesfa et al. (2009) also found that topographic attributes were a better predictor of regolith thickness than metrics of vegetation cover. Comparisons with modern vegetation patterns may be misleading, as soils form over longer timescales and reflect the influence paleo-vegetation patterns (i.e. regolith properties and vegetation may be out of phase with each other). If the lower moisture-limited treeline migrated downwards in elevation during glacial intervals, which have prevailed during most of the Quaternary (Petit et al., 1999), it is possible that the greatest differences in vegetation cover actually occurred at lower elevations for most of the timescale of landscape development. The impact of paleovegetation on regolith characteristics is difficult to explore, as vegetation migrations have not been reconstructed. For semi-arid regions of Arizona, USA, McGuire et al. (2014) suggest that vegetation patterns moved down in elevation by ~1000 m during glacial climates, and that much of the slope asymmetry evident on cinder cones actually developed during glacial climates under dramatically different vegetation conditions. In landscapes along elevation and climate related ecotones, such as the lower moisture-limited treeline in the DCEW, the ecotones have likely shifted in response to climate change, and it would be surprising if the associated dramatic changes in vegetation cover were not reflecting in regolith thickness and texture.

Elevation-related trends in regolith thickness and texture are most apparent from the data from the soil sensor sites (Figures 2.8a & 2.9; Smith, 2010; Smith et al., 2011), but the penetration and augering transects generally support these trends. The penetration transect at lower elevation (~1100 m) documented that the regolith was at least 1.7 times thicker on northern aspects (>144 vs. 83 cm thick, on average). Smith's (2010) thicknesses were lower on average (~65 and 35 cm for north and south aspects), perhaps due to a difference in measurement technique, but documented a similar magnitude of difference, with roughly 2 times thicker regolith for the north-facing soil pits. The blind penetration method could penetrate beyond the mobile/immobile regolith transition if the immobile bedrock is highly weathered, which may more accurately reflect the hydrologic reservoir, but could overestimate mobile regolith thickness.

The augering transect results also generally agree with the observations of Smith (2010) for comparable mid-high elevations (~1450 m). Although the average values were slightly higher on southern aspects (86 vs. 75 cm, on average), this difference is not significant given the range of variability (~50 cm standard deviation; Table 2.2). While Smith (2010) noted thicker regolith in one soil pit for the northern aspect at this elevation, the other three pits exhibit similar values to the pits for the south-facing aspect. Regolith was not significantly thicker on either aspect.

The average thickness for northern aspects from augering (86 cm) at mid-high elevations was lower than the average thickness for northern aspects at low elevations (>144 cm), which does not fit the trend for northern aspects found by Smith (2010), with regolith thickening with increasing elevation. This could reflect overestimation of thicknesses using blind penetration, as the penetration data were generally much thicker

than the soil pit data for the same elevations for both aspects (e.g. 144 vs. 65 cm for north, and 83 vs. 35 cm for south aspects, respectively).

### 2.6.2 Hillslope-Scale Variability

Along the augering transect, the occurrence of the thickest regolith on the upper mid-slope (~1/2 to 3/4 of the way upslope) and relatively gentle ridgeline segments appears to largely reflect geomorphic stability. Dense vegetation stabilizes these slopes at steep angles, while their distance from incising drainages buffers them from change, allowing weathering bedrock and dust to accumulate. The occurrence of thick soils on steep planar upper-mid slopes is unexpected; Steep planar hillslope forms suggest they are at the critical slope angle, above which they become unstable and erosion increases nonlinearly (Roering et al., 1999).

The augering data subset for the primary valley facets along the transect (Figure 2.10) are most representative of north and south-facing slopes, as the rest of the transect crosses intra-catchment slopes that vary in aspect orientation. Along this section, regolith is thicker on the upper-mid slopes, and thins upslope towards ridgelines and downslope towards foot slopes. This spatial variability suggests both bottom-up and top-down controls on regolith thickness that diminish toward mid-slope; diffusive processes may be outpaced by regolith delivery from upslope, while fluvial processes lack the drainage area to accumulate flow. The relatively thinner regolith and steeper gradients on foot slopes and along drainages can likely be explained by erosion (i.e. regolith thinning) and steepening in response to incision of adjacent streams. Incising drainages steepen adjacent slopes and degradation propagates this erosion signal upslope. This suggests landscape transience, which is difficult to account for in soil depth models, as prior

conditions often cannot be established. Measurements on foot slopes could be underestimated if the auger struck larger talus in the subsurface, but often these are the steepest slopes, suggesting that they are not depositional surfaces; Deposits tend to be gentler than the slopes that produced them.

The incision signal that has caused regolith thinning and slope steepening on the lower slopes does not appear to have reached the upper slopes. The slightly gentler gradients of the upper-mid slopes may grade to a higher pre-incision drainage level. This implies that the lower slope buffers the upper slope from change, maintaining stable slopes with lower erosion rates, which allows regolith to thicken. A combination of distance from drainages, and vegetation reinforcement, appears to promote stability, despite steep gradients.

Snow and/or dust drifting could influence regolith thickness and texture on the upper-mid slopes. The predominant wind direction in the area is from west of southwest, meaning that north-facing slopes are essentially leeward slope. Snowdrifts would provide more water, which could enhance bedrock weathering, causing weathering to outpace erosion, while dust accumulation would inflate soils and cause them to be finer-grained. However, since the pattern is repeated on the south-facing slope, it seems more likely that regolith thickening on the upper-mid slope is due to topographic position.

The model results (Tesfa et al., 2009) generally exhibit thicker soils on the upper slopes as well (Figure 2.11), suggesting that the pattern exhibited by the augering data may be repeated throughout the watershed. Augered regolith thicknesses matched the soil thicknesses modeled from topographic attributes (Tesfa et al., 2009) quite well for much of the augering transect (Figure 2.10), except on a gentler ridgeline segment, where the

model predicts shallower regolith (i.e. under-predicts), and on foot slopes where the model overestimated regolith accumulation. Importantly, the primary goal of the penetration measurement and soil depth modeling of Tesfa et al. (2009) was to predict the thickness of the hydrologic reservoir, not the mobile regolith thickness of geomorphic interest. Thus, thus the augering and blind penetration data may be measuring distinctly different subsurface characteristics. Differences in what the two methods measure might help explain why the penetration data for low elevations exceeded the soil pit data of Smith (2010).

The overestimation of regolith cover on the foot slopes by the model is likely related to the difficulty of accounting for the legacy effect of episodic depositional and erosional events, which influence regolith thickness variability both laterally and temporally. Overestimation in hollows may reflect wetter conditions and greater bedrock weathering, allowing the upper immobile regolith to be penetrated beyond the immobile/mobile boundary by the blind penetration measurements the model was based upon.

The augering transect also documented thicker, finer-grained regolith on a relatively gentler section of a ridgeline between two south-facing catchments, suggesting that these ridgeline segments form relatively stable uplands, which reduces erosion (i.e. increase residence time), increases weathering, and/or increases dust accumulation. When looking down-valley, these gentler segments of the ridgelines are evident as stair-steps in the ridgeline profiles (Figure 2.14). Interestingly, these gentler uplands are more frequent on the south-facing side of the valley. The model appears to under-estimate soil depth in this area, so it remains unclear if this pattern is repeated throughout the watershed. Along

the penetration transect at lower elevations, stair-stepping was evident in the subsurface bedrock topography. Perhaps, similar processes are responsible for both ridgeline and subsurface stair-stepping topography.

Many processes might contribute to the formation of the stable ridgeline steps. The stair steps do not appear to be terrace remnants, as they occur at different heights on adjacent ridgelines, trend lines parallel to the main valley stream could not be fit through them, and the surfaces of the steps often slope up-valley. They may occur where more pronounced drainage incision on either side of the ridgeline accelerates ridgeline lowering locally, but we would expect this to produce thinner soils. The gentler areas on ridgelines may be produced on the top of back-rotated slump blocks, as some of the larger stable uplands exhibit possible head scarps. Landslide-like features seem to be more frequent on the south-facing valley side, which could be promoted by higher water tables within the south-facing valley side, which has been observed in well logs for granitic south-facing slopes of the central rockies (Anderson and Rock, 2015; Boulder CZO, Upper Gordon Gulch). Alternatively, the stable uplands may be remnants of a landscape adjusted to a higher baselevel and gentler slopes, as ridgelines should be the last area to respond to a drop in base level following drainage incision.

Regardless of what causes these relatively gentle and stable ridgeline segments to form, they appear to be associated with eco-hydro-pedologic feedbacks. Chemical weathering amounts are likely higher on stable ridgeline segments because the denser sagebrush ecosystem it supports likely increases organic acids from root exudates and microbial decomposition, and the thick, fine-grained soils hold more water, all of which are inter-related through positive feedbacks. Preferential spring-flow due to bedrock

structure could also promote faster critical zone development, but no evidence of spring-flow was noted and springs in the area are usually much closer to drainage outlets.

Physical weathering rates are also likely to be higher locally on stable ridgeline segments, as the denser, deeper-rooted vegetation exploits and expands fractures in saprolitic rock, but thick regolith might also distance the bedrock from interaction with roots. More dust may have accumulated within the regolith on the stable uplands. The gentler slopes and denser vegetation cover of the gentler ridgeline segments likely result in slower erosion by water, creep, and wind. Reduced erosion rates increase soil residence times, which might allow more weathering to occur before soils are removed. Multiple eco-hydro-pedo-geomorphic feedbacks may be involved in thickening regolith on gentle ridgeline segments.

## **2.7 Conclusions**

Mobile regolith was thicker on north-facing slopes at low and mid-low elevations, but more similar among aspects at mid-high and high elevations, suggesting an elevation limit on the sensitivity of regolith thickness to aspect. Regolith thickness increased with elevation among the low and mid elevation sites for both aspects, albeit faster for southern aspects, but decreased at higher elevations, further suggesting a limit to regolith sensitivity to elevation and aspect-induced climate trends. Among south-facing sites, regolith textures fined with increasing elevation; increases in precipitation and reductions in temperature appear to alleviate plant water stress, supporting denser and different vegetation (e.g. conifers), and promoting stability, all of which appear to increase weathering rates and/or soil residence time. In contrast, among north-facing sites, regolith textures coarsened and thicknesses varied less with increasing elevation, suggesting

north-facing slopes at lower elevations have experienced more chemical weathering due to higher air temperatures compared to higher elevations where tree and freeze-driven physical weathering are more dominant, but that denser vegetation at all elevations promotes soil thickening. The opposing trends in regolith weathering and soil development with increasing elevation appear to converge to similar values at high elevations, which is reinforced by the convergence of many other eco-hydro-pedologic characteristics (Smith, 2010). Importantly, the elevations that this convergence occur across (1450-1825 m) are the same elevations that valley asymmetry diminishes across, with little variability in slope with aspect evident at ~2000 m throughout the region (Poulos et al., 2012). Elevation appears to alter the sensitivity of valleys to aspect-induced microclimate throughout the semi-arid Idaho batholith.

At hillslope scales, thicker mobile regolith occurred on steep upper mid-slopes, which appears to reflect geomorphic stability due to distance from incising basal streams, as both aspects displayed this pattern, regardless of vegetation cover. Some of the thickest regolith also occurred on an anomalously gentle south-facing ridgeline segment (e.g. a stair-step), which supports dense sagebrush. Many other gentler ridgeline segments are evident from afar on south-facing ridgelines when looking down valley. Ridgelines are even more disconnected from base level changes, and gentler segments likely erode slower and may be largely relict features of difficult-to-constrain past geomorphic influences. The relative stability of gentler ridgeline segments may promote regolith thickening. Incorporating geomorphic stability and history into models, while difficult, could improve regolith thickness predictions.

Field data compared well with modeled regolith thickness, but models under predicted regolith thickness on the stable ridgeline segments, and over predicted thicknesses for foot slopes and hollows. Given the models different focus on hydrologic storage, rather than mobile regolith, a geomorphic model accounting for a wider range of geomorphic processes such as the formation of stable ridgeline segments and the episodic foot-slope and hollow erosion induced by knickpoint migration and drainage incision, might produce better predictions of mobile regolith thickness.

Field data compared well with modeled regolith thickness, but models under predicted regolith thickness on the stable ridgeline segments, and over predicted thicknesses for foot slopes and hollows. Given the models different focus on hydrologic storage, rather than mobile regolith, a geomorphic model accounting for a wider range of geomorphic processes such as the formation of stable ridgeline segments and the episodic foot-slope and hollow erosion induced by knickpoint migration and drainage incision, might produce better predictions of mobile regolith thickness.

## 2.8 References

- Aishlin, P., & McNamara, J. P. (2011). Bedrock infiltration and mountain block recharge accounting using chloride mass balance. *Hydrological Processes*, 25(12), 1934-1948.
- Anderson, R. S., Anderson, S. P., & Tucker, G. E. (2013). Rock damage and regolith transport by frost: an example of climate modulation of the geomorphology of the critical zone. *Earth Surface Processes and Landforms*, 38(3), 299-316.
- Anderson, S. P., & Rock N. (2015). "CZO Dataset: Betasso - Well Water Levels (2013-2015) - (BT\_GW\_1\_Pducer)." Retrieved 10 Jan 2016, from <http://criticalzone.org/boulder/data/dataset/3742/>
- Barry, R. G. (2013). *Mountain Weather and Climate*. Routledge.
- Birkeland, P. W. (1984). *Soils and geomorphology*. Oxford University Press.
- Brantley, S. L., Goldhaber, M. B., & Ragnarsdottir, K. V. (2007). Crossing disciplines and scales to understand the critical zone. *Elements*, 3(5), 307-314.
- Budyko, M. I. (1974), *Climate and Life*, Academic, Orlando, Fla.
- Bull, W. B. (1991). *Geomorphic responses to climatic change*. New York, Oxford University Press, 326 p.
- Burnett, B. N., Meyer, G. A., & McFadden, L. D. (2008). Aspect-related microclimatic influences on slope forms and processes, northeastern Arizona. *Journal of Geophysical Research: Earth Surface* (2003–2012), 113(F3).
- Clayton, J. L., Megahan, W. F., & Hampton, D. (1979). *Soil and bedrock properties: weathering and alteration products and processes in the Idaho batholith*. United States. Intermountain Forest and Range Experiment Station. USDA Forest Service research paper INT (USA).
- Clemens, D. M. (1993). *Tectonics and Silicic Volcanic Stratigraphy of the Western Snake River Plain, Southwestern Idaho* (Master's thesis, Arizona State University).

- Ferrier, K. L., Kirchner, J. W., & Finkel, R. C. (2011). Estimating millennial-scale rates of dust incorporation into eroding hillslope regolith using cosmogenic nuclides and immobile weathering tracers. *Journal of Geophysical Research: Earth Surface* (2003–2012), 116(F3).
- Foster, M. A., Anderson, R. S., Wyshnytzky, C. E., Ouimet, W. B., & Dethier, D. P. (2015). Hillslope lowering rates and mobile-regolith residence times from in situ and meteoric  $^{10}\text{Be}$  analysis, Boulder Creek Critical Zone Observatory, Colorado. *Geological Society of America Bulletin*, B31115-1.
- Gabet, E. J., & Mudd, S. M. (2010). Bedrock erosion by root fracture and tree throw: A coupled biogeomorphic model to explore the humped soil production function and the persistence of hillslope soils. *Journal of Geophysical Research: Earth Surface* (2003–2012), 115(F4).
- Geroy, I. J., Gribb, M. M., Marshall, H. P., Chandler, D. G., Benner, S. G., & McNamara, J. P. (2011). Aspect influences on soil water retention and storage. *Hydrological Processes*, 25(25), 3836-3842.
- Hack, J. T., & Goodlett, J. C. (1960). *Geomorphology and forest ecology of a mountain region in the central Appalachians* (No. 347). United States Government Printing Office.
- Hansen, M. C., Egorov, A., Roy, D. P., Potapov, P., Ju, J., Turubanova, S., ... & Loveland, T. R. (2011). Continuous fields of land cover for the conterminous United States using Landsat data: First results from the Web-Enabled Landsat Data (WELD) project. *Remote Sensing Letters*, 2(4), 279-288.
- Heimsath, A. M., Dietrich, W. E., Nishiizumi, K., & Finkel, R. C. (1997). The soil production function and landscape equilibrium. *Nature*, 388(6640), 358-361.
- Howard, A. D. (1965). Geomorphological systems; equilibrium and dynamics. *American Journal of Science*, 263(4), 302-312.
- Istanbulluoglu, E., Yetemen, O., Vivoni, E. R., Gutiérrez-Jurado, H. A., & Bras, R. L. (2008). Eco-geomorphic implications of hillslope aspect: Inferences from analysis

- of landscape morphology in central New Mexico. *Geophysical Research Letters*, 35(14).
- Jenny, H. (1941). *Factors of soil formation* (p. 281). New York, NY: McGraw-Hill Book Company.
- Kunkel, M. L., Flores, A. N., Smith, T. J., McNamara, J. P., & Benner, S. G. (2011). A simplified approach for estimating soil carbon and nitrogen stocks in semi-arid complex terrain. *Geoderma*, 165(1), 1-11.
- Loughridge, R. (2014). *Identifying Topographic Controls of Terrestrial Vegetation Using Remote Sensing Data in a Semiarid Mountain Watershed, Idaho, USA*.
- McGuire, L. A., Pelletier, J. D., & Roering, J. J. (2014). Development of topographic asymmetry: Insights from dated cinder cones in the western United States. *Journal of Geophysical Research: Earth Surface*, 119(8), 1725-1750.
- McNamara, J. P., Chandler, D., Seyfried, M., & Achet, S. (2005). Soil moisture states, lateral flow, and streamflow generation in a semi-arid, snowmelt-driven catchment. *Hydrological Processes*, 19(20), 4023-4038.
- Nicotina, L., Tarboton, D. G., Tesfa, T. K., & Rinaldo, A. (2011). Hydrologic controls on equilibrium soil depths. *Water Resources Research*, 47(4).
- National Research Council (US). Committee on Basic Research Opportunities in the Earth Sciences. (2001). *Basic Research Opportunities in Earth Science*. National Academy Press.
- National Research Council (US). Committee on Challenges and Opportunities in Earth Surface Processes. (2010). *Landscapes on the Edge: New Horizons for Research on Earth's Surface*. National Academies Press.
- Othberg, K. L., & Stanford, L. R. (1992). *Geologic map of the Boise Valley and adjoining area, western Snake River Plain*. Idaho: Idaho Geological Survey Geologic Map, 18.
- Pelletier, J. D., & Rasmussen, C. (2009). Geomorphically based predictive mapping of soil thickness in upland watersheds. *Water Resources Research*, 45(9).

- Pelletier, J. D., Barron-Gafford, G. A., Breshears, D. D., Brooks, P. D., Chorover, J., Durcik, M., ... & Meixner, T. (2013). Coevolution of nonlinear trends in vegetation, soils, and topography with elevation and slope aspect: A case study in the sky islands of southern Arizona. *Journal of Geophysical Research: Earth Surface*, 118(2), 741-758.
- Pelletier, J. D., Brad Murray, A., Pierce, J. L., Bierman, P. R., Breshears, D. D., Crosby, B. T., ... & Lancaster, N. (2015). Forecasting the response of Earth's surface to future climatic and land use changes: A review of methods and research needs. *Earth's Future*, 3(7), 220-251.
- Petit, J. R., Jouzel, J., Raynaud, D., Barkov, N. I., Barnola, J. M., Basile, I., ... & Delmotte, M. (1999). Climate and atmospheric history of the past 420,000 years from the Vostok ice core, Antarctica. *Nature*, 399(6735), 429-436.
- Poulos, M. J., Pierce, J. L., Flores, A. N., & Benner, S. G. (2012). Hillslope asymmetry maps reveal widespread, multi-scale organization. *Geophysical Research Letters*, 39(6).
- Rasmussen, C., Pelletier, J. D., Troch, P. A., Swetnam, T. L., & Chorover, J. (2015). Quantifying topographic and vegetation effects on the transfer of energy and mass to the critical zone. *Vadose Zone Journal*, 14(11).
- Reheis, M. C., Goodmacher, J. C., Harden, J. W., McFadden, L. D., Rockwell, T. K., Shroba, R. R., ... & Taylor, E. M. (1995). Quaternary soils and dust deposition in southern Nevada and California. *Geological Society of America Bulletin*, 107(9), 1003-1022.
- Reynolds, R., Neff, J., Reheis, M., & Lamothe, P. (2006). Atmospheric dust in modern soil on aeolian sandstone, Colorado Plateau (USA): variation with landscape position and contribution to potential plant nutrients. *Geoderma*, 130(1), 108-123.
- Roering et al 1999
- Rinaldo, A., Dietrich, W. E., Rigon, R., Vogel, G. K., & Rodrlguez-Lturbe, I. (1995). Geomorphological signatures of varying climate. *Nature*, 374(6523), 632-635.

- Rodríguez-Iturbe, I., & Rinaldo, A. (2001). *Fractal river basins: chance and self-organization*. Cambridge University Press.
- Roering, J. J., Kirchner, J. W., & Dietrich, W. E. (1999). Evidence for nonlinear, diffusive sediment transport on hillslopes and implications for landscape morphology. *Water Resources Research*, 35(3), 853-870.
- Roering, J. J., Marshall, J., Booth, A. M., Mort, M., & Jin, Q. (2010). Evidence for biotic controls on topography and soil production. *Earth and Planetary Science Letters*, 298(1), 183-190.
- Smith, T. J. (2010). *Using Soil Moisture Trends Across Topographic Gradients to Examine Controls on Semi-arid Ecosystem Dynamics* (Master's thesis, Boise State University).
- Smith, T. J., McNamara, J. P., Flores, A. N., Gribb, M. M., Aishlin, P. S., & Benner, S. G. (2011). Small soil storage capacity limits benefit of winter snowpack to upland vegetation. *Hydrological Processes*, 25(25), 3858-3865.
- Stark, B. J. (2012). *Assessing Eolian Dust Inputs to Soils in Dry Creek Experimental Watershed, SW Idaho* (Doctoral dissertation, Boise State University).
- Tesfa, T. K., Tarboton, D. G., Chandler, D. G., & McNamara, J. P. (2009). Modeling soil depth from topographic and land cover attributes. *Water Resources Research*, 45(10).
- Thomas, C. A. (1963). *Cloudburst Floods at Boise, Idaho, August 20, September 22, 26, 1959*. United States, Department of the Interior, Geological Survey, 12 p.
- West, N., Kirby, E., Bierman, P., & Clarke, B. A. (2014). Aspect-dependent variations in regolith creep revealed by meteoric  $^{10}\text{Be}$ . *Geology*, 42(6), 507-510.
- Williams, C. J., McNamara, J. P., & Chandler, D. G. (2009). Controls on the temporal and spatial variability of soil moisture in a mountainous landscape: the signature of snow and complex terrain. *Hydrology and Earth System Sciences*, 13(7), 1325-1336.

Yetemen, O., Istanbuluoglu, E., & Vivoni, E. R. (2010). The implications of geology, soils, and vegetation on landscape morphology: Inferences from semi-arid basins with complex vegetation patterns in Central New Mexico, USA. *Geomorphology*, 116(3), 246-263.

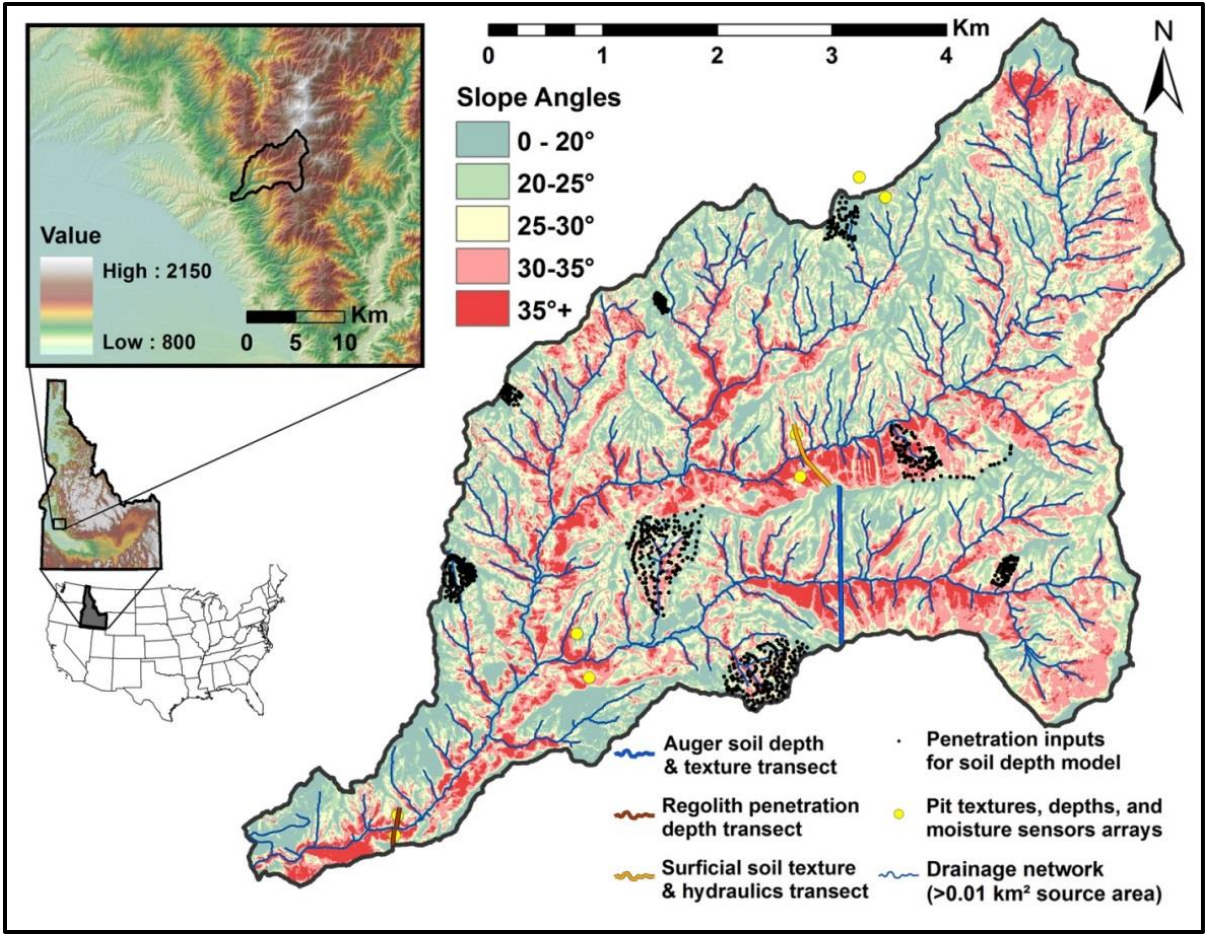


**Figure 2.1** Location map of the Dry Creek Experimental Watershed (DCEW), with locations of depth and texture measurements of regolith and soil by this study and previous studies. Penetration inputs were used in a soil depth model by Tesfa et al. (2009). Pit textures, depths and moisture measurements were assessed by Smith et al. (2012). Surficial soil and hydraulic properties were assessed by Geroy et al. (2012).



Figure 2.2 Example of penetration rod and auger piercing the upper darker, finer-grained mobile regolith, and set into the underlying coarser immobile regolith (granodiorite). The methods yielded similar results when tested side-by-side.

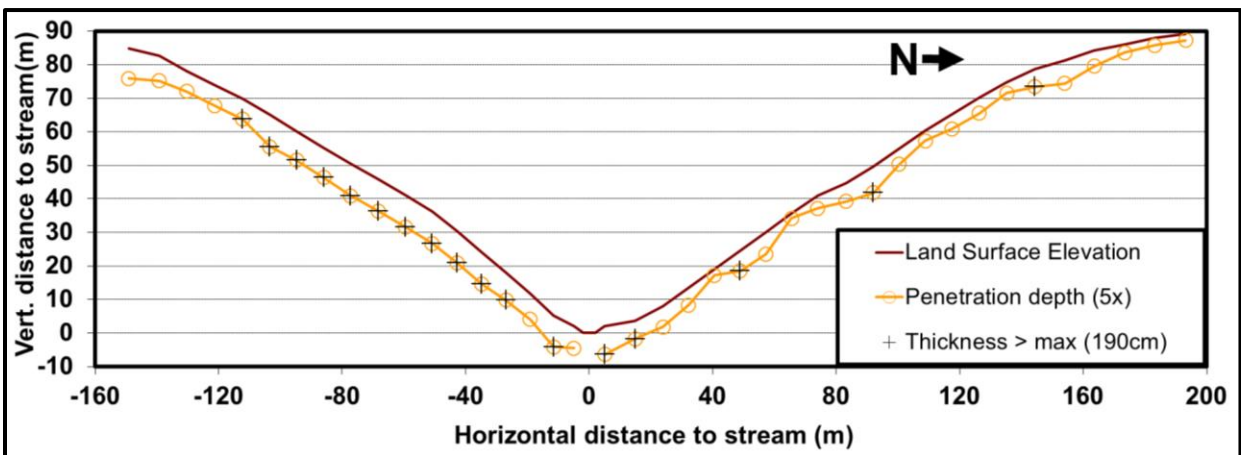
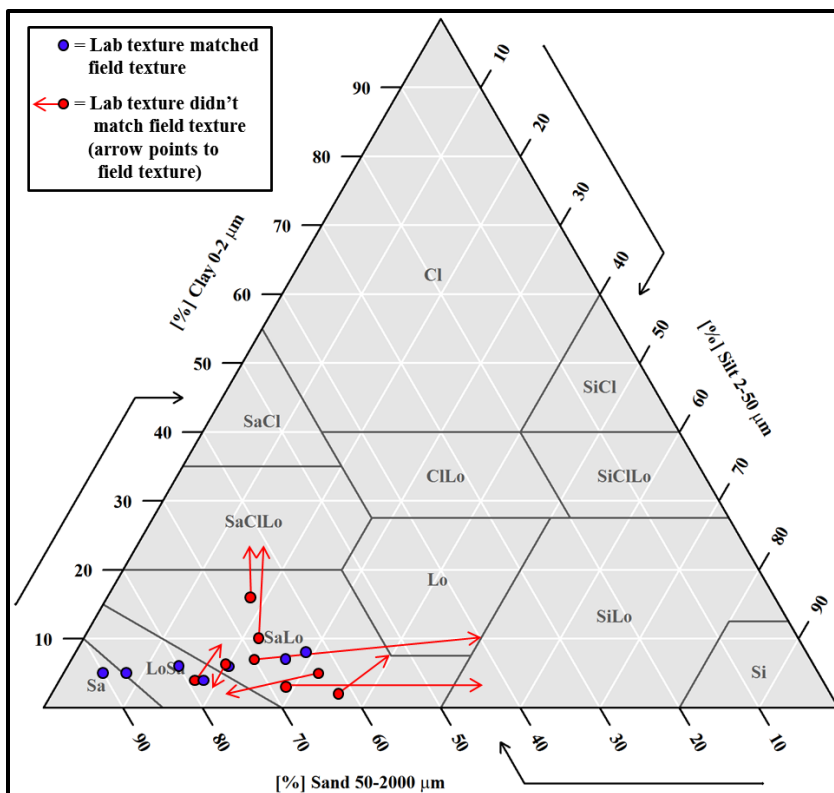


Figure 2.3 Cross-sectional view of regolith 'blind' penetration transect showing thicker, and possibly less variable, unconsolidated regolith. Each circle shows the average of 2-3 measurements, with sites where at least one measurement exceeded the maximum measurable depth indicated with crosses.



**Figure 2.4** Comparison of lab textures (circles) with field classification. Blue circles indicate that field classification correctly identified the correct soil class, while red circles indicate incorrect classification and include a red arrow pointing to the texture class or intermediate boundary (e.g. SaLo/Lo boundary) identified in the field.



Depth (cm)	0-13	20-30	39-48	60-71	80-92	102-110	120-130	138-146	154-163
Gravel (%)	10-15	10	10	15	15	20	20	35	50
Field Texture (USDA)	Sandy Loam	Loam / Silt Loam	Loam	Loam	Clay Loam	Sandy Loam	Sandy Loam	Sandy Loam / Loam	Loamy Sand / Sand
Munsell Color (7.5 YR)	2.5/2	3/2	3/3	4/3	4/4	4/4	4/6	4/6	5/6

**Figure 2.5** Example auger samples from a site with relatively thick mobile regolith (152 cm), located on a gentle upland of a south-facing ridgeline supporting dense sagebrush cover. Note the change to immobile regolith (saprolitic granodiorite bedrock) is characterized by an increase in gravel content, a transition to a loamy sand or sand texture, and a lighter and redder color.

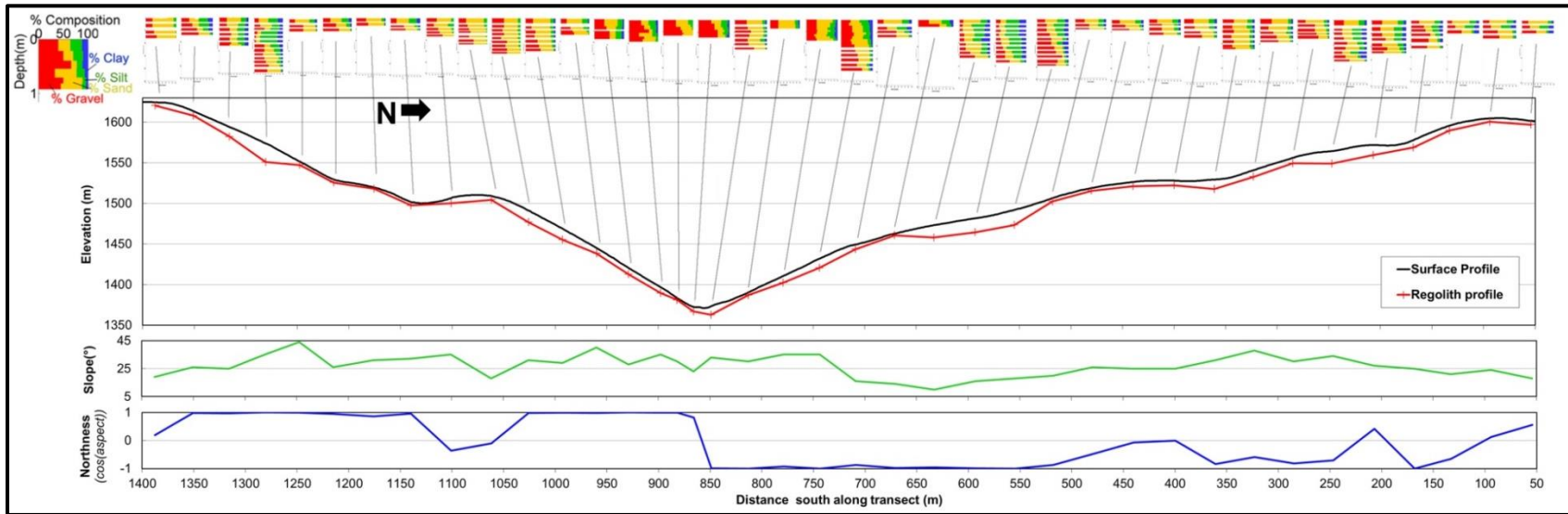


**Figure 2.6** Augering transect figure showing, from top to bottom, grain-size data, land surface and mobile/immobile regolith transition profiles, local slope, and local northness, which is calculated from aspect.

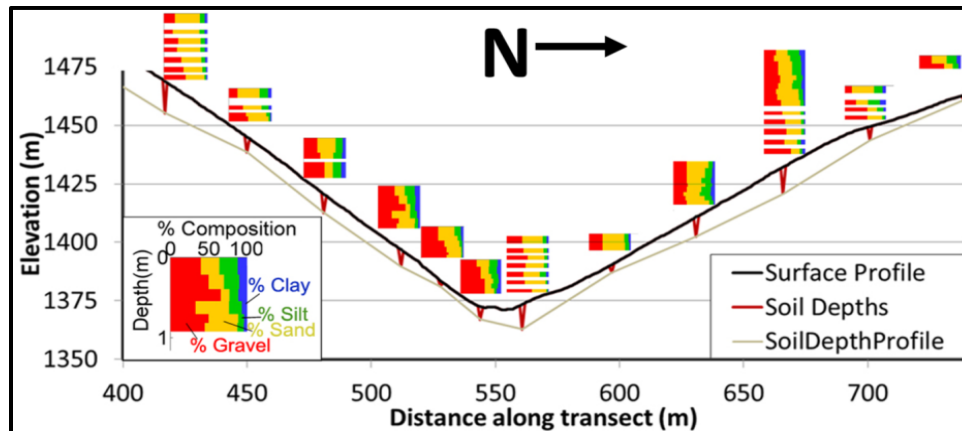


**Figure 2.7** Zoomed in figure showing soil textures and mobile regolith (i.e. soil) depths for the north and south-facing hillslopes in the middle of the transect (facets).

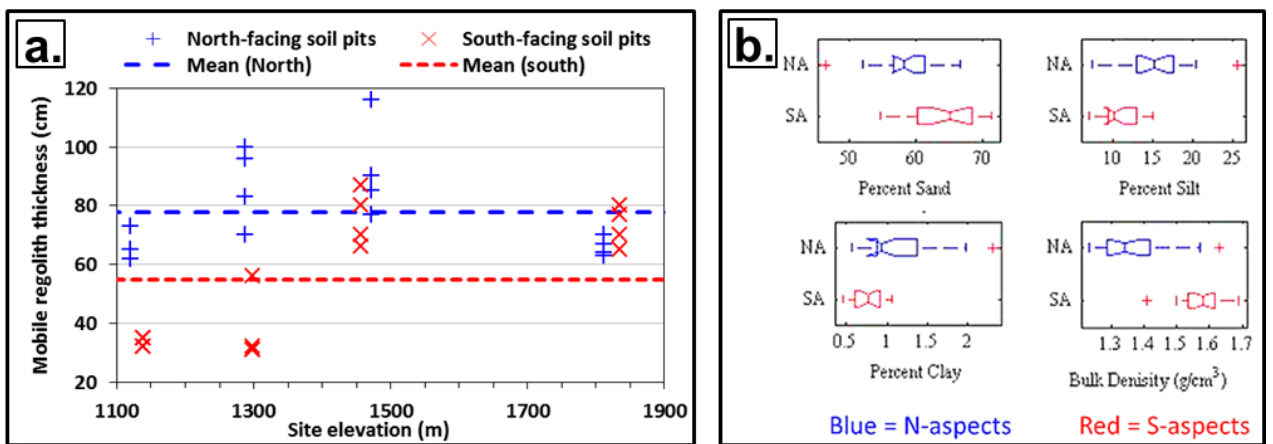


Figure 2.8 a.) Summary of aspect-related differences in soil depth and variability with elevation (replotted from Smith, 2010), and b.) Aspect-related differences in surficial soil texture and density (graphs from Geroy et al., 2011).

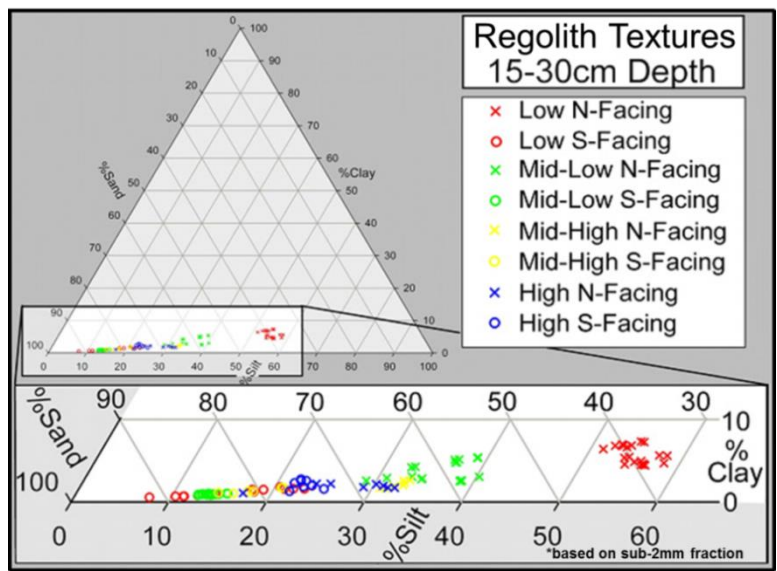


Figure 2.9 Differences in regolith textures (sub-2mm fraction) vary the most with between north and south-facing slopes at low elevations, but differences with aspect decrease with increasing elevation. Replotted using laser-diffraction texture data from Smith (2010). Grain-size data displayed similar trends with aspect and elevation for 0-2 cm, 2-15 cm, and bedrock depths.

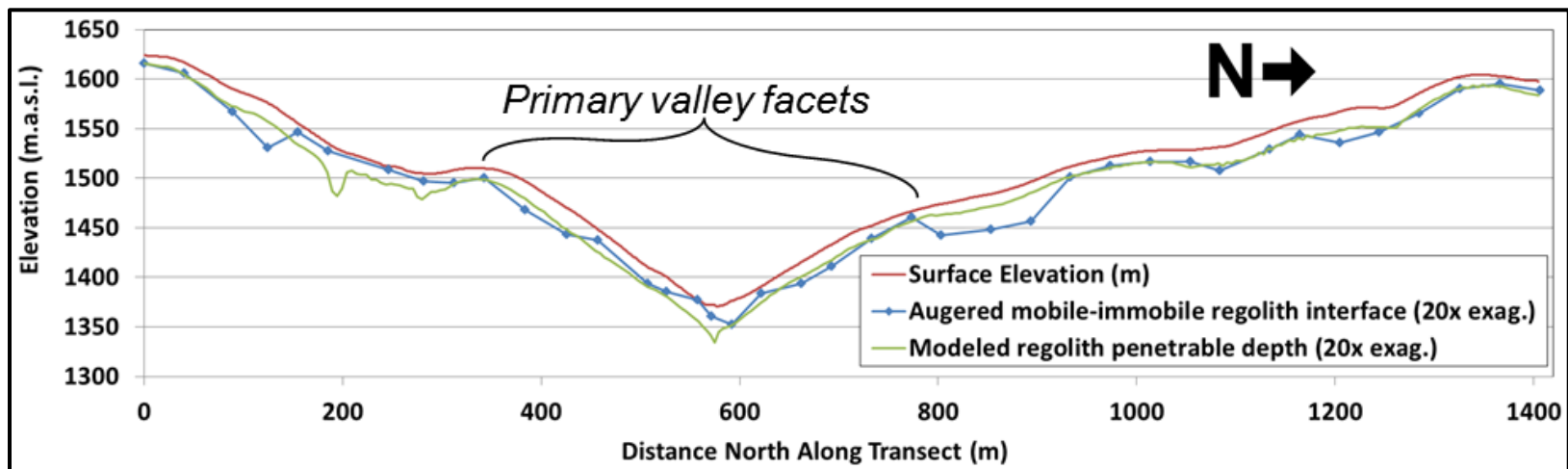
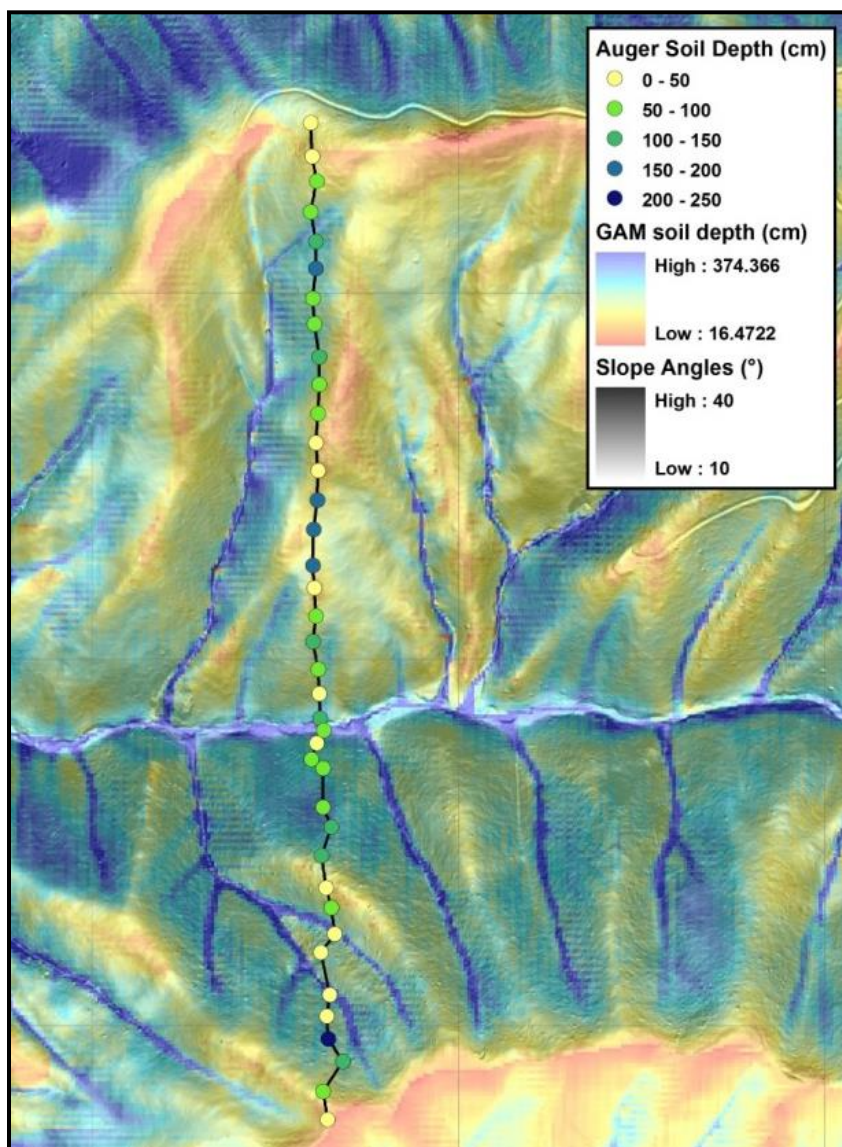
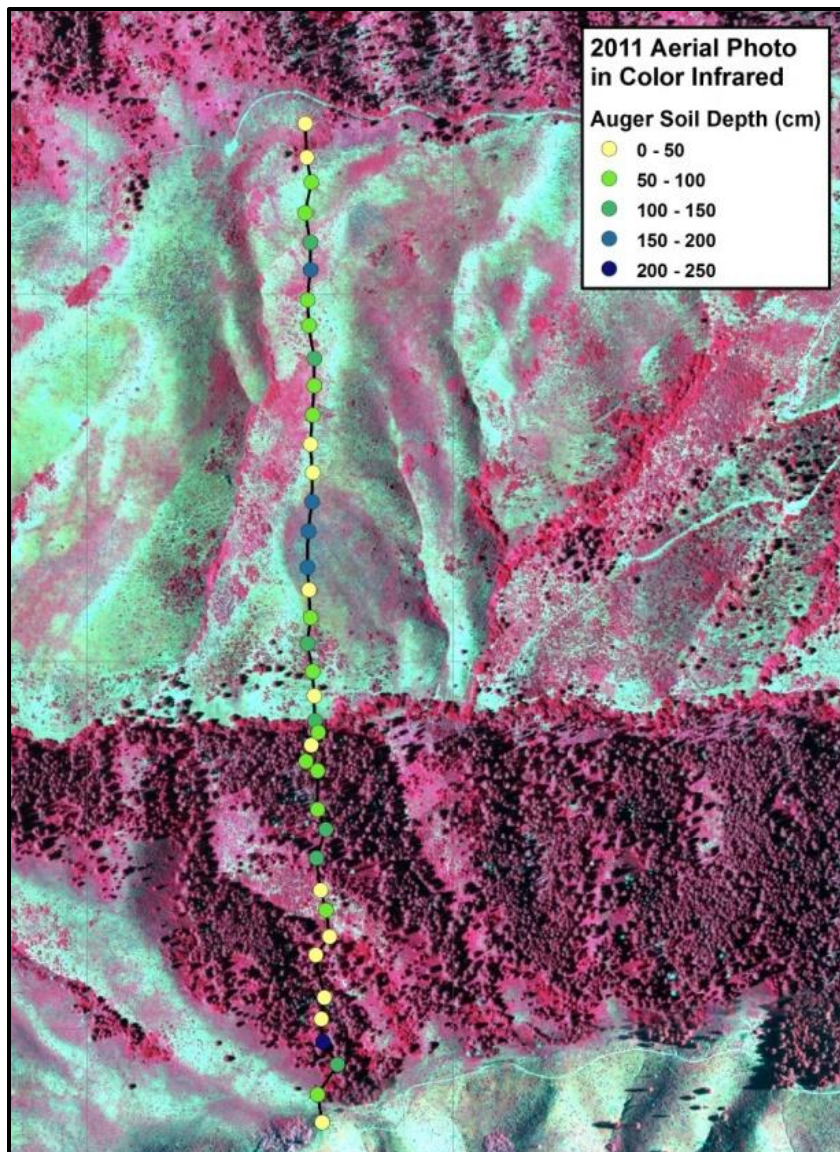


Figure 2.10 a.) Valley cross-section with no vertical exaggeration of topography, showing augered mobile regolith thicknesses with GAM modeled penetrable regolith thickness, which are exaggerated 20 times to make changes in regolith thickness more visible on graphs.



**Figure 2.11** Augered mobile regolith depths plotted over modeled penetrable regolith depths (Tesfa et al, 2009), with added slope-shaded to show topography.



**Figure 2.12** Auger-based mobile regolith thickness transect plotted over color-infrared aerial photograph showing increased vegetation reflectance of infrared (red colors above). Note that, at least on the south-facing slope, thicker soils occur where near-infrared is brighter, which is generally characteristic of productive vegetation.

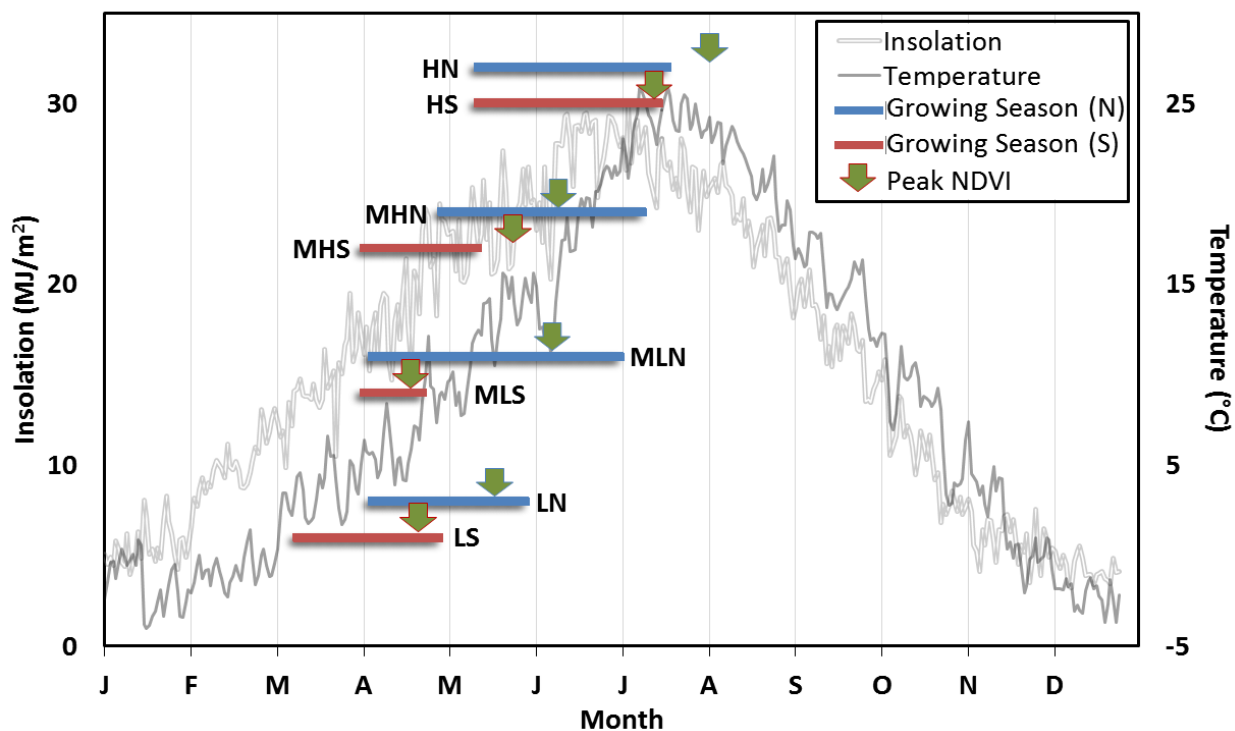


**Figure 2.13** Annual time-series of insolation and temperature, with overlays of growing season durations and timing of peak NDVI (vegetation productivity), with vertical positions denoting general elevations (not to scale).

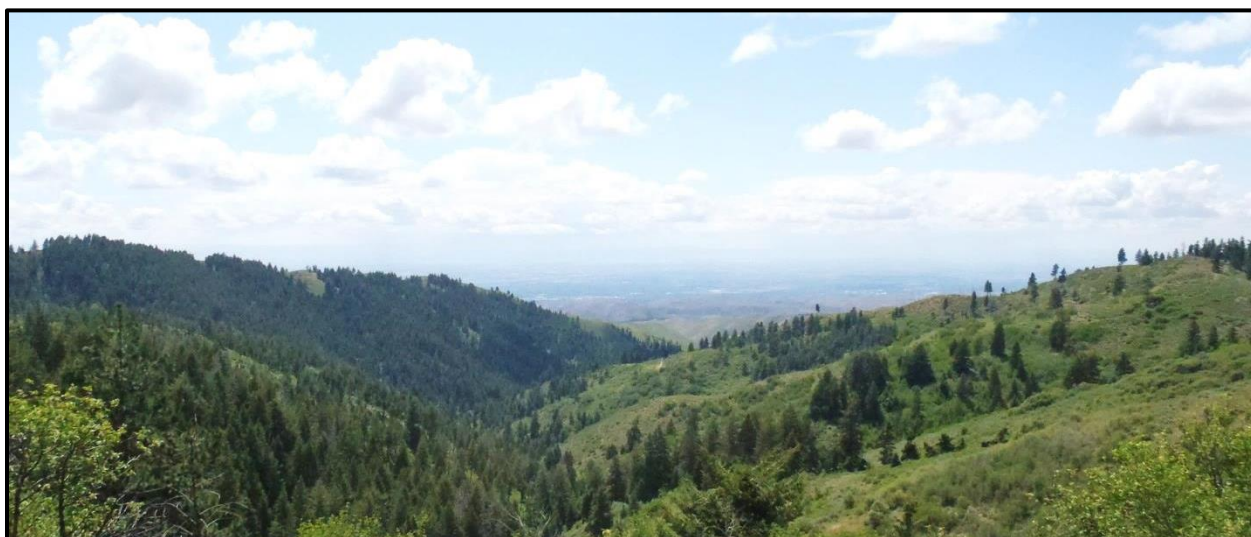


**Figure 2.14** Down-valley view of the location of the augering transect. Note the gentler ridgeline segments on the south-facing valley side (i.e. stair-steps in ridgelines), which contrast with the linear north-facing ridgelines.

**Table 2.1 Penetration-based regolith depth (thickness) measurements along a valley transect. Note that actual mean depths are likely higher where depths exceeded measurement capabilities (bold values), and the means for each aspect represent minimum values. Average surface-normal depths are plotted in cross-section in Figure 2.3.**

	Horizontal distance N. of stream (m)	distance above stream (m)	Slope (°)	Regolith depth 1 (cm)	Regolith depth 2 (cm)	Regolith depth 3 (cm)	Surface-normal mean soil depth (cm)	
<b>South-facing hillslope</b>	193.2	89.1	7	29	34	48	37	
	183.2	88.0	11	47	37	51	44	
	173.4	86.1	10	31	69	46	48	
	163.6	84.3	18	113	87	84	90	
	154.0	81.3	15	120	179	114	133	
	144.4	78.7	24	<b>190</b>	60	71	98	
	135.2	74.7	27	57	61	66	55	
	126.3	70.1	29	82	81	110	80	
	117.6	65.3	30	100	72	94	77	
	108.9	60.3	32	59	81	40	51	
	100.4	55.0	33	137	111	38	80	
	92.0	49.6	29	<b>190</b>	116	163	137	
	83.3	44.7	22	110	166	52	101	
	74.0	41.0	32	125	91	15	65	
	65.5	35.7	34	33	15	44	25	
	57.2	30.1	34	180	177	34	109	
	48.9	24.6	33	<b>190</b>	154	19	101	
	40.5	19.1	34	33	36	48	32	
	32.2	13.6	34	50	75	<b>190</b>	87	
	23.9	8.0	25	130	139	100	111	
14.8	3.7	10	<b>190</b>	10	130	108		
5.0	2.0	6	<b>190</b>	122	<b>190</b>	166		
<b>North-facing hillslope</b>	-5.0	2.0	20	141	119	127	121	
	-11.5	5.3	27	183	<b>190</b>	<b>190</b>	167	
	-19.1	11.8	41	156	152	154	117	
	-26.9	18.1	39	159	<b>190</b>	149	129	
	-34.8	24.2	38	<b>190</b>	<b>190</b>	-	151	
	-42.7	30.4	38	<b>190</b>	<b>190</b>	-	150	
	-50.8	36.2	36	<b>190</b>	<b>190</b>	-	155	
	-59.5	41.2	30	<b>190</b>	<b>190</b>	-	165	
	-68.3	45.9	28	<b>190</b>	<b>190</b>	-	168	
	-77.2	50.4	27	<b>190</b>	<b>190</b>	-	169	
	-86.0	55.2	29	152	<b>190</b>	<b>190</b>	155	
	-94.7	60.2	30	<b>190</b>	167	165	151	
	-103.4	65.0	29	<b>190</b>	<b>190</b>	<b>190</b>	166	
	-112.2	69.9	29	<b>190</b>	67	108	106	
	-121.3	73.9	24	163	100	104	111	
	-130.4	78.2	25	135	132	100	111	
-139.3	82.7	27	162	158	130	134		
-149.1	84.8	12	189	184	159	173		
" - " indicates only 2 measurements taken							<b>Mean soil depth for S-aspects (cm)</b>	<b>83</b>
<b>Bold</b> indicates depth exceeded length of rod							<b>Mean soil depth for N-aspects (cm)</b>	<b>144</b>

**Table 2.2 Soil thickness and compiled land surface characteristics for each soil augering site, sorted from north to south.**

Auger Pit #	Easting (m)	Northing (m)	Elevation (m)	Aspect (°)	Slope (°)	Regolith thickness (cm)
22S	570798	4840730	1598	304	18	48
21S	570800	4840690	1604	277	24	41
20S	570806	4840650	1602	229	21	60
19S	570798	4840610	1584	181	25	92
18S	570805	4840570	1571	295	27	124
17S	570805	4840530	1567	225	34	155
16S	570801	4840490	1557	215	30	66
15S	570803	4840460	1545	234	38	80
14S	570810	4840410	1531	213	31	117
13S	570810	4840380	1528	270	25	56
12S	570808	4840340	1527	266	25	51
11S	570805	4840300	1519	241	26	33
10S	570808	4840260	1510	209	20	42
9S	570807	4840220	1494	175	18	186
8S	570802	4840180	1483	170	16	172
7S	570801	4840130	1473	163	10	152
6S	570803	4840100	1465	169	14	20
5S	570805	4840060	1451	151	16	57
4S	570801	4840020	1433	180	35	113
3S	570808	4839990	1411	158	35	84
2S	570810	4839950	1391	184	30	33
1S	570811	4839920	1374	189	33	107
1N	570816	4839900	1372	325	23	55
2N	570806	4839890	1382	8	30	25
3N	570799	4839860	1400	9	35	71
4N	570815	4839850	1410	2	28	80
5N	570815	4839800	1450	348	40	65
6N	570826	4839770	1470	9	29	137
7N	570813	4839730	1497	10	31	144
8N	570819	4839690	1510	264	18	48
9N	570826	4839660	1508	249	35	65
10N	570831	4839630	1505	343	32	42
11N	570812	4839600	1512	330	31	17
12N	570824	4839540	1535	342	26	38
13N	570820	4839510	1555	9	44	43
14N	570822	4839480	1576	3	35	229
15N	570842	4839450	1591	14	25	118
16N	570815	4839410	1617	12	26	56
17N	570821	4839370	1624	281	19	40
<b>South-facing regolith thickness - Average (cm)</b>						<b>86</b>
<b>South-facing regolith thickness - Standard deviation (cm)</b>						<b>49</b>
<b>North-facing regolith thickness - Average (cm)</b>						<b>75</b>
<b>North-facing regolith thickness - Standard deviation (cm)</b>						<b>54</b>

CHAPTER THREE: ASPECT-INDUCED ASYMMETRIC DEGRADATION, DIVIDE  
MIGRATION, AND LAND SURFACE ELONGATION DRIVE VALLEY  
ASYMMETRY DEVELOPMENT TOWARDS A DYNAMIC EQUILIBRIUM

**Abstract**

Insolation varies with hillslope aspect, producing a persistent and ubiquitous climate perturbation. Over million-year timescales, aspect-induced insolation changes drive feedbacks among vegetation, soils and hydrology that alter landscape evolution and cause valley asymmetry development. Because lithology, tectonics, and past climate are often similar for valley sides, asymmetric valleys can be used to constrain how climate affects landscape evolution. We integrate eco-hydro-pedo-geomorphic data from steep semi-arid montane terrain to develop a conceptual model of how pedon-scale changes in vegetation, soil, and regolith alter the water balance, which impacts drainage incision, expansion, and competition. South-facing slopes receive more insolation, which increases moisture stress, shortens growing seasons, reduces vegetation cover, and produces thin, coarse, and dense soils that retain less water. South-facing catchments, on average, have 30% denser drainage networks, are  $\sim 5\text{-}10^\circ$  gentler, and are  $\sim 40\%$  longer than similar north-facing slopes. Reduced water storage and evapotranspiration at pedon-scales on south-facing slopes allows more water to drain through the subsurface, increasing runoff potential, which, in conjunction with reduced cohesion, promotes drainage incision and expansion. Accelerated denudation of south-facing catchments likely makes them more responsive to incision signals, increases competition for drainage area, and causes divide

migration and catchment elongation. However, asymmetric denudation and elongation produce gradient changes that counteract and attenuate aspect-induced erosion differences and drive valley asymmetry development toward a dynamic equilibrium. Valley asymmetries appear to reflect landscape climate-sensitivity and proximity to stable states, and may be useful for predicting landscape responses to climate change.

### **3.1 Introduction**

Climate is a primary control of landscape evolution; different climates produce contrasting landscapes. Spatial variations in climate affect pedogenic and biotic processes (e.g. mineral weathering, photosynthesis, plant and soil respiration, nutrient cycling, and soil and root cohesion), which alter hydrologic storage and partitioning, and ultimately dictate the forces driving erosion (e.g. runoff, diffusive processes, and mass wasting) and resisting erosion (e.g. soil and root cohesion, and particle size and texture). Spatial variability in climate affects a range of hillslope and catchment characteristics (Carson and Kirkby, 1972; Rodríguez-Iturbe and Rinaldo, 2001), including drainage density and slope steepness, weathering and transport limited erosion, and types of dominant geomorphic processes (e.g. glacial, fluvial, and diffusive erosion).

Landscape responses to climate are inherently complex; Landforms arise from landscape processes, while simultaneously moderating those processes. Landforms coevolve with and are dynamically coupled with ecologic, biologic, hydrologic, and geologic processes (Rinaldo et al., 1995; Rodríguez-Iturbe and Rinaldo, 2001; Troch et al., 2015). Negative feedbacks among land surface processes cause landscapes to evolve towards dynamic equilibria (i.e. stable states; Pelletier et al., 2015). However, landscape response timescales are long relative to the response timescales of vegetation ( $10^3$ - $10^6$  vs

$10^0$ - $10^2$  years; Whipple, 2001), and older landscapes may reflect a range of past climates, and be in disequilibrium with modern climate (e.g. glacial landscapes; Howard, 1965; Bull, 1975; Rinaldo et al., 1995), effectively chasing their equilibrium conditions. However, while landscapes may be in disequilibrium with climate over shorter time-scales, over longer time-scales they may be near equilibrium with time-averaged climatic conditions.

Landform aspect can be used to assess how landscapes evolve under different climates because it produces a consistent unidirectional climate forcing. Equator-facing slopes get more sunlight and are warmer than pole-facing slopes, driving eco-pedo-hydro-geomorphic feedbacks that result in different landforms, and culminate in valley asymmetry. Aspect-related differences in slope steepness are widespread and globally prevalent on the majority of mountainous landforms, producing patterns with latitude, elevation, and mountain range-scale topography (Poulos et al., 2012). Valleys serve as natural laboratories for studying how aspect-induced climate perturbation affects landscape evolution. Valley side-slopes face opposite directions, producing aspect-induced climate variability, while other sources of variability are often similar between adjacent slopes (e.g. past regional climates, lithology, and base level). Investigating the specific mechanisms of valley asymmetry development may help us understand how landscapes respond to climate.

At pedon-scales, we know that aspect affects insolation and the surface energy balance, which has cascading effects on coupled ecologic, hydrologic, and pedologic characteristics. Subsurface characteristics (e.g. the field capacity) dictate the pedon-scale water balance, altering water retention and partitioning, and growing season length

(Smith, 2010; Geroy et al., 2011). In most landscapes, runoff is primarily generated from soil and groundwater drainage along subsurface flow paths, rather than via overland flow, because infiltration generally greatly exceeds precipitation rates in semi-arid terrain (Anderson and Anderson, 2010; Dingman, 2015). Where runoff dominantly occurs along subsurface flow paths, storage deficits dictate how much water must be supplied before runoff occurs. It follows that aspect-induced perturbations to the pedon-scale water balance should affect catchment-scale runoff processes.

At catchment-scales, we know that runoff production affects the efficacy of fluvial processes and drainage development, and that this is reflected in drainage scaling relationships (e.g. drainage density and slope/drainage area relationships; Montgomery and Dietrich, 1989; Rodríguez-Iturbe and Rinaldo, 2001; McNamara et al., 2006). However, we don't know how aspect-induced differences in hydrologic processes at pedon-scales are linked with catchment-scale drainage evolution. Are there aspect-related differences in water-balance-dependent landforms (i.e. drainage networks)?

Although some works present differences in fluvial efficacy with aspect (e.g. Gutiérrez-Jurado et al., 2007; Yetemen et al., 2010), most studies of aspect occur in relatively small catchments, where drainage development is minimal or absent on one or both of the opposing sides, and the complexities of drainage form cannot be rigorously studied. We investigate the relationship between drainage forms and hydrologic processes within larger scale valleys, where drainages on both valley sides are sufficiently developed to exhibit measurable differences in form.

This work establishes a mechanistic link between aspect-induced changes in eco-hydro-pedo-geomorphic processes at pedon-scales and valley-scale development of

drainage and slope asymmetry. We show that aspect-induced differences in water balances at the soil pedon scale result in differences in subsurface runoff generation at catchment scales. Hydrologic data are used to demonstrate that south-facing valley side slopes have a lower water storage deficit, which increases their potential for runoff generation, while landform data shows that their drainages are more deeply incised, extensive, and dense, which, when coupled with gradient-induced acceleration of diffusive processes, allows them to compete more effectively for drainage area, resulting in divide migration and elongation of catchments and land surfaces and more-pronounced valley asymmetry. Erosion rate data are used to show that, despite the dramatic aspect-related differences in landscape characteristics, asymmetry is not actively developing over Holocene timescales, demonstrating that the faster degradation of south-facing slopes and divide migration serve as negative feedbacks, via gradient reductions, that drive valley asymmetry development toward a dynamic equilibrium.

### **3.2 Study Area**

We build upon existing aspect-related eco-pedo-hydrologic data from the Dry Creek Experimental Watershed (DCEW; <http://earth.boisestate.edu/drycreek/>). The watershed is ~27 km<sup>2</sup> in size and spans elevations from 1025 to 2130 m.a.s.l. in the foothills of the Idaho batholith northeast of Boise, Idaho, USA (Figure 3.1). Average annual precipitation increases with elevation from ~300 to 1000 mm, and roughly half the precipitation occurs as snow, with more snow at higher elevations (McNamara, 2005; Aishlin and McNamara, 2011).

Aspect-induced microclimates significantly influence the water balance and ecosystems in the DCEW. Prior research has characterized aspect-related variability in

snowpack distribution, snowmelt dynamics, soil moisture variability, soil depth, soil texture, soil bulk density, soil hydrologic properties, soil carbon and nitrogen availability, vegetation type and productivity, and growing season length (Table 3.1; Tesfa et al., 2009; Smith, 2010; Geroy et al., 2011; Kunkel et al., 2011; Smith et al., 2011; Anderson et al., 2014; Kormos et al., 2014; Loughridge, 2014; Kormos et al., 2015). North-facing slopes within valleys in the DCEW are visibly steeper, shorter, and more densely vegetated than the opposing south-facing slopes, producing a strikingly asymmetric view in cross-section (Figure 3.2). The abundant existing data, methods, and instrumentation for the area facilitate understanding how land surface aspect affects water retention, evapotranspiration, vegetation characteristics, and runoff production, as well as how drainages erode, incise, and expand, and how catchment and hillslope forms evolve.

The DCEW is incised into the southwestern margin of the Atlanta lobe of the Idaho batholith, and is underlain by mostly-homogenous granodiorite that varies in composition (e.g. potassium feldspar content) and degree of hydrothermal alteration (Clayton et al., 1979; Clemens, 1993), and hosts occasional Tertiary intrusive dikes (Kiilsgaard et al., 1997). Jointing is evident in exposed bedrock, but the orientation of the valleys does not coincide with the prevailing fracture orientations of the underlying bedrock (Hoffman, 2008), nor with the orientation of major faults in the region (Clemens, 1993).

Insolation reductions on north-facing slopes in the DCEW effectively reduce energy budgets for snowpack melt, sublimation, and evapotranspiration, allowing snowpack and soil moisture to persist longer on north-facing slopes (Smith et al., 2011; Anderson et al., 2014; Kormos et al., 2014). North-facing slopes generally retain

moisture later into the year and have a longer growing season, which allows them to support denser and different vegetation (Smith, 2010).

Vegetation covaries with hillslope aspect and elevation. Lower elevations and south-facing slopes tend to support sagebrush-steppe ecosystems, composed of big sagebrush (*Artemisia tridentata*), rubber rabbitbrush (*Ericameria nauseosa*), antelope bitterbrush (*Purshia tridentate*), cheatgrass (*Bromus tectorum*), and rush skeletonweed (*Chondrilla juncea*), while higher elevations and north-facing slopes often support coniferous forests composed primarily of Douglas fir (*Pseudotsuga menziesii*) and ponderosa pine (*Pinus ponderosa*). Insolation reductions allow conifers to exist at lower elevations on northern aspects, effectively shifting the moisture-limited lower treeline down in elevation (Figures 3.1 and 3.2).

### 3.3 Methods

Topography was characterized from Digital Elevation Models (DEMs), which were derived at 1 m and 5 m resolution from airborne Light Detection and Ranging (LiDAR) point cloud elevations (e.g. Shallcross et al., 2011) using the BCAL LiDAR Tools (<http://bcal.boisestate.edu/tools/lidar>). The LiDAR-derived DEMs were used to calculate slope, aspect, curvature, annual (2011) insolation, and flow direction and accumulation (i.e. upslope drainage area), which were used to delineate drainage networks and catchments. Insolation and slope angles were compared to aspects by calculating the frequency and average values of insolation and slope angles within 1° aspect bins, as well as by assessing insolation and slope angle distributions within 90° aspect bins.

For 21 catchments incised into the prevailing north and south-facing valley side-slopes, drainage networks and catchment boundaries were delineated using a flow accumulation (i.e. drainage area) threshold of  $\sim 10,000 \text{ m}^2$ , which was selected based on the fit with catchment heads evident in 1 m hillshaded elevation and slope rasters. Drainage networks and catchments extents were used to calculate drainage density (e.g. drainage length / catchment area) and ruggedness (e.g. catchment relief \* drainage density).

When valley side slopes have been dissected by drainage development, such as in the DCEW, linear valley cross-sections cut across smaller-scale ridgelines and catchments, making it difficult to unbiasedly select cross-section locations for studying valley asymmetry. To avoid bias, we produced valley cross-sections of drainages and ridgelines by extracting non-linear longitudinal profiles from 1 m DEMs along main drainages (i.e. following the greatest drainage area up the network) for each catchment incised into the larger-scale valley side-slopes as well as along the ridgelines between catchments (i.e. divides). Longitudinal profiles were used to visually compare land surface length, linearity, vertical relief, and overall gradient. Ridgelines are the landforms that are visually prominent when looking up and down-valley, and thus capture the valley asymmetry evident in the field (e.g. Figure 3.2).

We estimated the minimum volumes of material eroded, or missing, from each of the 21 catchments incised into the larger-scale north and south-facing hillslopes by reconstructing the prevailing land surface over these drainages (Figure B1). Interpolation of ridgeline elevation data across catchments yielded a new DEM where catchments were effectively filled to ridgeline elevations. The total volume missing from each catchment

was calculated by subtracting the original DEM from the filled surface, multiplying by the pixel size, and summing all pixels. Minimum eroded volumes do not reflect total erosion rates, because we cannot account for ridgeline lowering. Rather, the minimum volumes of material removed (i.e. missing) from catchments reflect differences in the efficacy of fluvial processes, which deepen valleys and increase volumes, and diffusive processes, which lower ridgelines and decrease volumes. Normalizing (i.e. dividing) volume estimates by catchment size resulted in catchment-averaged incision depths.

Active ephemeral channel heads for several catchments incised into north and south-facing slopes were surveyed using a handheld GPS and compared to channel heads derived from 1 m DEMs. Active channels and channel heads were identified by evidence of recent surface flow, such as sediment sorting, observable channels forms, absence of soil cover, and defined banks.

Slopes and curvatures were compared with drainage areas to study hydro-geomorphic scaling relationships, which reflect changes in process efficacy between diffusive and fluvial domains, channel initiation, and hydro-geomorphic process coupling (Tarboton et al., 1992; Dietrich et al. 1993; McNamara et al., 2006; Istanbuluoglu et al., 2008; Yetemen et al., 2011). Curvatures were calculated from 5 m resolution DEMs because they are scale-dependent and we sought to capture the curvature of landforms rather than smaller natural heterogeneities (e.g. burrows and tree-throw pits).

### **3.4 Results**

Southern aspects are less steep in general in the Dry Creek Experimental Watershed (DCEW), with gentler slopes on convexities and ridgelines (Figure 3.3). Northern aspects are  $\sim 6^\circ$  steeper on average, with a median value of  $31.1^\circ$  vs  $24.9^\circ$

(Figure 3.4). Slopes of  $\sim 33^\circ$  and  $\sim 27^\circ$  are the most frequent slope angles for north and south-facing slopes, respectively. Slope angles on north-facing valley sides are consistently steep at most hillslope and catchment positions, while slopes on south-facing valley sides are more variable (Figures 3.3 and 3.4). North-facing slopes had a higher kurtosis value of 4.3, indicating a sharper and narrower distribution, while south-facing slopes had a kurtosis of 3.0. North-facing slope distributions (Figure 3.4) exhibit greater negative skew (-0.96) indicating the prevalence of steeper slopes, while south-facing slopes exhibit less skew (-0.27), indicating more gentle slopes. Slope distributions change gradually with aspect (Figure B2); slope angles gradually increase, and slope distributions become tighter, transitioning from southern aspects to northern aspects.

South-facing slopes occupy  $8.7 \text{ km}^2$  of the  $27 \text{ km}^2$  DCEW, whereas only  $4.6 \text{ km}^2$  faces north, which is also reflected in valley side-slope (i.e. land surface) lengths. Hillslope aspect varies significantly at scales smaller than the dominant valley side-slopes within the Dry Creek Experimental Watershed (DCEW). The fractal nature of smaller-scale drainage development produces a wide-range of aspect orientations within the drainages incised into the prevailing north and south-facing valley side-slopes. However, a majority of northern and southern aspects are associated with the dominant north and south-facing valley side-slopes, respectively, along the two major east-west trending valleys at mid-high elevations ( $\sim 1400\text{-}1800 \text{ m}$ ; Figure 3.2a), as well as along the east-west trending segment at low elevations ( $\sim 1000\text{-}1400 \text{ m}$ ; Figure 3.2b).

Median modeled annual clear-sky insolation (i.e. potential insolation) values (Figure 3.5) were  $\sim 1.5 \times 10^6 \text{ WH/m}^2$  for south-facing slopes, compared to  $\sim 0.9 \times 10^6 \text{ WH/m}^2$  for north-facing slopes. Frequency plots of specific insolation/aspect

combinations (Figure B3) show that, similar to the changes in average slope angles with aspect, insolation distributions change gradually with aspect. Reduced insolation on northern aspects is associated with steeper slopes, while increased insolation on southern aspects correlates with gentler slopes; median insolation values are inversely-correlated with median slope angles across all aspects (Figure 3.6).

Stream networks are more extensive on south-facing land surfaces, and appear to have expanded headwards (Figure 3.1). Within the three major east-west trending valleys segments analyzed, longitudinal stream profiles for the catchments incised into the north and south facing valley side-slopes show that drainages on north-facing hillsides are consistently steeper, shorter, and more linear in form than drainages incised into south-facing slopes, which exhibit more variability in form (Figure 3.7; Figures B4-B5). For the two upper elevation valleys, stream profiles for south-facing slopes were ~60% longer (Figure 3.7) which is primarily due to differences in the horizontal relief, as vertical relief is similar among streams on either side of the valley.

Profiles of the ridgelines between the catchments incised into the larger-scale north and south-facing slopes (i.e. the ridgelines that define the v-shaped valley form) show that north-facing ridgelines are also steeper, shorter, and more linear in form (Figure 3.7; Figures B6-B7). Similar to the streams, the ridgelines in the upper valleys were ~60% longer on south-facing slopes, which, primarily reflect differences in the horizontal distance from drainage-divide to basal stream, rather than vertical relief which is similar among the ridgelines on either side of each east-west trending valley assessed (Figure 3.7).

North-facing slopes are  $\sim 5\text{-}10^\circ$  steeper than south-facing slopes, on average, at most drainage areas (Figure 3.8a), despite changes in process dominance from diffusive to fluvial domains. Comparison of changes in average slope angles with upslope drainage area show that slopes generally increase with increasing drainage area until they reach a turn-over point after which slopes generally decrease with increasing drainage area (Figure 3.8a). This turn-over occurs at a critical drainage area which roughly corresponds with the transition from convex to concave topography, and the change from diffusive to fluvial process dominance (Dietrich et al., 1993; McNamara et al., 2006; Istanbuluoglu et al., 2008; and Yetemen et al., 2011). Both north and south-facing slopes turn over at roughly the same drainage area ( $50\text{-}60\text{ m}^2$ ), but slopes decline much more rapidly with increasing drainage area for south-facing slopes, and the greatest differences in slope occur at high drainage areas.

The transition from convex to concave topography occurs at  $\sim 40\text{ m}^2$  drainage area for both north and south-facing slopes (Figure 3.8b), which is similar to the  $\sim 60\text{ m}^2$  turn-over point observed for the slope trends (Figure 3.8a). Total curvature (measured over a 5 m scale) is not significantly different at low drainages (Figure 3.8b), but north-facing slopes have slightly less negative total curvatures (i.e. concavities) at higher drainage areas.

Catchments incised into south-facing land surfaces were 51% larger, on average, compared to north-facing slopes (Figure 3.3; Table 3.2). Additionally, total stream network lengths for catchments incised into south-facing valley side-slopes were 94% longer, on average, than those for north-facing valley side-slopes. South-facing catchments had 30% greater drainages densities, and were 24% more rugged. Relief was

not significantly different between north and south-facing slopes. The total volumes of material removed (i.e. missing) from south-facing catchments were 29% greater than those for north-facing slopes.

Most of the increased drainage area of south-facing catchments (Figure 3.8c) occurs at drainage areas  $<60 \text{ m}^2$  (i.e. the slope turn-over point in Figure 3.8a) and with positive curvature (i.e. gentle and convex upper hillslopes; Figure 3.8b). Drainage areas were less than  $60 \text{ m}^2$  in south-facing catchments 80% of the time, compared to 72% of the time in north-facing catchments, indicating that south-facing slopes contain more low drainage areas (i.e. upper hillslopes).

North and south-facing catchments exhibited a similar number of pixels at intermediate drainage areas, but south-facing slopes exhibit more high drainage area pixels (i.e. greater probability of exceedance in Figure 3.8d). Drainage areas exceeded  $10^4 \text{ m}^2$  in south-facing catchments 0.70% of the time, but only 0.56% of the time for north-facing catchments, indicating that south-facing catchments have ~24% more high drainage areas (i.e. streams). The probability of exceeding a given drainage area declined more rapidly with increasing drainage area for north-facing catchments (Figure 3.8d).

North and south-facing catchments exhibited a similar amount of intermediate drainage areas (Figure 3.8c), despite the greater abundance of low and high drainage area pixels for south-facing catchments.

Active channel heads occurred near catchment heads for all four catchments surveyed on south-facing valley sides. In contrast, for north-facing catchments, active channel heads were absent or occurred near the catchment outlets, and the drainage

networks evident in catchment landforms were mantled by soil, leaf litter, and dense vegetation, with no evidence of fluvial transport.

### **3.5 Discussion**

#### **3.5.1 North-Facing Catchment Response to Decreased Insolation**

Insolation reductions on northern aspects in semi-arid ecosystems generally stabilize slopes at steeper angles by reducing soil and regolith erodability. Northern aspects support denser vegetative biomass with larger woody roots (e.g. trees vs shrubs and grasses; Smith, 2010; Loughridge, 2014), and produce finer-grained (i.e. more clay and silt), organic-enriched, and more cohesive soils (Smith, 2010; Geroy et al., 2011). Stabilizing north-facing slopes while drainages incise induces steepening, which further reduces insolation (i.e. a positive feedback). However, as slopes approach a critical angle of stability (e.g. angle of repose) erosion rates increase exponentially (Roering et al, 1999), and degradation acts as a negative feedback that prevents further steepening and maintains slopes near the critical angle of repose. This explains why the north-facing slopes are consistently steep and planar (Figures 3.2-3.4). It is often inferred that steeper slopes erode more quickly, but the characteristics of the north-facing slopes suggest that stability promotes steepening (i.e. the ability to maintain steepness reflects stability), they are stable at steeper slopes angles, and have eroded less overall (e.g. overall land surface gradient).

The increased stability of north-facing slopes appears to promote thickening of the regolith cover. If erosion is slower on north-facing slopes, this might allow regolith production to outpace denudation and the regolith mantle will become thicker. However, as the regolith mantle thickens, the bedrock becomes increasingly distanced and buffered

from weathering and production slows. Additionally, thicker soils become prone to shallow landsliding and accelerated erosion (Heimsath et al., 2005), especially if the slopes are near critical slopes angles and are disturbed (e.g. following fire). The convergence of regolith production and denudation drives regolith thickness to a dynamic equilibrium soil depth (Heimsath et al., 1997).

Aspect-induced eco-pedo-hydrologic feedbacks also appear to increase the erosivity of processes in north-facing catchments. The finer-grained, less dense, and more organic rich soils mantling northern aspects retain more water per-unit volume (i.e. higher field capacity), while thicker regolith cover increases the total volume (Tesfa et al., 2009; Geroy et al., 2011; Smith et al., 2011; Kormos et al., 2015). A relatively larger proportion of water will be retained on north-facing slopes and lost as evapotranspiration, rather than runoff. Plants build a storage deficit by depleting stored water, and more water is required to fill the available water storage before connectivity and drainage to the ground water can occur. Increased water storage demand and retention on north-facing slopes reduces subsurface drainage potential, which likely reduces stream flow production and fluvial process efficacy.

Aspect-induced insolation reductions appears to promote stabilization and regolith mantle thickening, which increases soil water retention and evapotranspiration , and decreases fluvial process dominance (Figure 3.9). Simultaneously, regolith thickening increases diffusive and mass wasting process efficacy, and appears to produce north-facing catchments that are simple, linear, and chute-like, with a lower drainage density.

Both the erodability of the regolith and the erosivity of processes appear to be decreased for north-facing catchments and land surfaces. In north-facing catchments, if

less water is allowed to drain through the subsurface or over the surface to streams, naturally more drainage area will be required to concentrate enough water to saturate hollows or cause overland flow and promote channel initiation. North-facing drainages do not transition to slope-drainage-area space power-log exponent (slope) values typical of developed channels (e.g. Flint, 1974; McNamara et al., 2006) until higher drainage areas (Figure 3.8a). In fact, modern channel heads were often located near the outlets of north-facing catchments, far below the catchment head, and their steep chute-like catchment bottoms above the channel heads appear relatively inactive and are mantled by unincised colluvium that likely gets eroded and flushed out episodically following fire.

### 3.5.2 South-Facing Catchment Response to Increased Insolation

In south-facing catchments, eco-pedo-hydrologic feedbacks appear to produce shallower, coarser, denser, and less porous soil and regolith that decreases water retention and evapotranspiration (Smith, 2010; Geroy et al., 2011), shortens growing seasons (Smith, 2010), and allows more water to drain freely into the subsurface (Figure 3.9; Kormos et al., 2015). In addition, increased regolith density and reduced porosity likely reduce infiltration rates and make south-facing catchments more prone to infiltration-excess overland flow. Additionally, the more arid conditions on south-facing slopes promote hydrophobicity and overland flow, and increase post-fire response (Noske et al., 2016). South-facing drainages are active under modern conditions, with incised channels, defined banks, and evidence of sediment sorting and ephemeral flow. Increased runoff potential per unit drainage area, in conjunction with increased regolith erodability (e.g. reduced root and soil cohesion), appear to increase the efficacy of fluvial processes. Fluvial processes scale more strongly with drainage area in south-facing catchments,

which causes their channel slopes to decline more rapidly with increasing drainage area (Figure 3.8a). Catchments incised into south-facing land surfaces exhibit drainages that are more deeply incised (e.g. volume removed; Table 3.2), more extensive (e.g. drainage length and density, and catchment area), and have gentler channels (i.e. more degraded; Figure 3.7). Greater fluvial process efficacy on south-facing slopes explains why south-facing drainage networks are more incised, extensive, denser, and complex.

The upper hillslopes in south-facing catchments are also gentler (i.e. more degraded). Average gradients are  $\sim 5\text{-}10^\circ$  gentler on south-facing slopes at all drainage areas (Figure 3.8a), indicating that diffusive processes are able to keep up with accelerated drainage incision. Diffusive process may be more efficient on south-facing slopes because of reduced soil and root cohesion, increased exposure to rain, and more extreme daily temperature cycles (Smith, 2010), which likely increases the number of freeze thaw cycles (e.g. Anderson et al., 2015).

### 3.5.3 Fluvial-Diffusive Process Coupling and Incision Signal Propagation

In steep landscapes, hillslopes are intimately connected with drainage networks because drainage incision defines the lower boundary conditions of hillslopes. Steep gradients inhibit sediment storage in valley bottoms, which can disconnect hillslopes from drainage incision signals. In the absence of floodplains, connectivity is dictated by the transitional zone of mass wasting between zones of diffusive and fluvial process dominance. Sediment stored within small upland catchment hollows serve as dynamic buffers between drainages and hillslopes. North-facing catchments are steeper at all drainage areas, but the greatest aspect-related differences in slope occur at steep transitional drainage areas (i.e. lower slopes and hollows). Differences in mass wasting

processes (e.g. colluvial hollow failure) in transitional drainage areas appear to produce the strongest slope asymmetry between north and south-facing catchments.

Interestingly, despite accelerated fluvial processes in south-facing catchments, the transitions from the convex upper to concave lower slopes (i.e. slope-drainage-area turn-over points in Figure 3.8a), which reflect a change from diffusive to mass-wasting process dominance (McNamara et al., 2006), occur at similar critical drainage areas (e.g.  $\sim 60 \text{ m}^2$ ) for both north and south-facing catchments. However, the transitional mass-wasting zone on north-facing slopes spans two orders of magnitude in drainage area, on average (flatter section of blue line at intermediate drainage areas; Figure 3.8a), which buffers, and may disconnect, the upper hillslopes from the bottom-up influence of drainage incision, making them less geomorphically-responsive. Diffusive processes on both sides of the valley appear to adjust and scale with their different rates of drainage incision. Drainage-hillslope coupling is evident in the scaling between average slope angles and drainage area (Figure 3.8a); despite changes from diffusive processes to mass-wasting and fluvial processes with increasing drainage area, differences in average slope angles between north and south-facing slopes change gradually. Additionally, stream and ridgeline profiles across valleys (Figure 3.7) exhibit similar gradients and valley asymmetries, suggesting that diffusive hillslope processes scale with fluvial processes, and that they share a common control, such as the bottom-up control of changes in base level and knick point propagation.

As drainages incise, adjacent toe slopes are steepened, but over time they degrade faster to reduce their gradients to stable conditions (a negative feedback). Degradation propagates incision signals upslope in a wave-like fashion (Wood, 2013). Knick zone

migration rates within drainage networks exhibit a power-law dependency on drainage area (Crosby and Whipple, 2006). Extrapolating this concept to hillslopes, knick zone migration rates likely decline exponentially as they migrate upslope, with an overwhelming majority of the catchment response time depending upon diffusive processes on the upper hillslope. This suggests that although drainage incision drives land surface lowering rates, diffusive process efficacy is the rate-limiting factor of catchment response time.

#### 3.5.4 Catchment Competition, Divide Migration, and Valley Asymmetry Development

On north-facing valley sides, the efficacy of both fluvial and diffusive processes appear to be decreased due to reductions in both the erosivity of processes and the erodability of substrate. This likely reduces north-facing catchment response time, and their ability to compete at drainage divides for drainage area.

Rather than producing differences in vertical relief, enhanced drainage incision and land surface lowering of south-facing land surfaces appears to have allowed them to compete more effectively at the divides for drainage area, causing the divides between the north and south-facing valley sides of adjacent valleys to shift northward. This leads to horizontal lengthening of south-facing valley sides, further reducing overall gradients, and shortening and steepening of north-facing valley sides, which enhances valley asymmetry.

If divide migration were to continue unchecked, one might expect south-facing land surfaces to continue to elongate and eventually capture all drainage area from north-facing slopes. Such a one-directional response would reflect a predominance of positive feedbacks. For example, divide migration and elongation of south-facing valley sides

should cause them to intercept more precipitation, further increasing differences in runoff and maximum flow accumulation. Runaway drainage dynamics like this might be an explanation for the dramatic differences in land surface horizontal lengths observed for some environments (e.g. the Gabilan Mesa; Dohrenwend, 1978; Richardson et al., 2014).

Importantly, negative feedbacks counteract positive feedbacks and slow valley asymmetry development. Asymmetric denudation and gradient reduction serves as a negative feedback that reduces aspect-induced differences in erosion and competition at divides. Additionally, divide migration inherently alters the gradient of the land surfaces by changing horizontal land surface relief, while the vertical relief is held similar between land surfaces sharing a divide; Divide migration causes south-facing land surfaces to become lower gradient (i.e. degrade), while north-facing land surfaces maintain or increase their gradients. Additionally, increased south-facing land surface length increases the distance knick-point-driven land surface lowering signals must travel to reach the divide, while the effect is opposite for north-facing land surfaces.

Valley asymmetry development appears to counteract aspect-induced erosion differences, serving as a negative feedback that slows valley asymmetry development and drives the system towards a stable state (i.e. a dynamic equilibrium) (Figure 3.10). Essentially, valley asymmetry development is a mechanism by which landscapes adjust towards a state of energy minimization and equalize erosion between opposite valley sides.

If the DCEW valleys are near a stable state, and valley asymmetry has not been actively developing, it could explain why Holocene (0-8 Ma) erosion rates did not differ significantly between north and south-facing catchments (Chapter 1), despite the

dramatic differences in landforms, soils, and vegetation. Erosion rates for north and south-facing land surfaces in other landscapes with pronounced asymmetry were also not significantly different over Holocene and late Quaternary timescale (e.g. West et al., 2014; Foster et al., 2015). In addition to reflecting how landscapes respond to climate perturbation over longer timescales, valley asymmetry may serve as useful remotely-measurable indicator of a landscape's proximity to dynamic equilibrium.

We hypothesize valley asymmetry develops as an initial system response to aspect-induced erosion differences following drainage initiation, when the system is far from equilibrium, and that rates of development diminish over time. Valley asymmetry may also readjust when the system is disturbed from dynamic equilibrium (e.g. longer term changes in climate, land cover, and uplift). Counterintuitively, landscapes with more pronounced asymmetry may exhibit little difference in erosion rates with aspect.

### **3.6 Conclusions**

In the semi-arid, montane, and granodioritic Dry Creek Experimental Watershed (DCEW), aspect-induced differences in water balances at the soil pedon scale appear to result in differences in subsurface runoff generation at catchment scales, which increases fluvial process efficacy and scaling with drainage area, accelerates tightly coupled diffusive processes, and alters drainage incision, expansion, and competition. South-facing valley sides exhibit more deeply incised drainages that appear to have expanded headward, resulting in longer, lower-gradient catchments, and shifting divides between north and south-facing catchments northwards. Valley asymmetry appears to be driven by a combination asymmetric degradation, divide migration, and changes in the length of valley sides, but this response appears to serve as a negative feedback that slows valley

asymmetry development. Asymmetric valley side degradation and elongation (i.e. valley asymmetry development) counteracts aspect-induced erosion differences and causes land surface lowering rates to become increasingly similar. This negative feedback drives landscape evolution towards a dynamic equilibrium where valley asymmetry is preserved and divides are stabilized. This suggests that landscapes respond to aspect-related differences in insolation and microclimate by evolving to mitigate differences in erosion, and that landscapes with more developed asymmetry are more essentially more geomorphically mature, with similar erosion rates throughout the system despite dramatic variability in factors affecting erosion (e.g. vegetation, soils, and landforms). In addition to inherently reflecting the climate sensitivity of a landscape, aspect-related differences in land surface characteristics (e.g. valley asymmetries) may serve as useful and mappable indicators of the geomorphic maturity of landscapes and their proximity to dynamic equilibria (i.e. stable states).

### 3.7 References

- Anderson, R. S., Anderson, S. P., & Tucker, G. E. (2013). Rock damage and regolith transport by frost: an example of climate modulation of the geomorphology of the critical zone. *Earth Surface Processes and Landforms*, 38(3), 299-316.
- Anderson, B. T., McNamara, J. P., Marshall, H. P., & Flores, A. N. (2014). Insights into the physical processes controlling correlations between snow distribution and terrain properties. *Water Resources Research*, 50(6), 4545-4563.
- Bull, William B. (1975). Allometric change of landforms. *Geological Society of America Bulletin* 86.11, 1489-1498.
- Burnett, B. N., Meyer, G. A., & McFadden, L. D. (2008). Aspect-related microclimatic influences on slope forms and processes, northeastern Arizona. *Journal of Geophysical Research: Earth Surface*, 113(F3).
- Clayton, J. L., Megahan, W. F., & Hampton, D. (1979). *Soil and bedrock properties: weathering and alteration products and processes in the Idaho batholith*. United States. Intermountain Forest and Range Experiment Station. USDA Forest Service research paper INT (USA). Research: Earth Surface (2003–2012), 113(F3).
- Clemens, D. M. (1993). *Tectonics and Silicic Volcanic Stratigraphy of the Western Snake River Plain, Southwestern Idaho*. Master's thesis, Arizona State University.
- Churchill, R. R. (1982). Aspect-induced differences in hillslope processes. *Earth Surface Processes and Landforms*, 7(2), 171-182.
- Crosby, B. T., & Whipple, K. X. (2006). Knickpoint initiation and distribution within fluvial networks: 236 waterfalls in the Waipaoa River, North Island, New Zealand. *Geomorphology*, 82(1), 16-38.
- Dietrich, W. E., Wilson, C. J., Montgomery, D. R., & McKean, J. (1993). Analysis of erosion thresholds, channel networks, and landscape morphology using a digital terrain model. *The Journal of Geology*, 259-278.
- Dingman, S. L. (2015). *Physical hydrology*. Waveland press.

- Dohrenwend, J. C. (1978). Systematic valley asymmetry in the central California Coast Ranges. *Geological Society of America Bulletin*, 89(6), 891-900.
- Emery, K. O. (1947). Asymmetrical Valleys of San Diego Country, California. *Bulletin of the Southern California Academy of Science*, Vol. 46 (1947), pp. 61-71.
- Foster, M. A., Anderson, R. S., Wyshnytzky, C. E., Ouimet, W. B., & Dethier, D. P. (2015). Hillslope lowering rates and mobile-regolith residence times from in situ and meteoric  $^{10}\text{Be}$  analysis, Boulder Creek Critical Zone Observatory, Colorado. *Geological Society of America Bulletin*, 127(5-6), 862-878.
- Garrote, J., Cox, R. T., Swann, C., & Ellis, M. (2006). Tectonic geomorphology of the southeastern Mississippi Embayment in northern Mississippi, USA. *Geological Society of America Bulletin*, 118(9-10), 1160-1170.
- Geroy, I. J. (2010). *Factors influencing soil moisture at the hillslope scale in a semi-arid mountainous environment*. Master's thesis, Boise State University.
- Geroy, I. J., Gribb, M. M., Marshall, H. P., Chandler, D. G., Benner, S. G., & McNamara, J. P. (2011). Aspect influences on soil water retention and storage. *Hydrological Processes*, 25(25), 3836-3842.
- Gilbert, G. K. (1904). Systematic asymmetry of crest lines in the High Sierra of California. *The Journal of Geology*, 12(7), 579-588.
- Gutiérrez-Jurado, H. A., Vivoni, E. R., Istanbuluoglu, E., & Bras, R. L. (2007). Ecohydrological response to a geomorphically significant flood event in a semiarid catchment with contrasting ecosystems. *Geophysical Research Letters*, 34(24).
- Hack, J. T., & Goodlett, J. C. (1960). *Geomorphology and forest ecology of a mountain region in the central Appalachians (No. 347)*. United States Government Printing Office.
- Heimsath, A. M., Furbish, D. J., & Dietrich, W. E. (2005). The illusion of diffusion: Field evidence for depth-dependent sediment transport. *Geology*, 33(12), 949-952.

- Hoffman, B. A. (2008). *Scale and heterogeneity in hydraulic properties of the fractured granitic Boise front, Boise, Idaho* (Doctoral dissertation, Boise State University).
- Howard, Alan D. (1965). Geomorphological systems; equilibrium and dynamics. *American Journal of Science* 263.4, 302-312.
- Istanbulluoglu, E., Yetemen, O., Vivoni, E. R., Gutiérrez-Jurado, H. A., & Bras, R. L. (2008). Eco-geomorphic implications of hillslope aspect: Inferences from analysis of landscape morphology in central New Mexico. *Geophysical Research Letters*, 35(14).
- Kiilsgaard, T. H., Scanlan, T. M., & Stewart, D. E. (1997). Geology of the Boise Basin Vicinity, Boise, Ada, and Elmore Counties, Idaho. Idaho Geological Survey [University of Idaho].
- Kormos, P. R., Marks, D., McNamara, J. P., Marshall, H. P., Winstral, A., & Flores, A. N. (2014). Snow distribution, melt and surface water inputs to the soil in the mountain rain–snow transition zone. *Journal of Hydrology*, 519, 190-204.
- Kormos, P. R., McNamara, J. P., Seyfried, M. S., Marshall, H. P., Marks, D., & Flores, A. N. (2015). Bedrock infiltration estimates from a catchment water storage-based modeling approach in the rain snow transition zone. *Journal of Hydrology*, 525, 231-248.
- Kunkel, M. L., Flores, A. N., Smith, T. J., McNamara, J. P., & Benner, S. G. (2011). A simplified approach for estimating soil carbon and nitrogen stocks in semi-arid complex terrain. *Geoderma*, 165(1), 1-11.
- Loughridge, R. (2014). *Identifying Topographic Controls of Terrestrial Vegetation Using Remote Sensing Data in a Semiarid Mountain Watershed, Idaho, USA*. Master's thesis, Boise State University.
- McNamara, J. P., Chandler, D., Seyfried, M., & Achet, S. (2005). Soil moisture states, lateral flow, and streamflow generation in a semi-arid, snowmelt-driven catchment. *Hydrological Processes*, 19(20), 4023-4038.

- McNamara, J. P., Ziegler, A. D., Wood, S. H., & Vogler, J. B. (2006). Channel head locations with respect to geomorphologic thresholds derived from a digital elevation model: A case study in northern Thailand. *Forest Ecology and Management*, 224(1), 147-156.
- Melton, M. A. (1960). Intravalley variation in slope angles related to microclimate and erosional environment. *Geological Society of America Bulletin*, 71(2), 133-144.
- Noske, P. J., Nyman, P., Lane, P. N., & Sheridan, G. J. (2016). Effects of aridity in controlling the magnitude of runoff and erosion after wildfire. *Water Resources Research*.
- Poulos, M. J., Pierce, J. L., Flores, A. N., & Benner, S. G. (2012). Hillslope asymmetry maps reveal widespread, multi-scale organization. *Geophysical Research Letters*, 39(6).
- Powell, J. W. (1874). Remarks on the structural geology of the valley of the Colorado of the West. *Washington Philosophical Society Bulletin*, 1, 48 – 51.
- Richardson, P. W., Perron, J. T., & Miller, S. R. (2014, December). Microclimate-induced Lateral Channel Migration as a Driver for Hillslope Asymmetry in Semi-arid Landscapes. *AGU Fall Meeting Abstracts* (Vol. 1, p. 05).
- Rodríguez-Iturbe, I., & Rinaldo, A. (2001). Fractal river basins: chance and self-organization. *Cambridge University Press*.
- Roering, J. J., Kirchner, J. W., & Dietrich, W. E. (1999). Evidence for nonlinear, diffusive sediment transport on hillslopes and implications for landscape morphology. *Water Resources Research*, 35(3), 853-870.
- Shallcross, A. T. (2012). *LiDAR investigations of snow distribution in mountainous terrain*. Master's thesis, Boise State University.
- Smith, T. J. (2010). *Using Soil Moisture Trends Across Topographic Gradients to Examine Controls on Semi-arid Ecosystem Dynamics*. Master's thesis, Boise State University.

- Smith, T. J., McNamara, J. P., Flores, A. N., Gribb, M. M., Aishlin, P. S., & Benner, S. G. (2011). Small soil storage capacity limits benefit of winter snowpack to upland vegetation. *Hydrological Processes*, 25(25), 3858-3865.
- Tesfa, T. K., Tarboton, D. G., Chandler, D. G., & McNamara, J. P. (2009). Modeling soil depth from topographic and land cover attributes. *Water Resources Research*, 45(10).
- Tuck, R. (1935). Asymmetrical topography in high latitudes resulting from alpine glacial erosion. *The Journal of Geology*, 530-538.
- Weissel, J. K., & Seidl, M. A. (1997). Influence of rock strength properties on escarpment retreat across passive continental margins. *Geology*, 25(7), 631-634.
- Wende, R. (1995). Drainage and valley asymmetry in the Tertiary Hills of Lower Bavaria, Germany. *Geomorphology*, 14(3), 255-265.
- West, N., Kirby, E., Bierman, P., & Clarke, B. A. (2014). Aspect-dependent variations in regolith creep revealed by meteoric  $^{10}\text{Be}$ . *Geology*, 42(6), 507-510.
- Wood, R. (2013). *Transient Hillslope Response to an Incision Wave Sweeping up a Watershed: A Case Study from the Salmon River*. Master's Theses, San Jose State University, Paper 4322.
- Yetemen, O., Istanbuluoglu, E., & Vivoni, E. R. (2010). The implications of geology, soils, and vegetation on landscape morphology: Inferences from semi-arid basins with complex vegetation patterns in Central New Mexico, USA. *Geomorphology*, 116(3), 246-263.
- Zhang, K., Ma, Z., Grapes, R., & Peng, Z. (2014). Asymmetrical river valleys in response to tectonic tilting and strike-slip faulting, northeast margin of Tibetan Plateau. *Earth Surface Processes and Landforms*, 39(12), 1642-1650.

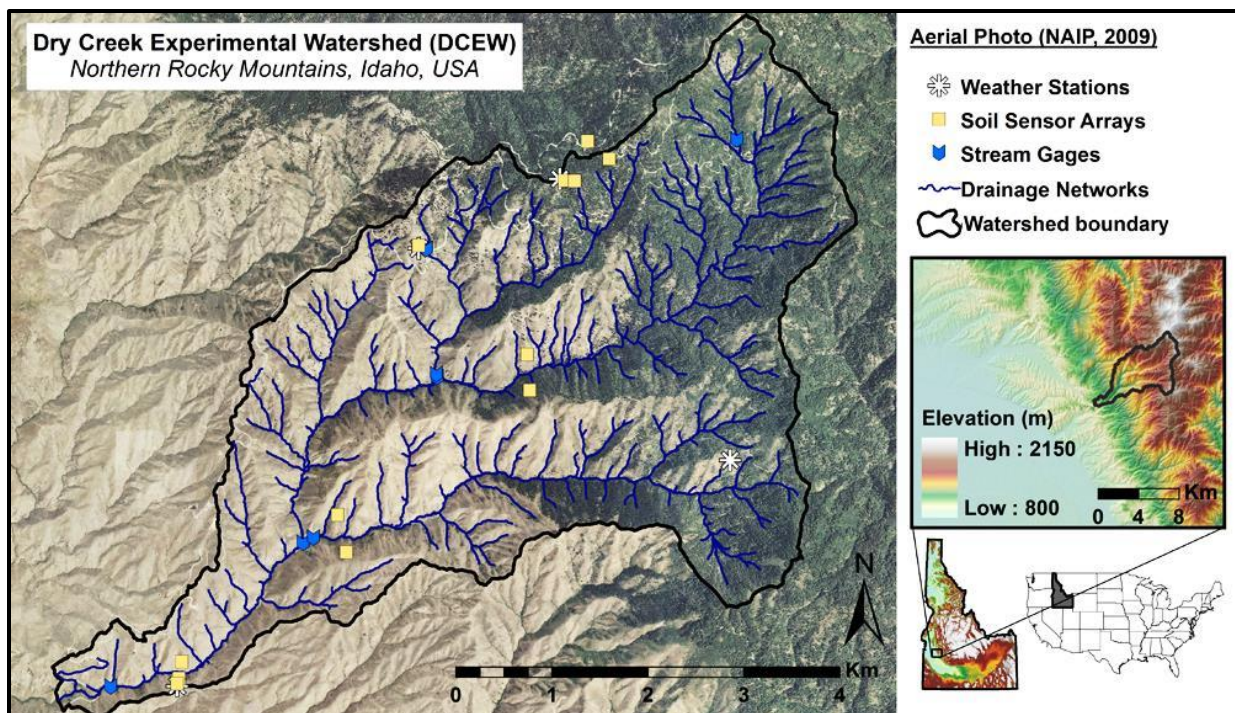


**Figure 3.1** Aerial photo of the Dry Creek Experimental Watershed (DCEW) showing forest cover (i.e. the moisture-limited lower treeline) extending to lower elevations on north-facing valley sides, and locations of instruments stratified across aspects and elevations. Note that drainage networks on south-facing land surfaces are generally more extensive and complex.



**Figure 3.2** Up-valley photos at a.) ~1400-1800 m elevation and b.) 1000-1400 m elevation. Note landform asymmetry, and position of the tree-line at lower elevations on northern aspects.

**Table 3.1 Summary of aspect-related variability in soils, water, and vegetation in the DCEW.**

<b>Variable Measured</b>	<b>Method</b>	<b>Aspect-related finding</b>	<b>Resulting publication</b>
<b>Snow Deposition &amp; Persistence</b>	Measured with 6 snow depth sensors, numerous snow surveys, and evident from 32 shallow soil temperature sensors, all stratified across aspects.	Snow deposits evenly across aspects. Snow pack persists later and accumulates deeper and denser on northern aspects.	Smith et al., 2011; Anderson et al., 2014; Kormos et al., 2014
<b>Snow Water Input Timing and Volume</b>	Evident from snow depth sensors, snow melt modeling, and moisture data from 32 shallow soil sensors on northern and southern aspects.	Snow melts and infiltrates more on southern aspects earlier in the spring, but more on northern aspects later in the spring.	Smith et al., 2011; Kormos et al., 2014
<b>Soil/Regolith Thickness</b>	Measured in 32 soil pits. Modeled from 949 distributed penetration measurements.	Soil and regolith cover is thicker on northern aspects.	Tesfa et al., 2009; Smith et al., 2011
<b>Soil/Regolith Texture</b>	Particle size distributions of 125 samples determined using hydrometer, sieving, and laser diffraction.	Soils on northern aspects are finer-grained, with more silt and clay, and less sand and gravel.	Geroy et al., 2011; Smith et al., 2011
<b>Soil Carbon &amp; Nitrogen</b>	Measured by soil sample combustion in an elemental analyzer for 923 soil samples.	Soils on northern aspects are richer in organic carbon and nitrogen, especially near the surface.	Kunkel et al., 2011; Smith et al., 2011
<b>Soil Bulk Density</b>	Measured by weighing 125 oven dried soil cores.	Soils on northern aspects are less dense, especially near the surface.	Geroy et al., 2011; Smith, 2010
<b>Soil Water Retention</b>	Measured by a progressive drainage laboratory experiment on 35 surficial soil core samples collected along a transect across north and south aspects.	Soils on northern aspects retain more water per unit soil volume at all soil water tensions (e.g. saturation, field capacity, wilting point).	Geroy et al., 2011; Smith et al., 2011
<b>Soil Water Persistence</b>	Evident from 121 soil moisture sensors at 3 to 4 depths among 32 pits on northern and southern aspects .	Soil water on northern aspects persists later into the dry season.	Smith et al., 2011; Kormos et al., 2015
<b>Soil Water Storage Capacity &amp; Drainage</b>	Capacity estimated by integrating field capacity values from moisture sensors with depth. Drainage estimated from a physically based energy-snow-soil model.	Soils on northern aspect store more water per unit volume and have higher total volumes, reducing subsurface drainage to bedrock.	Smith et al., 2011; Kormos et al., 2015
<b>Growing Season Length &amp; Productivity</b>	Inferred from seasonal changes in soil moisture and temperature, and vegetation productivity (NDVI).	Growing season lasts longer on northern aspects, yielding more vegetation productivity.	Smith, 2010
<b>Vegetation Type, Density, and Biomass</b>	Assessed across a range of aspects and elevations from vegetation plots, leaf area index, and field observations.	Northern aspects produce denser vegetation, greater biomass, and support forest down to lower elevations.	Kunkel et al., 2011; Smith et al., 2011; Loughridge, 2014

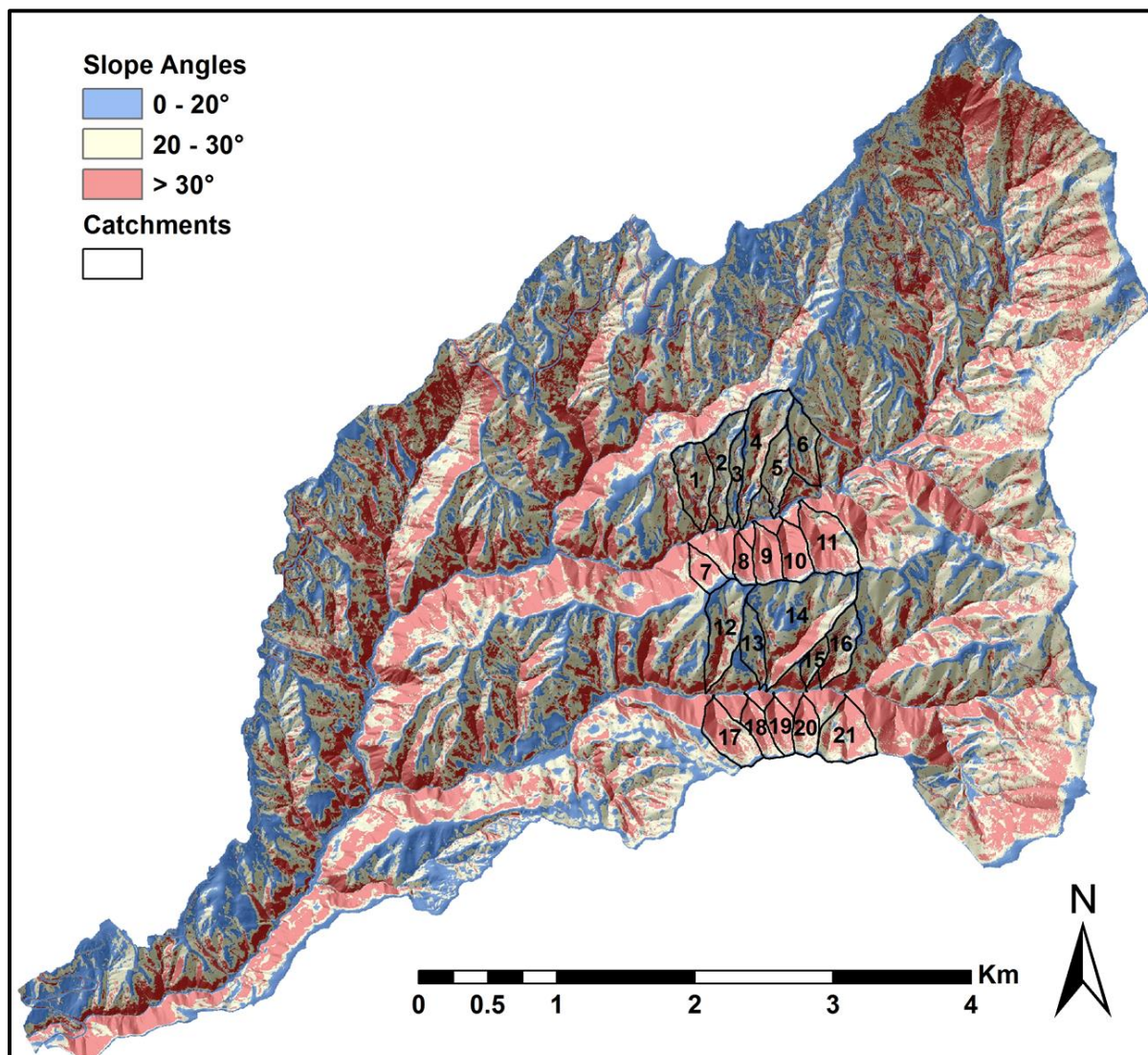


**Figure 3.3** Binned slope angle map showing difference in slope steepness between north and south-facing valley side-slopes. Note that north-facing slopes are consistently over  $30^\circ$  for the north-facing slopes along the major east-west trending drainages. The characteristics of the outlined north and south-facing catchments are summarized in Table 3.2.

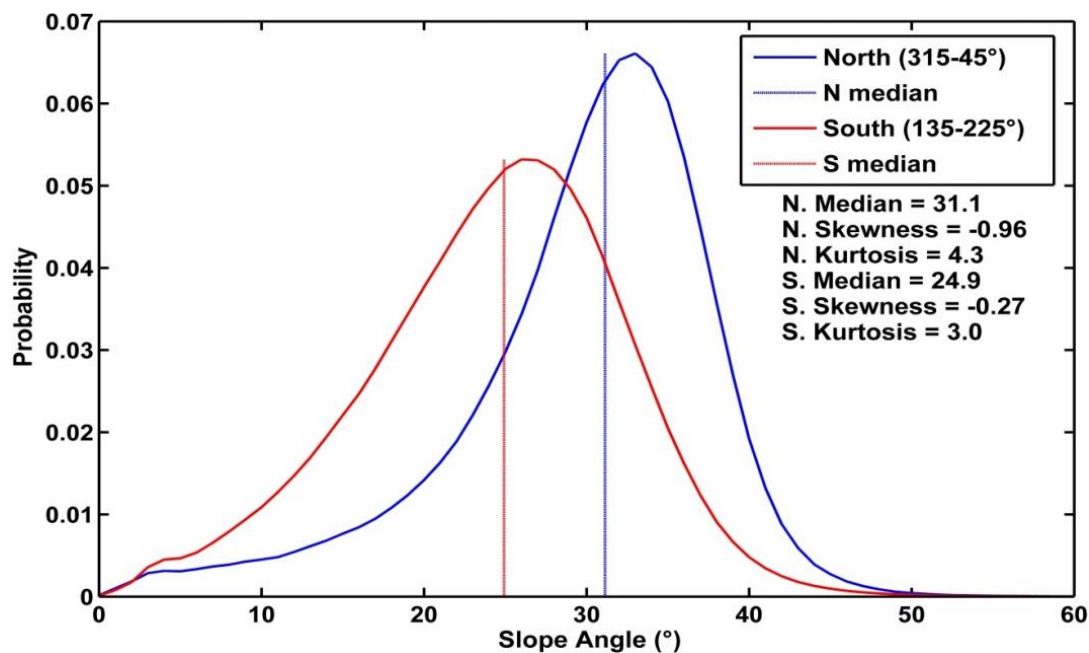


Figure 3.4 Non-parametric probability density function of aspect-binned (90° each) slope angles for north and south-facing slopes.

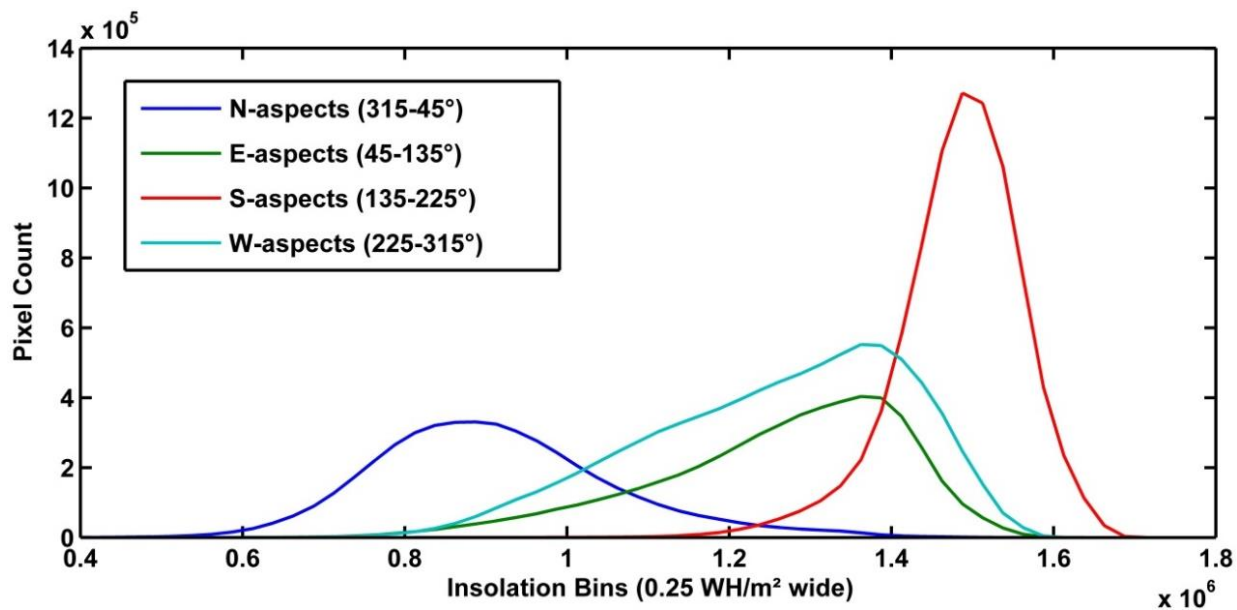


Figure 3.5 Topography-modeled insolation distributions for the cardinal directions. Insolation values represent annual cloud-free totals.

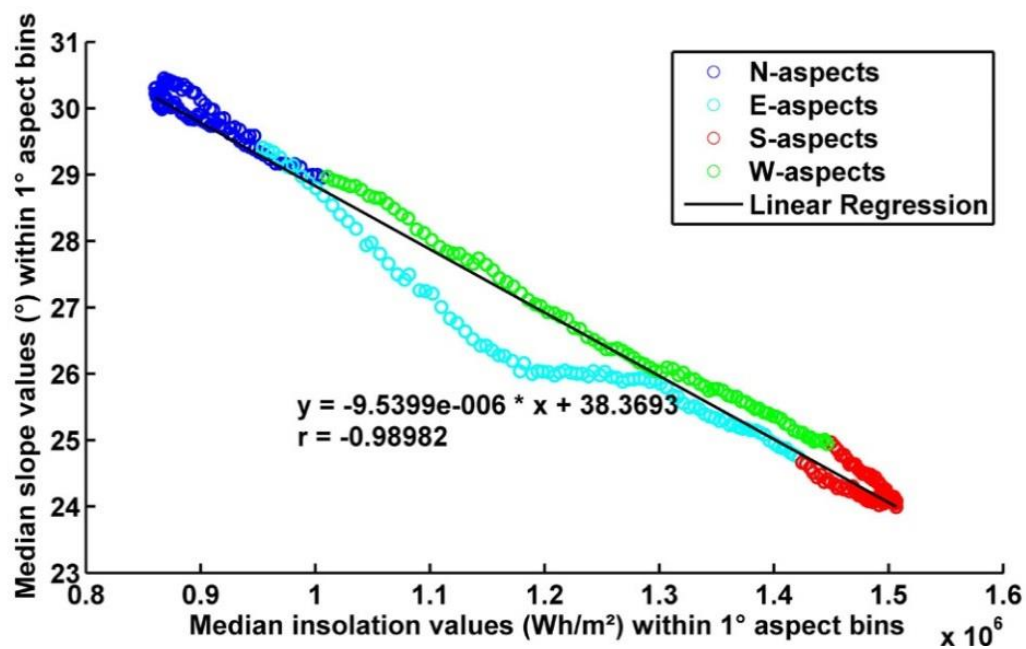
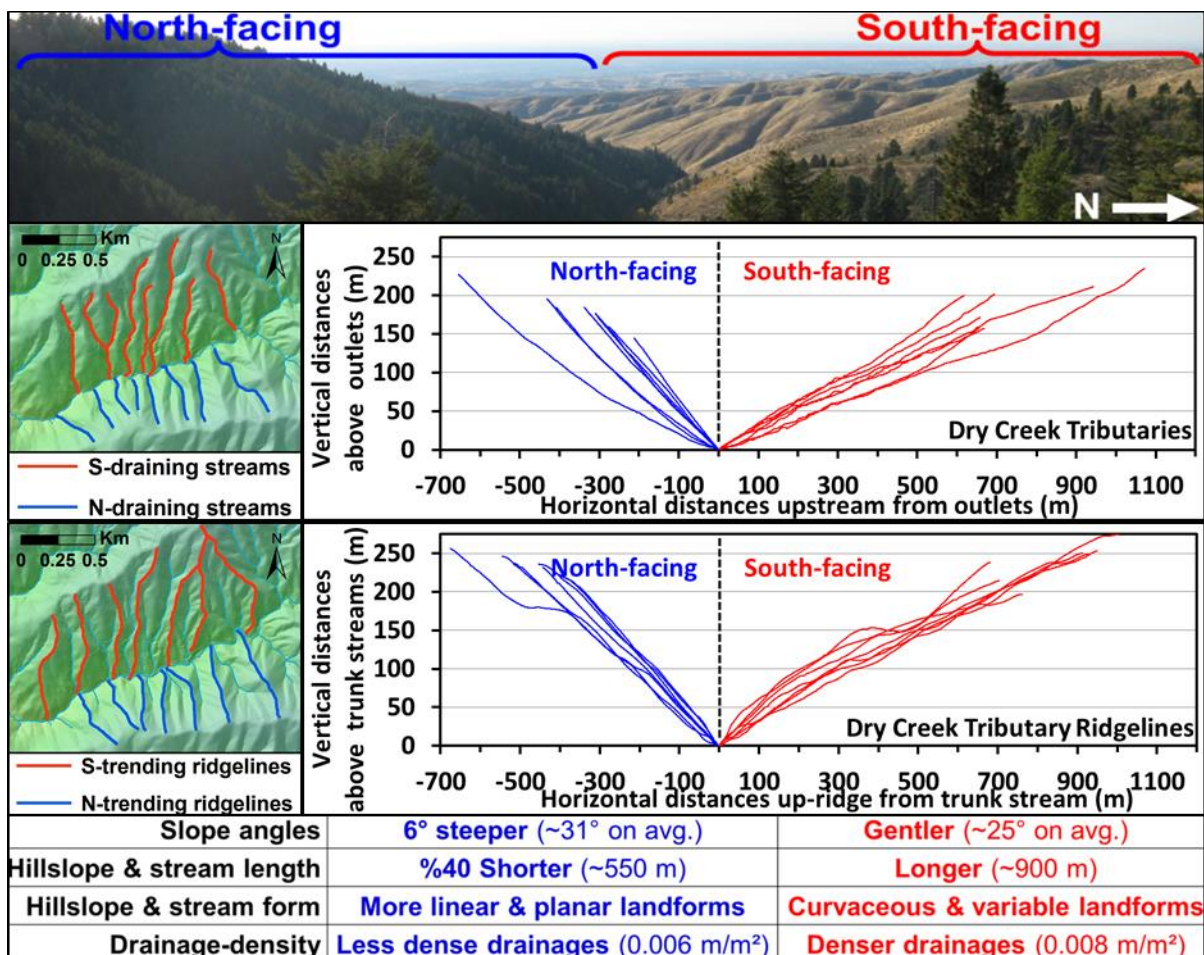
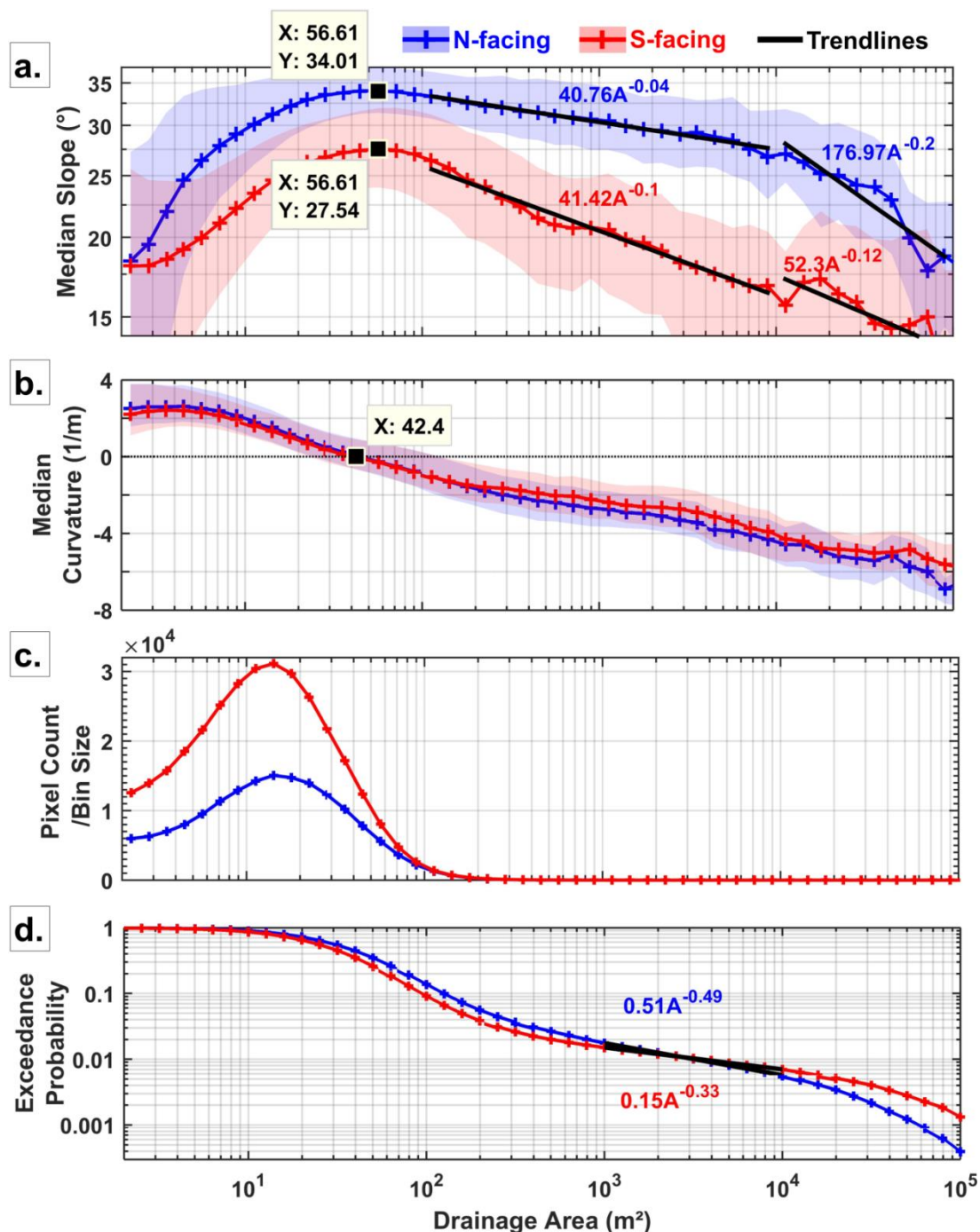


Figure 3.6 Scatter plot showing the inverse correlation between aspect-binned slope and insolation.



**Figure 3.7** Summary of aspect-related differences in stream and ridgeline forms. South-facing land surface extends beyond the photo extent. Data for all three valley segments can be viewed in Figures B4-B7 in Appendix B.



**Figure 3.8** a.) Changes in median slope with drainage area, with interquartile range envelopes, labeled slope turnover points, and transitional and channelized trends and power-law functions denoting scaling relationships. b.) Changes in curvature with drainage area, with interquartile range envelopes and the transitional drainage area from convex to concave topography labeled. c.) Drainage area pixel counts, normalized by bin size, depicting differences in total land surface area at different drainage areas. d.) Probabilities of exceeding given drainage areas, with trends and power-law functions for the linear sections of the distributions denoting scaling relationships.

**Table 3.2 Summary of characteristics of catchments shown in Figure 3.3.**

Catchment number	Orientation	Total drainage area (m <sup>2</sup> )	Minimum volume removed (m <sup>3</sup> )	Min. catchment-averaged denudation (m)	Maximum elevation (m.a.s.l.)	Minimum elevation (m.a.s.l.)	Basin vertical relief (m)	Basin horizontal relief (m)	Stream length (m)	Drainage density (m/m <sup>2</sup> )	Ruggedness (m <sup>2</sup> /m <sup>2</sup> )
1	S	131,183	847,806	6.5	1,607	1,365	241	663	1002	0.0076	1.84
2	S	116,681	936,329	8.0	1,631	1,372	259	758	1081	0.0093	2.40
3	S	54,628	197,623	3.6	1,604	1,381	223	738	612	0.0112	2.50
4	S	175,892	1,958,810	11.1	1,676	1,383	293	1011	1409	0.0080	2.35
5	S	86,358	817,116	9.5	1,622	1,397	225	685	696	0.0081	1.81
6	S	99,389	803,552	8.1	1,664	1,422	242	674	695	0.0070	1.69
7	N	54,740	237,992	4.3	1,593	1,359	233	394	292	0.0053	1.25
8	N	44,386	373,885	8.4	1,623	1,383	240	386	259	0.0058	1.40
9	N	76,023	857,906	11.3	1,629	1,389	240	461	607	0.0080	1.91
10	N	80,771	1,154,880	14.3	1,655	1,399	255	470	383	0.0047	1.21
11	N	149,254	3,239,750	21.7	1,680	1,409	271	624	842	0.0056	1.53
12	S	160,216	2,299,800	14.4	1,622	1,353	270	849	993	0.0062	1.67
13	S	75,304	392,835	5.2	1,602	1,383	219	672	625	0.0083	1.81
14	S	365,653	6,699,540	18.3	1,679	1,387	292	867	2656	0.0073	2.12
15	S	37,816	179,680	4.8	1,591	1,407	184	404	252	0.0067	1.23
16	S	98,919	1,236,360	12.5	1,648	1,414	235	675	569	0.0058	1.35
17	N	116,914	1,954,070	16.7	1,626	1,357	269	595	660	0.0056	1.52
18	N	58,879	567,403	9.6	1,645	1,374	271	466	417	0.0071	1.92
19	N	60,282	597,776	9.9	1,645	1,390	256	437	326	0.0054	1.38
20	N	66,055	600,557	9.1	1,657	1,405	252	447	411	0.0062	1.57
21	N	136,144	1,933,720	14.2	1,702	1,429	273	495	769	0.0056	1.54
<b>Averages for south-facing catchments</b>		<b>127,458</b>	<b>1,488,132</b>	<b>9.3</b>	<b>1,631</b>	<b>1,388</b>	<b>244</b>	<b>727</b>	<b>963</b>	<b>0.0078</b>	<b>1.89</b>
<b>Averages for north-facing catchments</b>		<b>84,345</b>	<b>1,151,794</b>	<b>12.0</b>	<b>1,645</b>	<b>1,389</b>	<b>256</b>	<b>478</b>	<b>497</b>	<b>0.0060</b>	<b>1.52</b>

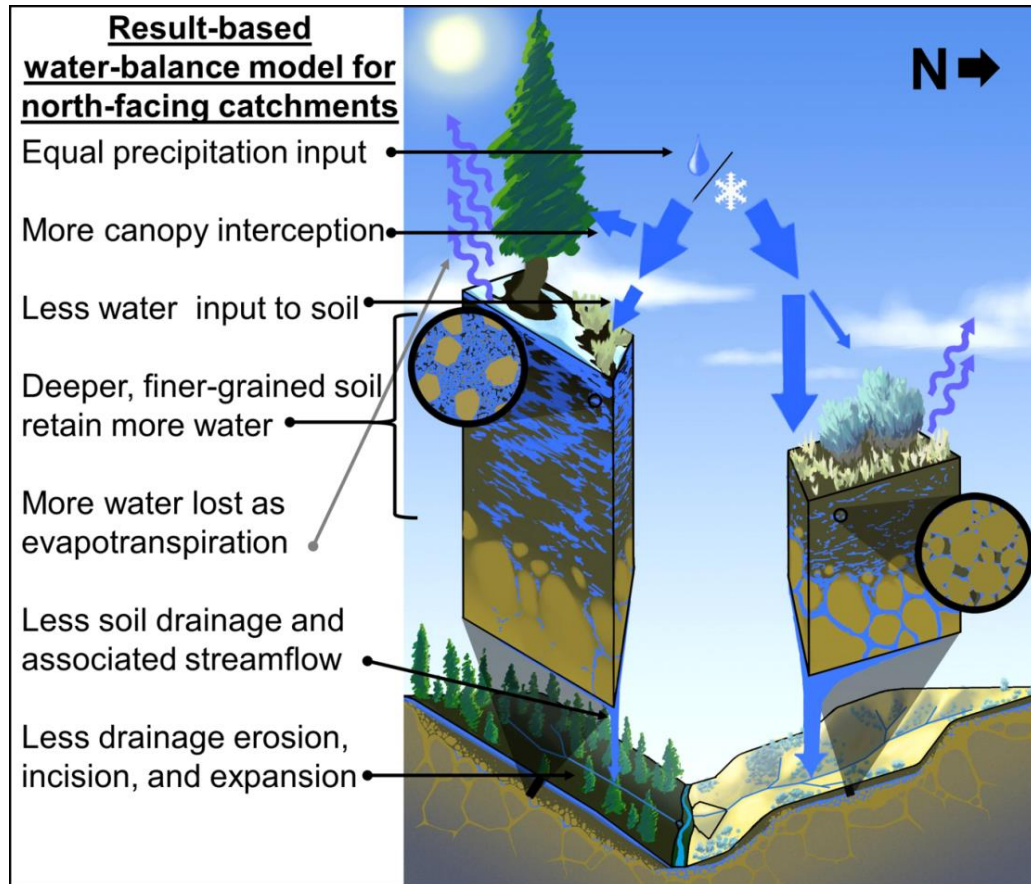


**Figure 3.9** Conceptual water balance model of interactions among modern aspect-related variability of vegetation, subsurface characteristics, water storage, hydrologic partitioning, runoff potential, and hillslope and drainage form.

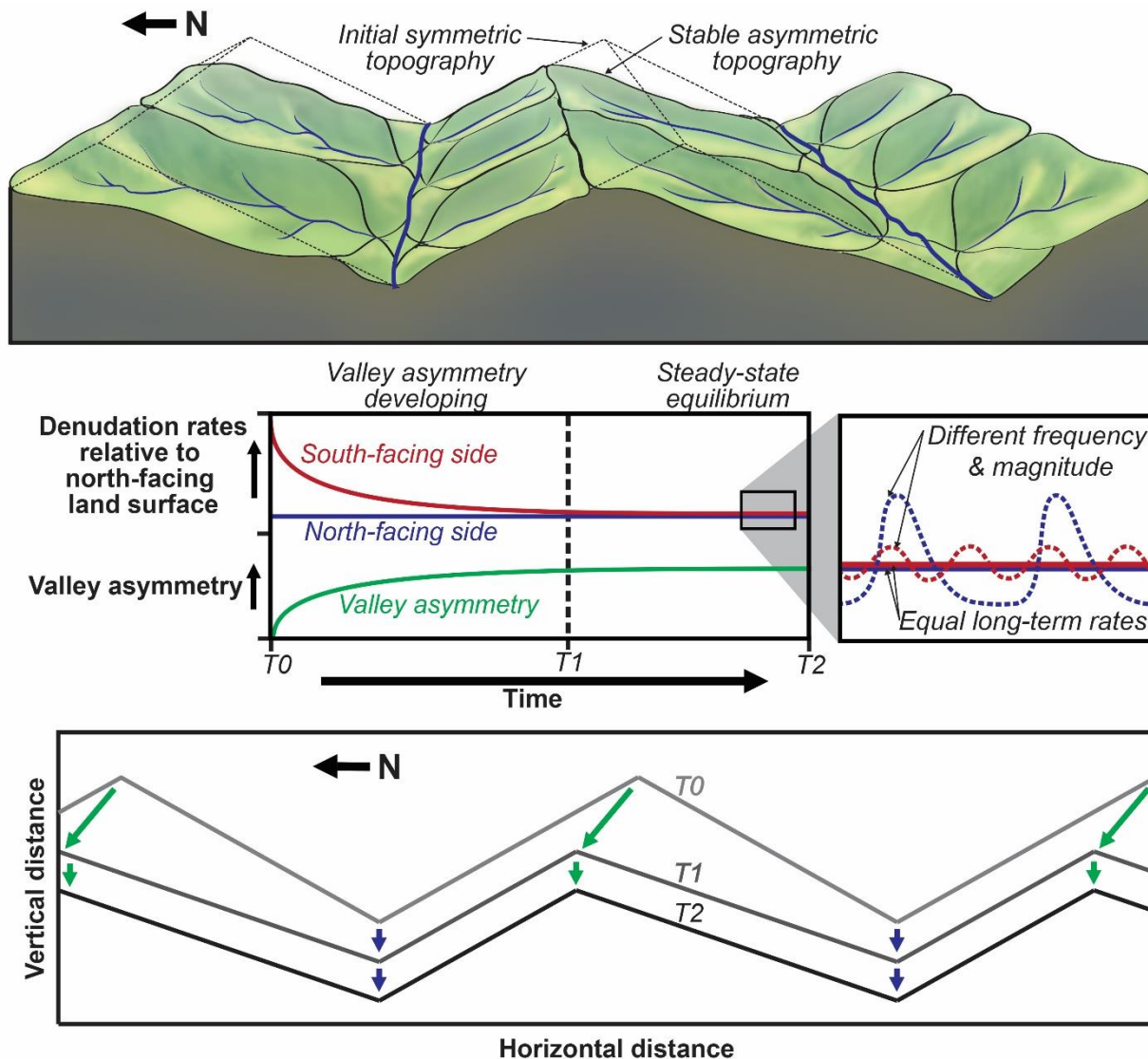


**Figure 3.10** Conceptual model of valley asymmetry development and dynamic equilibrium. a.) Valley geometry changes from a heterogeneously-lowering symmetric form to a homogeneously-lowering asymmetric form. b.) South-facing valley sides degrade faster initially, but negative feedbacks cause long-term denudation rates to attenuate to values similar to north-facing valley sides. Valley asymmetry also attenuates towards a stable asymmetric form. Although short-term denudation rates may be highly variable, due to differences in the frequency, magnitude, and type of erosional processes, long-term rates may still be similar. c.) Cross-section of valleys showing the combined effect of asymmetry development and trunk stream incision. Denudation rates between time-steps  $T_0$  and  $T_1$  vary with aspect, but are uniform between  $T_1$  and  $T_2$  when dynamic equilibrium has been achieved.

APPENDIX A

**Expanded Methods for Chapter 1: Coupling Alluvial Fans Records with Lidar to  
Compare Holocene Erosion Rates of North and South-Facing Catchments in the  
Idaho Batholith**

## **Expanded Methods for Chapter 1: Coupling Alluvial Fans Records with Lidar to Compare Holocene Erosion Rates of North and South-Facing Catchments in the Idaho Batholith**

### A.1 Methods Overview

For small steep ephemeral catchments facing north and south, erosion and fire records were characterized using datable charcoal fragments contained within the small alluvial fans deposited at their outlets. Our approach for estimating catchment-averaged erosion rates from alluvial fan deposits required: 1) radiocarbon dating the deposit, 2) determining the corresponding deposit volume, 3) distributing this volume across the source catchment, and 4) assessing uncertainties and limitations.

Various methods have been developed for measuring erosion rates at catchment and hillslope scales, including 1) direct measurement of modern erosion rates (e.g. sediment traps, tracers, and terrestrial LiDAR differencing), 2) estimates of erosion rates based on surface residence times in soil profiles or stream sediments (e.g. cesium and cosmogenic radionuclide (CRN) accumulations), and 3) estimates of erosion rates obtained by surveying and dating the deposits produced by erosion (e.g. radiocarbon dating or OSL methods). We chose to use radiocarbon dating because it is able to measure erosion over longer timescales and greater areas than direct measurements of erosion, is applicable to poorly-sorted debris flow deposits, and it is inexpensive compared to CRN and OSL-based methods. Radiocarbon dating of charcoal also allows us to reconstruct fire records, which are useful for assessing aspect-related variability in fire and understanding erosion.

Fan surfaces were reconstructed by fitting a conical surface through fan surface remnants, using high-resolution (0.5 m resolution) elevation data that we derived from LiDAR point clouds. Sample depths and ages were extrapolated across reconstructed fan surfaces to yield deposit volumes and volumetric rates of deposition. Normalization of deposit volumes by LiDAR-derived source-catchment surface areas yielded catchment-averaged denudation rates. Denudation rates were compared among small, steep ephemeral catchments incised into larger-scale north and south-facing valley side-slopes in order to investigate how erosion rates and fire activity vary with aspect. Catchment-averaged denudation rates were also compared to those previously measured for the broader Idaho Batholith region in order to validate our methodology.

#### A.2 Fan Identification, Excavation and Sampling

Catchment-scale erosion rates were measured using eight alluvial fan records for north-facing (n=3) and south-facing (n=5) catchments (Figure 1.2). Alluvial fans and catchments were selected for field investigations using 1 and 0.5 meter resolution LiDAR-derived bare-earth elevation data, followed by field excavation, deposit characterization, and charcoal sampling. Using existing exposures, such as where the toe of the fan had been undercut by the trunk stream, or where the fan-building channel had incised into the fan, we sampled charcoal at the greatest possible depth (i.e. the oldest charcoal available), in order to produce longer time-averaged erosion rates. For several sites, we sampled charcoal from multiple depths to assess how the timescales of measurement affect the resulting time-averaged erosion rates.

In-situ charcoal fragments or bulk deposit samples containing visible charcoal were cleanly collected from exposures, taking care to collect material from discrete depth

intervals of vertically cut and cleaned exposure surfaces. Sample depths used in the calculations are the median values of the depth intervals, but sampling ranges are propagated as uncertainty ranges (i.e. error bars). Larger charcoal fragments were picked from the profile where visible, but where fragments were small bulk samples of charcoal and sediment were collected.

### A.3 Radiocarbon Dating and Calibration

Radiocarbon ( $^{14}\text{C}$ ) ages of charcoal fragments from within alluvial fan deposits were dated at the Lawrence Livermore National Laboratory. We selected 20 high quality samples for radiocarbon dating (i.e. younger twigs, single large fragments, sufficient bulk charcoal), with preference given to charcoal from alluvial fans that would produce representative aspect groupings, and provide multiple dated deposits from a few individual fans. Large samples were subsampled into duplicates and dated to assess analytical replicability, and produced comparable results. One set of duplicates were dated as 585 $\pm$ 30 and 555 $\pm$ 35 radiocarbon years, while the second duplicates were dated as 3675 $\pm$ 30 and 3665 $\pm$ 30 radiocarbon years.

Radiocarbon dates were calibrated using the IntCal13 calibration curve in Calib 7.0.2 software (Stuiver and Reimer, 1993; [c14.arch.ox.ac.uk](http://c14.arch.ox.ac.uk)), yielding age probability distributions in calibrated years before present (cal yr BP). Probability distributions are difficult to use directly in calculations, as no single statistical value is truly representative (e.g. median). However, Telford et al. (2004) showed that the weighted mean appears to be the most representative of the radiocarbon age distribution. We calculated the weighted mean for each age probability distribution, as the sum of the products of years and probabilities (***Weighted Mean*** =  $\sum_{i=1}^n \text{Probability}_i * \text{Year}_i$ ), divided by the total

probability (i.e. 1). Uncertainties are quantified during calculations as the limits defining 95% of the probability distributions (i.e. 95% confidence intervals), and expressed as error bars. Individual calibrated age probability distributions were summed for each aspect to yield calibrated fire records for north and south-facing slopes.

#### A.4 Depth Correction

The depth of sample collection within the fan serves as one dimension of the sediment volume estimate. Sample depths are often measured vertically in soil pits. However, fans generally aggrade parallel to the surface, and the surface-normal depth better represents the volume of material deposited above a specific depth. Additionally, for comparisons across landforms of different slope, this introduces a slope bias, as vertical depth measurements on a steep slope will appear deeper than depth measurements normal to the surface. Because the alluvial fans varied in slope, we chose to convert the vertical depths to surface-normal depths using field measurements of fan slope, which were consistent within  $1^\circ$  with average fan surface slopes derived from high-resolution elevation data.

For pits at the fan surface, basic trigonometry was used to convert from vertical to surface-normal depth, where the surface normal depth is the product of the vertical depth and the cosine of the slope. For pits excavated on fan escarpments, where streams cut laterally or vertically into the fan, the pit top was sometimes located at the escarpment surface, rather than the fan surface. Surface-normal depths were calculated for these pits using additional measurements of the escarpment length and slope, and trigonometric relationships, in order to calculate the surface-normal depth to the top of the pit from the

extrapolated fan surface, which was added to the surface-normal depth in the pit.

#### A.5 Fan Reconstruction, Volumetric Deposition, and Catchment-Averaged Denudation

Often the fans of interest were partially dissected by nearby streams. In order to more accurately estimate the volume of material deposited above a charcoal sample, the fan 3D surfaces were reconstructed by creating a best-fit conical trend surface through relict fan surface elevations. First, raw airborne LiDAR point-cloud data were used to create 0.5 and 1.0 m resolution bare-earth digital elevation models (DEMs) using BCAL LiDAR Tools 1.5.3 (<http://bcal.boisestate.edu/tools/lidar>) in ENVI 5.0. Appropriate parameters for height-filtering LiDAR point returns (i.e. removing vegetation) were determined by manually iterating through canopy spacing and vegetation height thresholds, and visually comparing results to select parameters that best captured small-scale features (0.5 m resolution) or filtered out vegetation (1.0 m resolution). Height-filtered point clouds were then rasterized into bare-earth DEMs (i.e. interpolated into grids) at 0.5 m resolution for manual delineation of fan surface remnants, and 1 m resolution for catchment delineation.

Importantly, 0.5 m resolution bare-earth interpolation of airborne LiDAR data may not be useful for automated analyses, as this is pushing the data to its resolution limits, and often ground point elevations are not available within a 0.5 m area below coniferous trees, causing artifacts (e.g. tree trunks). However, this higher-resolution DEM was better able to capture details, such as fan edges and a known debris-flow levee on a fan, which was advantageous for manually and visually delineating fan surface remnants. Tree-related artifacts were apparent, but related point data were not used for fan surface interpolation (i.e. reconstruction).

In order to reconstruct fan surfaces in ArcGIS 10.1, gridded data were converted to point features so that points could be manually selected on the fan surface remnants and used to create a best-fit conical surface fit through the points. The reconstructed fan surfaces were then merged with the source DEM, effectively reconstructing missing fan extents at the time of deposition. The merged results allowed the reconstructed fan surfaces to be manually delineated, as the edges of the reconstructed fan surfaces were readily apparent where they intersected the confining hillslopes (Figure 1.3).

After the fan surfaces were delineated, the surface area was calculated by converting them to Triangulated Irregular Networks (TINs) and measuring their 3D surface area using the Polygon Volume tool in ArcGIS 10.1, which returns 3D surface area values. The 3D surface areas avoid bias associated with varying fan surface slopes, where map-view 2D surface areas increasingly underestimate true surface area for steeper slopes.

Multiplying reconstructed fan 3D surface areas by surface-normal sample depths yielded fan volume estimates above each sample. This volume was then used to calculate fan aggradation rates by dividing the volumes of material deposited above each sample by its weighted-mean calibrated age. Source-catchment 3D surface areas were produced using the ArcGIS 10.1 Spatial Analyst/Hydrology tools to delineate the catchments from 1.0 m resolution DEMs, which more completely filter vegetation than their 0.5 m counterparts, and then converting the bare-earth elevation data to TIN format to calculate 3D surface areas using the Polygon Volume tool. Fan aggradation rates were then converted to catchment-averaged denudation rates by dividing the aggradation rates by

the 3D surface areas of the source-catchments that produced each fan. This complete calculation is summarized as follows:

$$\mathbf{Denudation\ rate} \left( \frac{mm}{yr} \right) = \frac{\mathbf{Deposit\ Thickness} * \mathbf{Fan\ Area}}{\mathbf{Deposit\ Age} * \mathbf{Source\ Catchment\ Area}} \quad \frac{cm * m^2}{yr * m^2} \quad [\text{Eq. 1}]$$

Using 3D surface areas avoids the aforementioned slope-bias of 2D surface areas and yields an estimate of surface-parallel slope retreat.

Erosion was not evenly distributed across the catchment as ‘Catchment-averaged denudation’ implies. Rather material eroded from hillslopes accumulates and is stored temporarily in hollows and along channels and is episodically excavated and delivered to alluvial fans. We normalize the erosion rates by the total possible source area, but erosion may be highly variable within a catchment. However, as this stored sediment was originally produced by the contributing hillslopes, beyond the timescale of individual events the two should be similar.

#### A.6 Error Propagation

Maximum and minimum uncertainty ranges of fan aggradation and catchment averaged denudation rates were determined by propagating individual errors and uncertainties through the calculations (i.e. Equation 1 and depth corrections). In order to calculate minimum uncertainty range values, minimum error or uncertainty ranges were used in the calculations for variables positively correlated with the result (e.g. numerator variables), and maximum values used for inversely correlated variables (e.g. denominator variables). Maximum uncertainty ranges were calculated using the opposite approach. Some variables, such as sample age and depth range, had directly measurable error ranges, which were propagated in through the calculations. For depth corrections, we

assumed a  $\pm 1^\circ$  error on local slope measurements, based upon differences between slopes measured locally in the field and across the fans in high resolution elevation data. For fan and catchment surface areas, we assumed a  $\pm 1$  m (i.e.  $\pm 2$  pixels) accuracy in boundary delineation from the 0.5 m resolution elevation data, based upon our ability to distinguish features of similar scale (e.g. debris flow levees). Boundaries for fans and catchments were shrunk or grown, and the 3D surface areas were calculated to produce minimum and maximum uncertainty ranges.

Uncertainties for calibrated charcoal ages, based on 2 standard deviations (i.e. 95% confidence) of the probability distribution, ranged from  $\pm 24$  to 178 years ( $\pm 1$  to 18%) for all charcoal samples. The average calibrated age error was  $\pm 92$  years ( $\pm 6\%$ ). For the subset of deepest samples used to calculate aggradation and erosion rates, propagating age uncertainties with sampling depth interval uncertainties yielded errors for aggradation rates ranging from  $\pm 3$  to 12% of weighted mean values, with an average propagated aggradation error of  $\pm 7\%$ . For catchment-averaged denudation, propagated errors ranged from  $\pm 8$  to 14%, with an average value of  $\pm 11\%$ . The increased error for denudation rates is primarily due to the  $\pm 0.5$  m (i.e.  $\pm 1$  pixel) boundary uncertainty assumed for fan surface area delineation ( $\pm \sim 2$  to 6% error, varying inversely with fan area), as the source catchments were much larger than the estimated scale of measurement error ( $\pm 0.2$  to 0.4% error, varying inversely with catchment area).

#### A.7 Additional Assumptions & Uncertainties

Typically fan deposit thicknesses vary laterally; sample age/depth trends will vary depending on sampling locations. It was not possible to assess this variability, due to poor

exposure and a general absence of marker deposits. For simplification, our methods assume that the surface-normal sample depths are representative of our corresponding fan depositional volumes (i.e. deposits are of uniform thickness, lie parallel to the surface, and cover the entire fan). While this assumption certainly isn't valid over short time-scales, over longer timescales fans aggrade evenly and this variability is low relative to the overall sampling depth. In order to achieve a maximum timescale of measurement, we sought and excavated exposures where we could collect the deepest samples. The validity of this assumption was partially tested by characterizing the linearity of aggradation rates within multiple profiles. Additionally, variations in sample depths and associated timescales of measurement may reveal a characteristic timescale beyond which aggradation rates become relatively consistent.

Charcoal ages reflect the ages of the deposits at specific depth, plus any inbuilt age due to the age of the vegetation prior to the fire (Gavin, 2001) which includes any residence time within the catchment. These one-directional uncertainties will cause the timing of the fire inferred from radiocarbon dating to be overestimated by a corresponding amount. In order to reduce this error, preference was given to dating small twigs, identified under magnification by higher curvature growth rings, which were young at the time of the fire and have lower inbuilt ages. Some samples had unconstrainable inbuilt ages, which we could not account for in our error propagation. We assume that these overestimations are small compared to our uncertainty ranges, which spanned 64 to 343 years, and are somewhat counteracted by the underestimations caused by the inevitable inclusion of ingrown rootlets and microbes.

### References

- Gavin, D. G. (2001). Estimation of inbuilt age in radiocarbon ages of soil charcoal for fire history studies. *Radiocarbon*, 43(1), 27-44.
- Stuiver, M., Reimer, P.J., (1993). Extended 14C database and revised CALIB Radiocarbon Calibration Program. *Radiocarbon* 35, 215–230.
- Telford, R. J., Heegaard, E., & Birks, H. J. (2004). The intercept is a poor estimate of a calibrated radiocarbon age. *The Holocene*, 14(2), 296-298.

**APPENDIX B****Supplemental Figures for Chapter 3: Aspect-Induced Asymmetric Degradation,****Divide Migration, and Land Surface Elongation Drive Valley Asymmetry****Development towards a Dynamic Equilibrium**

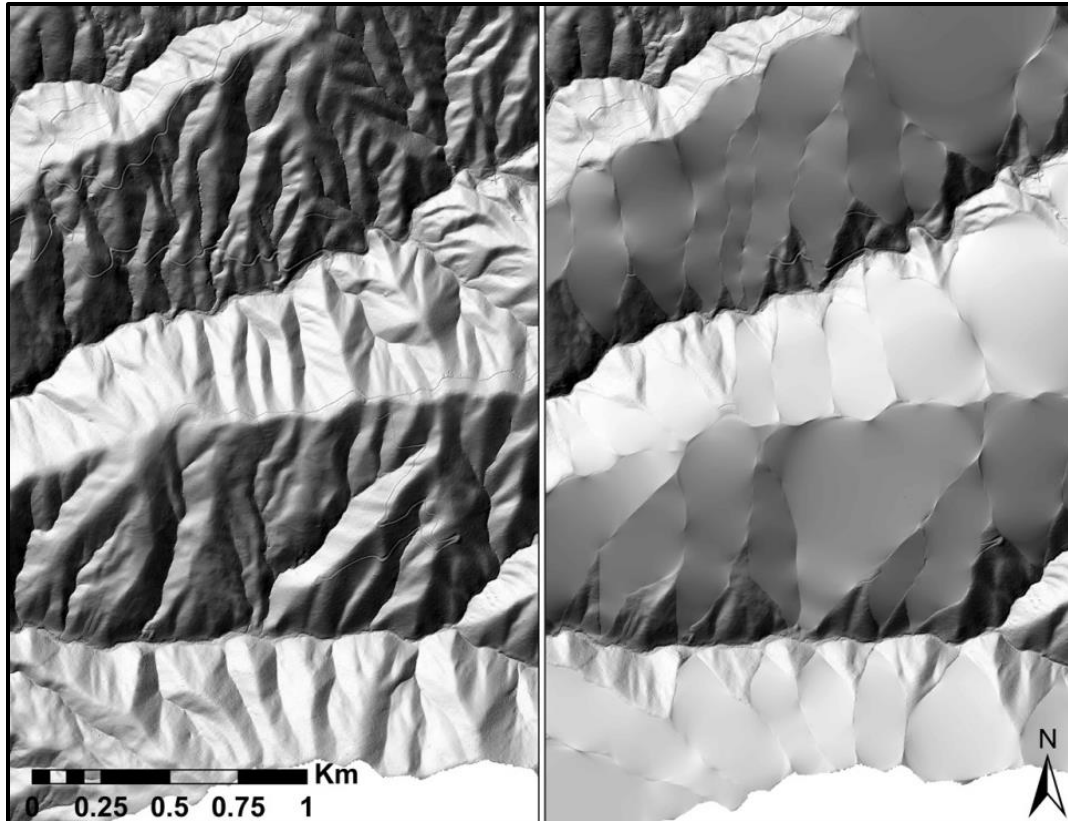


**Figure B1** Before (left) and after (right) hillshades showing how ridgeline elevations were interpolated to fill catchments and estimate the minimum volume of material removed. Ridgelines have likely eroded over time as well, so these volumes should not be viewed as total amounts of erosion, but are treated as a metric of the depth of drainage incision below ridgelines.

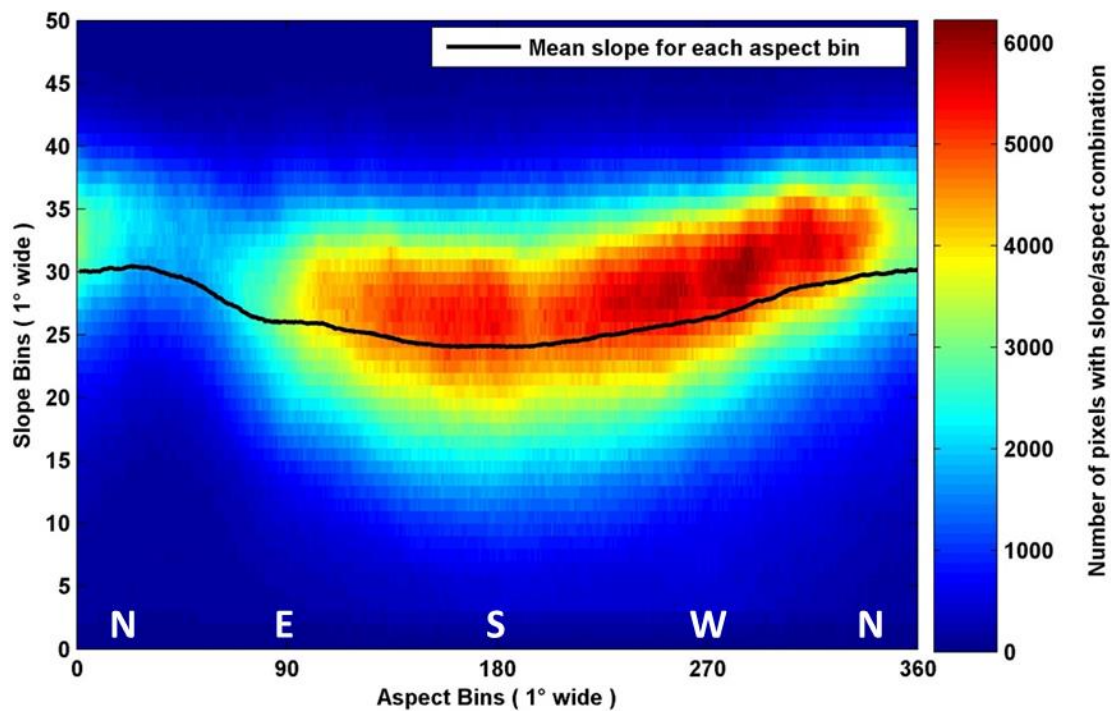


**Figure B2** Changes in slope with aspect. Colored data show the frequency of specific combinations of aspect and slope bins. The black line is the median slope value within each 1° aspect bin. The gap in the distribution at ~10 to 80° reflects the low abundance of north-east facing slopes.

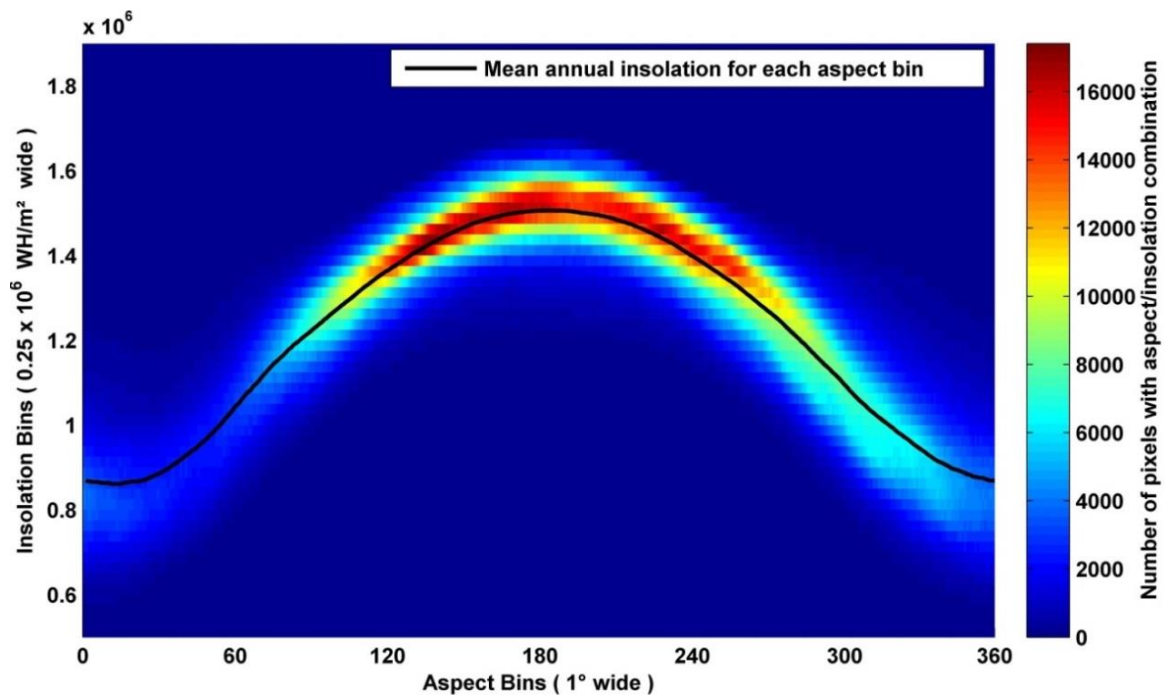


**Figure B3** Changes in insolation with aspect. Colored data show the frequency of specific combinations of aspect and insolation bins. The black line is the median insolation value within each 1° aspect bin.

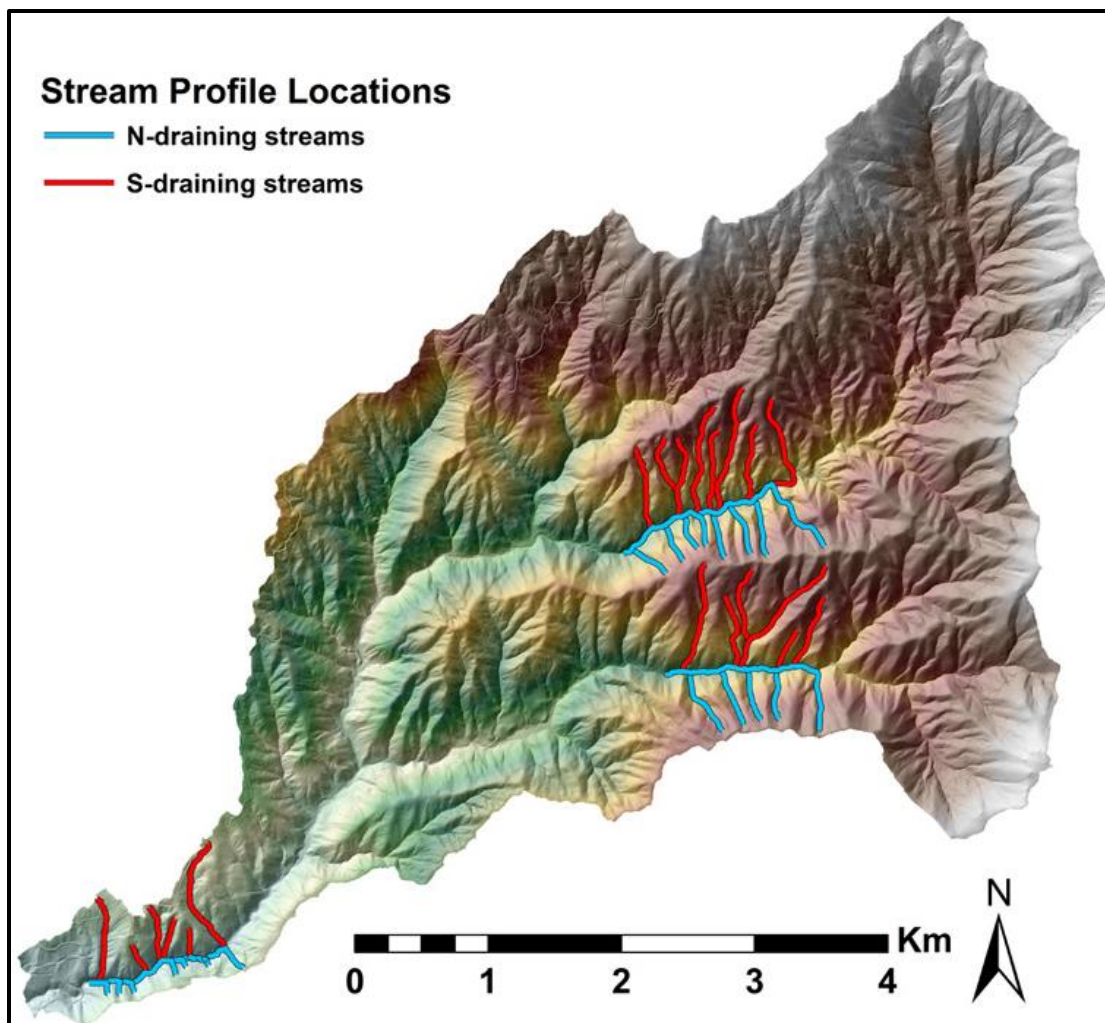


**Figure B4** Locations of stream profiles shown in Figure B5 for catchments incised into north and south-facing valley side-slopes. From top to bottom, these valleys are Upper Dry Creek, Shingle Creek, and Lower Dry Creek. Note the shorter length and more linear form of streams draining from north-facing slopes.

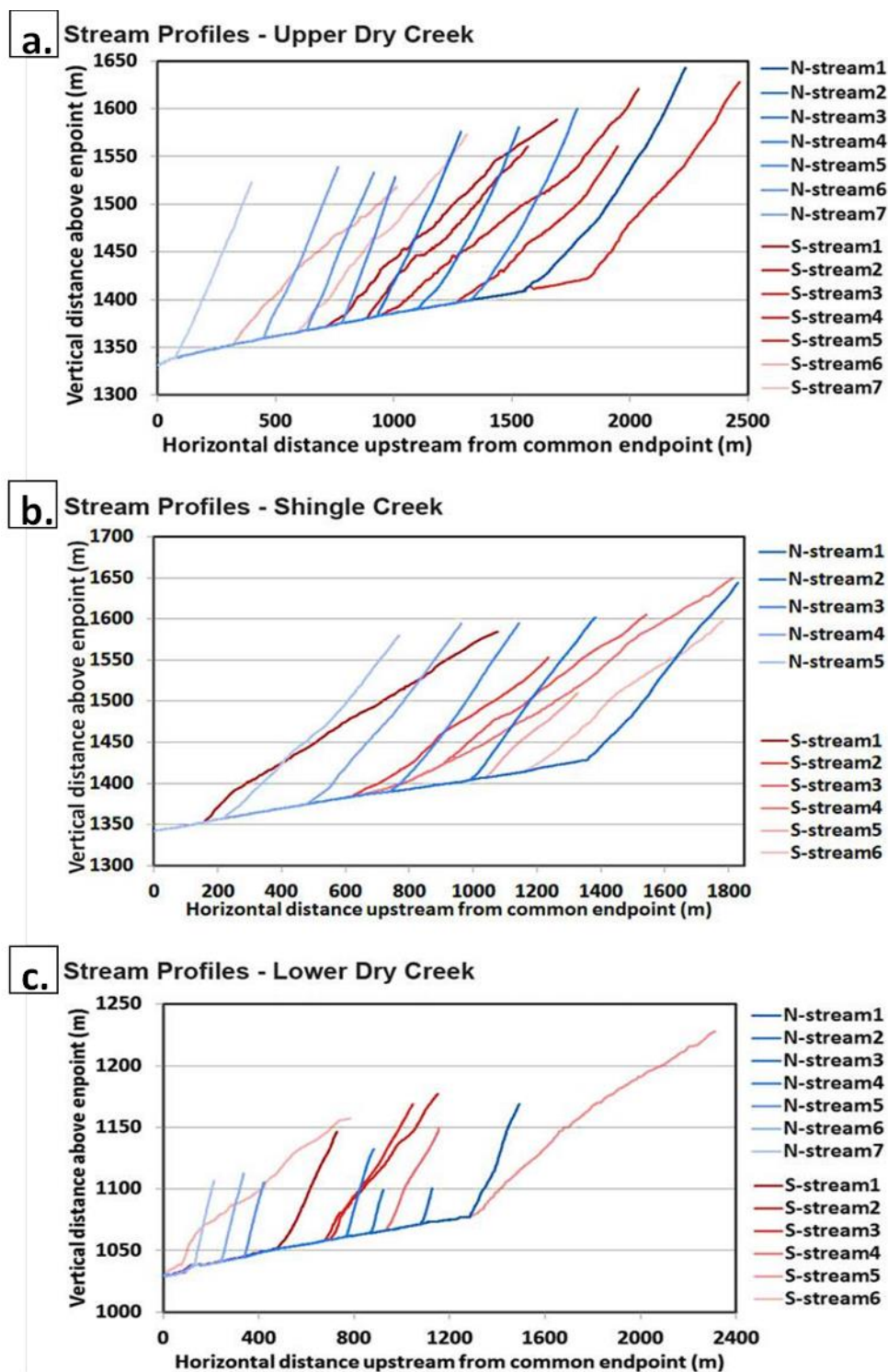


**Figure B5** Stream longitudinal profiles plotted draining to trunk streams for catchments incised into north and south-facing valley side-slopes along upper Dry Creek (a.), Shingle Creek (b.) and lower Dry Creek (c.). See Figure B4 for locations. Note that stream profiles for south-facing slopes less linear and longer horizontally, but similar in vertical relief, except along lower Dry Creek where south-facing landsurfaces have more relief.

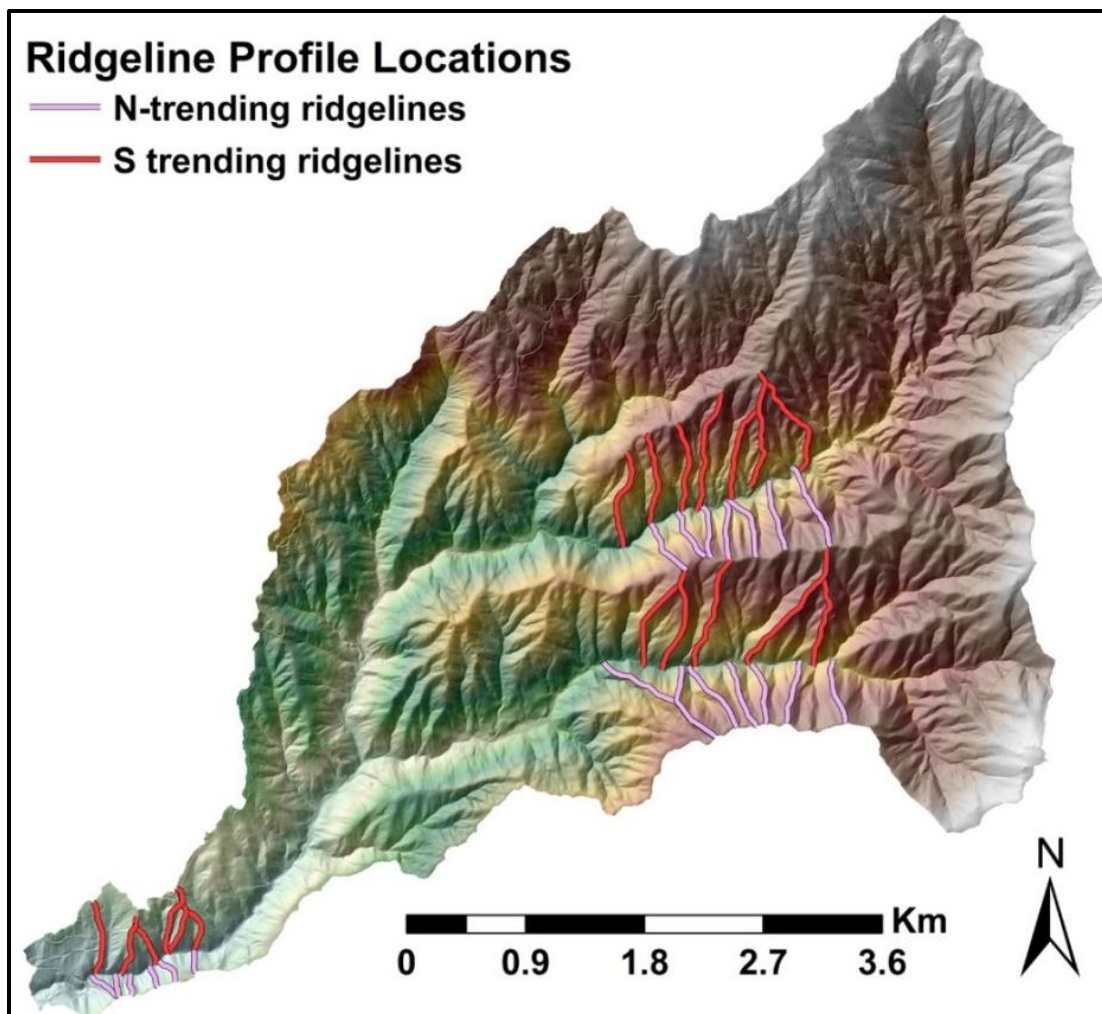


**Figure B6** Locations of profiles along ridgelines between catchments incised into north and south-facing valley side-slopes. From top to bottom, these valleys are Upper Dry Creek, Shingle Creek, and Lower Dry Creek. Note the shorter length of ridgelines, in general, for north-facing slopes. See Figure B7 for ridgeline profiles.

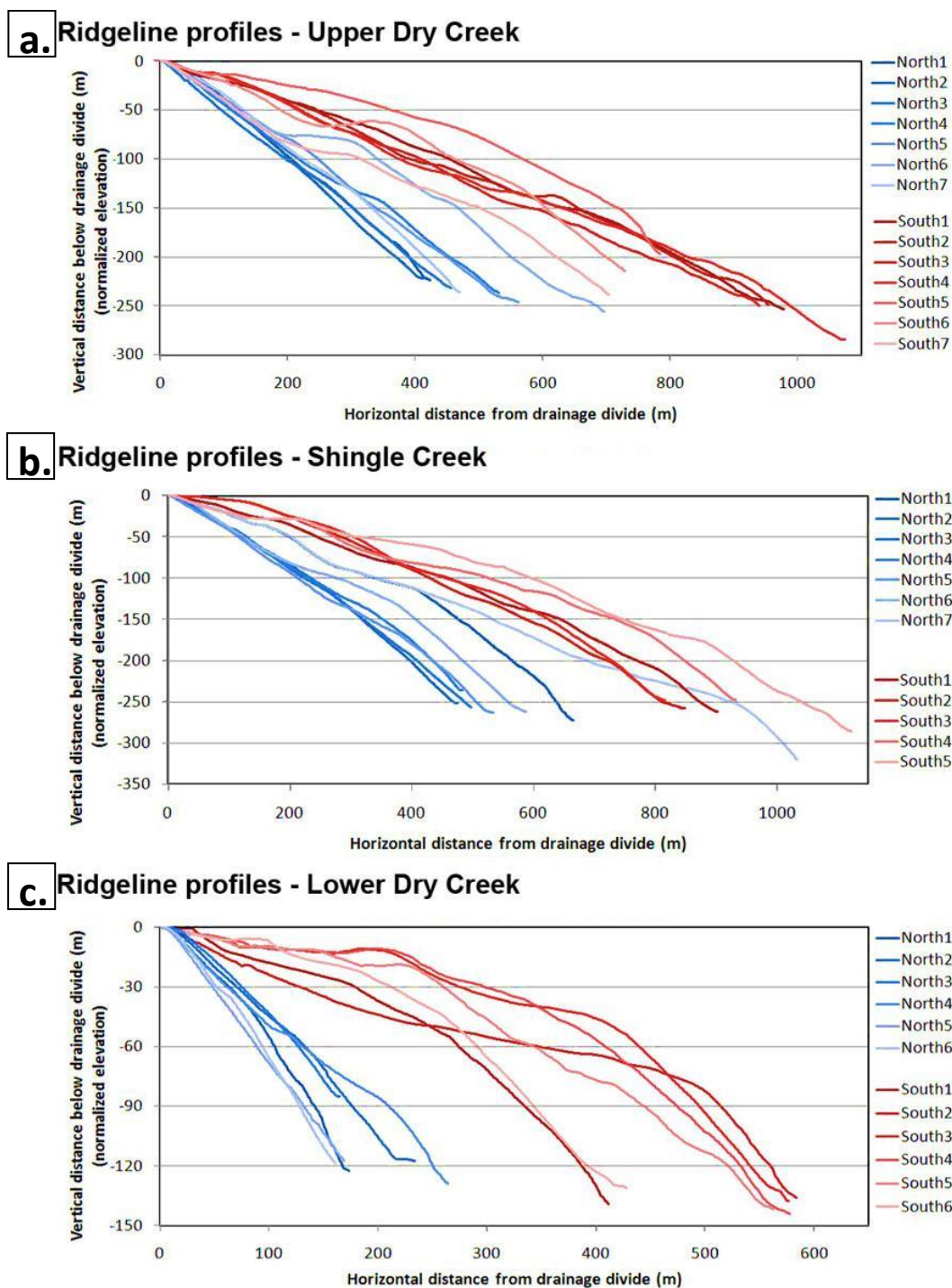


**Figure B7** Ridgeline (see Figure B6 for locations) profiles for ridgelines formed between catchments incised into north and south-facing valley side slopes along upper Dry Creek (a.), Shingle Creek (b.) and lower Dry Creek (c.). Distances are plotted relative to where each ridgeline intersects the divide between north and south-facing valley land surfaces. Ridgelines on south-facing slopes are longer horizontally, but similar in vertical relief, except in lower Dry Creek where south-trending ridgelines have more relief.